BEAMFORMING FOR UNDERLAY TWO-WAY RELAY NETWORKS

by

Yun CAO

A thesis submitted in partial fulfillment of the requirements for the degree of

Doctor of Philosophy

in

Communications

Department of Electrical and Computer Engineering
University of Alberta

Abstract

Although underlay networks mitigate the dual problems of spectrum congestion and spectrum under-utilization, the bi-directional (primary-to-secondary and secondary-to-primary) interference issues must be addressed to improve their reliability, coverage and capacity. To address these problems, this thesis investigates beamforming and two-way relaying. Specifically, the two underlay configurations considered are (a) multi-antenna terminals and one single-antenna two-way relay and (b) single-antenna terminals and multiple single-antenna two-way relays. First, for Configuration (a), assuming the availability of perfect channel state information, the performance of sub-optimal beamforming algorithms is characterized. Specifically, the exact and asymptotic outage probabilities in high transmit power and interference temperature limit region are derived considering both path loss effect and small-scale fading. Second, also for Configuration (a), efficient transmitter and receiver beamforming strategies are developed, e.g., transmit powers, transmitter-side beamforming and receiver-side beamforming vectors at the two multi-antenna terminals. Third, for Configuration (b), assuming the availability of second-order channel statistics, the joint relaying and transmitter designs are developed.

Overall, these research findings show the capability of beamforming and relaying in addressing the bi-directional interferences problems in underlay networks and thus improving their reliability.

$\sim$

Preface

This thesis is an original work conducted by Yun CAO.

Chapter 3 of this thesis has been accepted for publication as Y. CAO and C. Tellambura, "Outage Analysis of ZFB-MRT/MRC underlay Two-way Relay Systems," *IEEE Communication Letter*, March 2015. I was responsible for the concept formation, technical apparatus, simulation data collection and manuscript composition. C. Tellambura was the supervisory author and was involved with concept formation and manuscript composition.

Chapter 4 of this thesis has been submitted as Y. CAO and C. Tellambura, "Cognitive Beamforming in Underlay Two-way Relay networks with Multi-Antenna Terminals," *IEEE Transactions on Cognitive Communication and Network*, January 2015. I was responsible for the concept formation, technical apparatus, simulation data collection and manuscript composition. C. Tellambura was the supervisory author and was involved with concept formation and manuscript composition.

Chapter 5 of this thesis has been published as two papers, including Y. CAO and C. Tellambura, "Joint Distributed Beamforming and Power Allocation in Underlay Cognitive Two-Way Relay Links Using Second-Order Channel Statistics," *IEEE Transactions on Signal Processing*, vol. 62, no. 22, November 2014, P5950-5961; and Y. CAO and C. Tellambura, "Distributed beamforming and power allocation in two-way multi-relay networks with second-order channel statistics," *2013 International Conference in Wireless Communications and Signal Processing (WCSP)*, October 2013, Hangzhou, China. I was responsible for the concept formation, technical apparatus, simulation data collection and manuscript composition. C. Tellambura was the supervisory author and was involved with concept formation and manuscript composition.

~

Acknowledgement

I wish to express my sincere gratitude and respect to my supervisor, Dr. Chintha Tellambura for his brilliant advice and constant encouragement, which has helped me to perform my research timely and efficiently. His rich knowledge and experience in wireless communications have significant influence on my research and make working with him a memorable experience. I greatly appreciate him for supporting me throughout my research life.

My thanks also go to members of PhD examining committee, Dr. Hai Jiang and Dr. Yindi Jing, for their time reviewing my thesis and for their valuable suggestions for improvement. I am also grateful to the faculty and the staff of the Department of Electrical and Computer Engineering for their full support.

I am also grateful to my fellow lab-mates for their invaluable help and advice for my research and the pleasant lab environment they created.

My deepest gratitude goes to my beloved parents, my grandparents, my husband, my son, and other family members for their unequivocal supports.

Last but not least, I also wish to thank the China Scholarship Council (CSC) for the financial support throughout the past four years in the form of a CSC Scholarship.

$\sim$

Table of Contents

List of Tables

List of Figures

List of Symbols

Elementary & Special Functions

Notation	Definition
$\psi(x)$	diagamma function
$\Gamma(\cdot)$	Gamma function
$\gamma(\cdot, \cdot)$	lower incomplete Gamma function
$P(\cdot, \cdot)$	regularized lower incomplete Gamma function
$B(\cdot, \cdot)$	Beta function
$B(\cdot; \cdot, \cdot)$	incomplete Beta function
$\mathcal{K}_\nu(\cdot)$	modified Bessel function of the second kind of order ν
$\log_2(\cdot)$	logarithm to base 2

Probability & Statistics

Notation	Definition
$\mathbb{E}\{X\}$	expected value of X
$f_X(\cdot)$	probability density function (PDF) of X
$F_X(\cdot)$	cumulative distribution function (CDF) of X
$X \sim \text{Exp}(\lambda)$	exponential random variable X
$X \sim \text{Gamma}(\cdot, \cdot)$	Gamma random variable X
$X \sim \text{Beta}(\cdot, \cdot)$	Beta random variable X
$X \sim \mathcal{CN}(\cdot, \cdot)$	circularly symmetric complex Gaussian random variable X

Miscellaneous

Notation	Definition
$\mathbb{C}$	set of complex numbers
$\lvert a \rvert$	absolute value of scalar a
$\lVert \boldsymbol{a} \rVert$	L^2-norm of vector $\boldsymbol{a}$

Notation	**Definition**
$k!$	factorial of k
$\binom{n}{k}$	binomial coefficient n choose k
$\mathcal{H}_i$	Hypothesis i
$\lim_{x \to a} f(x)$	the limit of function $f(x)$ as x tends to a
$\max(a_1,\, a_2)$	maximum of scalars a_1 and a_2
$\min(a_1,\, a_2)$	minimum of scalars a_1 and a_2
$\boldsymbol{A}^{-1}$	inverse of $\boldsymbol{A}$
$\boldsymbol{A}^{T}$	transpose of $\boldsymbol{A}$
$\boldsymbol{A}^{H}$	Hermitian of $\boldsymbol{A}$
$\boldsymbol{A}^{*}$	conjugate of $\boldsymbol{A}$
$\boldsymbol{I}_n$	identity matrix of rank n
$\mathrm{Tr}(\boldsymbol{A})$	trace of matrix $\boldsymbol{A}$
$\mathrm{rank}(\boldsymbol{A})$	rank of matrix $\boldsymbol{A}$
$diag\{\boldsymbol{a}\}$	diagonal matrix with diagonal elements given by vector $\boldsymbol{a}$
$\boldsymbol{A} \circ \boldsymbol{B}$	Hadamard product of matrices $\boldsymbol{A}$ and $\boldsymbol{B}$
$\lambda_{max}(\boldsymbol{A})$	principle eigenvalue of matrix $\boldsymbol{A}$
$\lambda_{max}(\boldsymbol{A},\, \boldsymbol{B})$	generalized principle eigenvalue of matrices $(\boldsymbol{A},\, \boldsymbol{B})$

List of Abbreviations

Abbreviation	Definition
AF	Amplify-and-Forward
AWGN	Additive white Gaussian noise
CDF	Cumulative distribution function
CSI	Channel state information
DF	Decode-and-Forward
MIMO	Multiple-Input Multiple-Output
MRC/MRT	Maximal-ratio combining/transmission
P2S	Primary-to-secondary
PDF	Probability density function
POPA	Potential optimal power allocation
QCQPs	Quadratically constrained quadratic programs
Rx	Receiving
RZFB	Regularized zero-forcing beamforming
S2P	Secondary-to-primary
SDR	Semidefinite relaxation
SINR	Signal-to-interference-and-noise ratio
SNR	Signal-to-noise ratio
SOS	Second-order statistics
Tx	Transmitting
ZFB	Zero-forcing beamforming
ZFB-MRC/MRT	ZFB and MRC/MRT

Chapter 1

Introduction

This thesis explores beamforming and two-way relaying to mitigate the dual problems of spectrum congestion and spectrum under-utilization. These problems can be alleviated by the use of underlay cognitive radio networks. However, their reliability, capacity, and coverage depend on bi-directional (primary-to-secondary (P2S) and secondary-to-primary (S2P)) interference constraints. Therefore, this thesis uses beamforming and two-way relaying to improve these important performance measures.

This chapter starts with the current state of wireless communications, then introduces cognitive radio, beamforming and relaying. Next, the motivation, objectives and significance of this thesis are discussed. Finally, the contributions and outline of this thesis are discussed.

1.1 Wireless Communications

With the rapid growth of wireless devices, such as smart phones and tablets, wireless has recently been the fastest growing segment of telecommunications. For instance, the global mobile wireless data traffic has increased from 250 PetaBytes to over 2250 PetaBytes per quarter from 2010 to 2014 (Fig. 1.1a). And the increase from the first quarter of 2013 to 2014 is 65%. Such dramatic increases are expected to continue in the next four years (Fig. 1.1b) [4], e.g. as much as 15.9 ExaBytes per month in 2018, which is over 10-fold of that in 2013 (1.5 ExaBytes per month).

This dramatic growth of mobile wireless traffic leads to two critical questions:

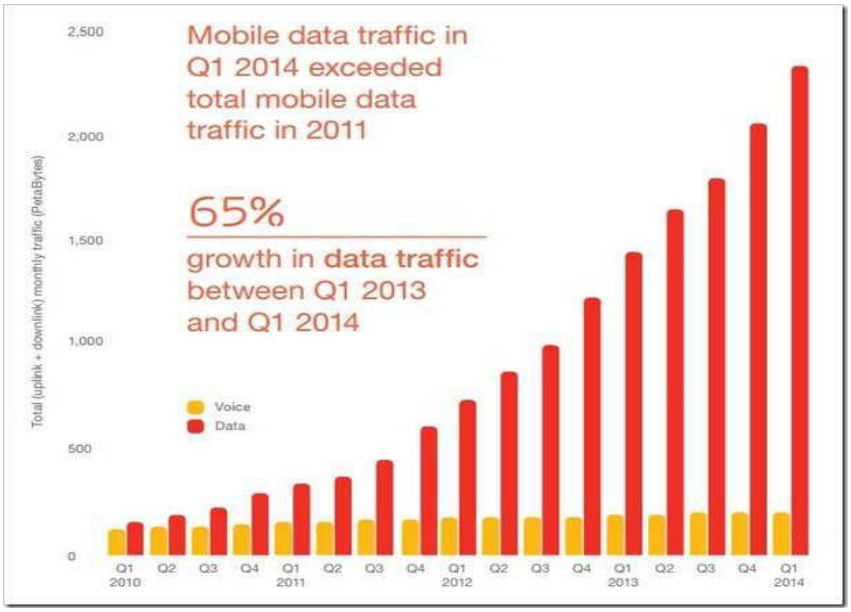

(a) Global Mobile Data Traffic [3]

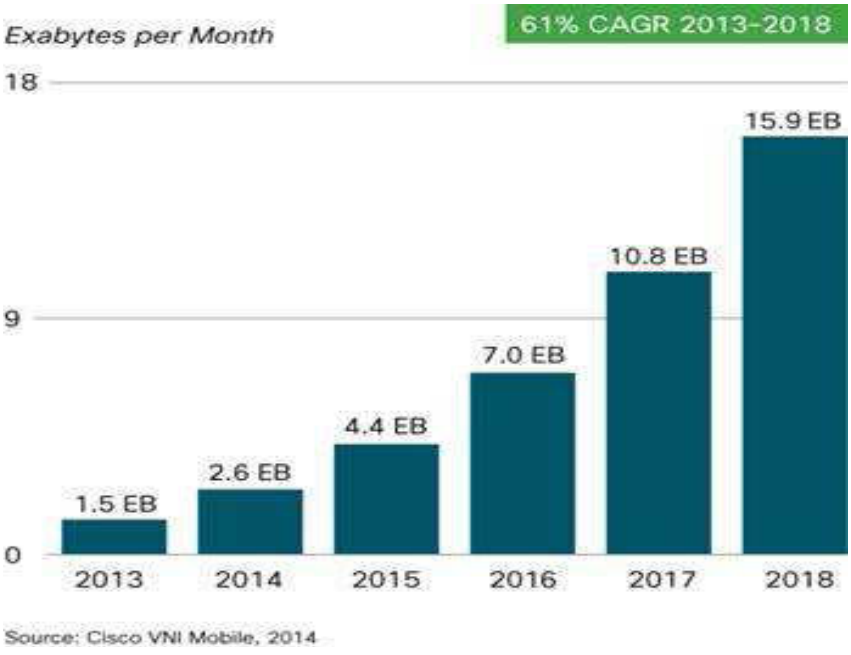

(b) Global Mobile Traffic Forecast [4]

Figure 1.1: Global Mobile Data Traffic

1. What are the possibilities to release more spectrum for wireless communications?

2. Is the pre-allocated spectrum currently being used as efficiently as possible?

On the first question, releasing more spectrum appears impossible with current radio spectrum allocation policies. For example, in UK, radio bands allocated for 2G, 3G and 4G services are fixed (Fig. 1.2). Such fixed spectrum allocations make it difficult to release additional radio spectrum to meet the dramatic growth, predicted to be over 10-fold in the mobile data traffic. Therefore, higher frequencies such as 30 GHz-300 GHz (millimetre wave) are being considered for next generation wireless systems. But their feasibility for large scale mobile wireless networks is contingent upon many technical challenges [5].

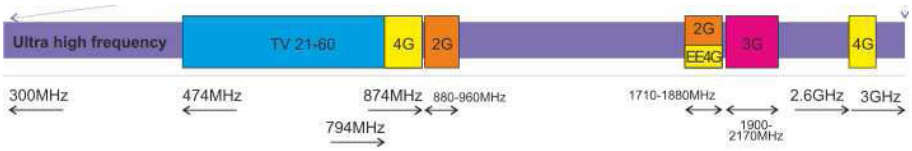

Figure 1.2: Spectrum Allocation in the UK [1]

On the second question, it has been reported that many of the currently allocated spectrum chunks are under-utilized. This may be partly due to the current exclusive-use-only spectrum access policies [6]. The sparse utilization of the licensed spectrum has been shown in the Federal Communications Commission (FCC) experiments [7], e.g., less than 25% licensed spectrum is in heavy use (Fig. 1.3).

Therefore, congestion and under-utilization of spectrum are the critical challenges. As a remedy, cognitive radio provides intelligent spectrum access policies to allow the unlicensed users to coexist with licensed users. A brief discussion of cognitive radio is provided next.

1.1.1 Cognitive Radio

Cognitive radio includes a hierarchical access model [8]. In such a model, the primary nodes, e.g. the existing network infrastructure, have the highest priority

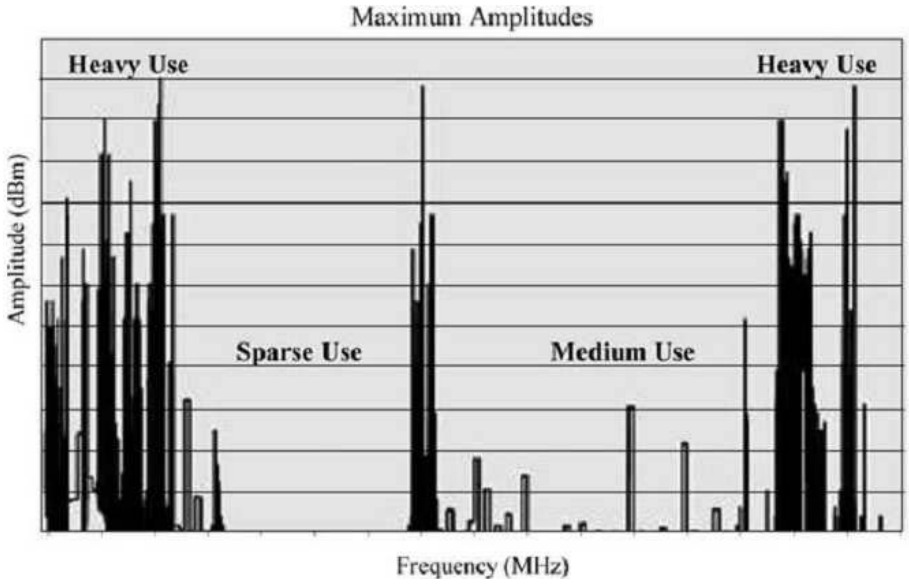

Figure 1.3: Spectrum Utilization [2]

any-time access to the spectrum, which is compatible with the current licensing-based spectrum access policy [6]. However, to reduce spectrum congestion and to mitigate spectrum under-utilization, secondary nodes, who have no spectrum allocated to them for their exclusively use, are allowed to access the spectrum as long as the interference power levels received at primary nodes are under some threshold, known as interference temperature limit [8]. This limit is the maximum interference power that a primary receiver can accept.

Fig. 1.4 shows an example of a cognitive radio network architecture, where both secondary and primary networks share the licensed radio spectrum. In the secondary network, the secondary base station (SBS) communicates with the secondary user (SU), while in the primary network, the primary base station (PBS) communicates with the primary user (PU). In this network, both primary and secondary signals may overlap in time/frequency slots (Fig. 1.5). Thus, the coexistence of both primary and secondary networks gives rise to the bi-directional interferences issues, e.g., the P2S interference (I_{P2S}) and S2P interference (I_{S2P}), where the later one (I_{S2P}) must be properly controlled under the interference temperature limit to protect the primary communication. Depending on the interference tolerance of the primary nodes, secondary networks can use one of the three modes: (1) interweave,

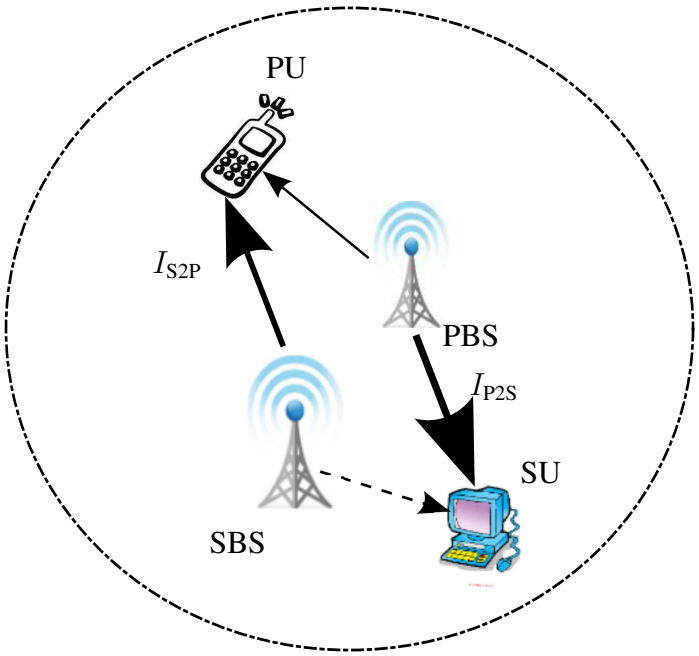

Figure 1.4: Co-existence of Primary and Secondary Networks

(2) overlay, and (3) underlay (see Section 2.1.6), to access the licensed spectrum. The underlay mode is the main focus of this thesis. However, the beamforming algorithms developed in this research may also be adapted for the interweave and overlay modes.

Standardization and Applications of Cognitive Radio

The concept of cognitive radio is officially defined in the IEEE 1900.1 Standard [9]. Its first implementation is in the IEEE 802.22 Standard [10], where the Physical and Medium Access Control layers are developed for cognitive radio based Wireless Regional Area Networks (WRANs) to operate in the television (TV) broadcast bands without causing interference to TV receivers [11, 12]. The reuse of TV bands for cognitive radio is also enabled in the ECMA 392 [13] standard, which is the first international standard enabling portable devices to operate in TV band [14].

Other applications of cognitive radio include smart grid networks, public safety networks and cellular networks. In smart grid networks, IEEE 802.15.4g [14] and IEEE 802.11af [15] cognitive radio standards address the distance limitation in the conventional power line communications. In public safety networks, the National

Broadband Plan considers cognitive radio to increase the reliability and data rate [16]. This plan also suggested that TV bands may become available to cellular operators.

Interference Issues with Underlay Mode

The cognitive radio mode investigated in this thesis is the underlay mode, where secondary nodes may transmit simultaneously with primary nodes as long as the interference on the primary nodes is under the interference temperature limit. This limit is the maximum amount of interference that a primary receiver can tolerate [8].

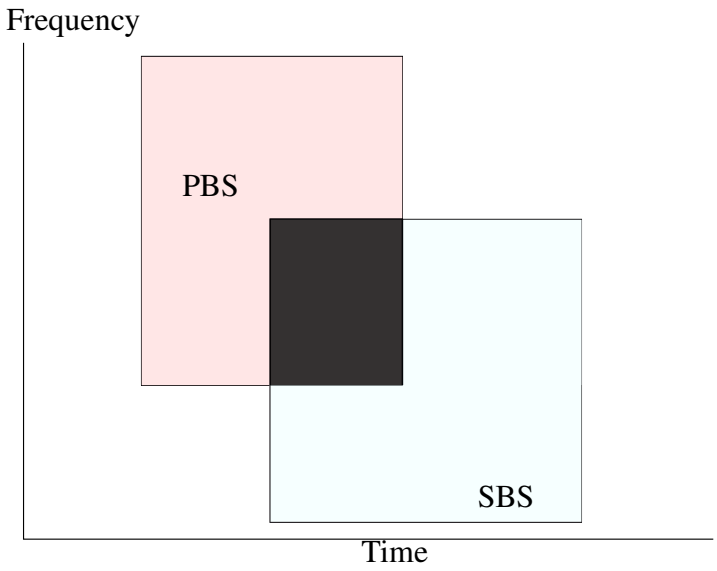

Figure 1.5: Transmissions of Primary and Underlay Secondary Base Stations

An example of the underlay mode is shown in Fig. 1.5, where the transmissions of a PBS and an underlay SBS overlap in both time and frequency domain (dark area). This overlap gives rise to the mutual interferences between primary and secondary networks. Moreover, because the S2P interference must be kept below the interference temperature limit, the secondary transmit power is constrained. This constraint may limit the coverage area of the secondary network. On the other hand, the P2S interference will decrease the received single-to-interference-and-noise ratio (SINR), which is critical for the secondary receiver to recover the secondary transmitter's signal. Both the constrained secondary transmit power and decreased

received SINR will result in secondary capacity loss (see Section 2.1.6 for discussion) and reduced secondary communication range, and thus must be addressed.

1.1.2 Beamforming

Beamforming [17], also known as spatial filtering, is a potential solution to manage the interference problems. It exploits space diversity to constructively combine desired signals while reducing interference and noise. Therefore, the achievable received SINR and thus the data rate can be improved in a fading and interference wireless environment. Due to these benefits, beamforming has been developed for the wireless local area network (WLAN) (IEEE 802.11ad [18]) standards, the LTE cellular communication standards [19], the multiple-input multiple-output (MIMO) based 4G networks [20, 21], and also being investigated for the 5G wireless networks [22].

1.1.3 Relays

Although beamforming mitigates interferences, it dose not necessarily improve the coverage area of the secondary networks, which is limited because of the constraint on the transmit power of secondary nodes in order to comply with the interference temperature limit. However, the coverage may be enlarged by introducing relay nodes, which use the broadcast nature of the wireless channels to exploit space and user cooperative diversities [23–25] and hence improve the reliability and coverage of the traditional point-to-point communications. Therefore, they have also been included in the WLAN (IEEE 802.11ad [18]) standards, the LTE cellular communication standards [19, 26], the MIMO based 4G networks [20, 21], and also being investigated for the 5G wireless networks [22].

1.2 Motivation, Objectives and Significance

Motivation: As mentioned before, the extraordinary wireless data traffic growth (Fig. 1.1) and the spectrum under-utilization (Fig. 1.3) require intelligent spectrum access policies. Both problems are mitigated by the use of the underlay mode to

share the spectrum. Thus, wide scale deployment of underlay secondary networks has the potential to reduce spectrum congestion and under-utilization. However, there are many open research problems that arise mainly due to the co-existence of primary and secondary networks. In particular, due to their simultaneous transmissions, both bi-directional (P2S and S2P) interference signals will limit the coverage range and reliability of underlay secondary networks. Therefore, successfully addressing these interference issues will increase the secondary coverage and improve the reliability. Then, the use of secondary networks can be increased to serve the expected wireless growth in the coming decades.

Objectives: To address the interference issues and thus to enhance the coverage, reliability and capacity, this thesis integrates two-way relaying and beamforming with an underlay network. The main objectives of this thesis include:

1. To characterize the performance of low-complexity sub-optimal beamforming algorithms. In particular, the outage performance of zero-forcing beamforming and maximal-ratio transmission/reception (ZFB-MRT/MRC) at multi-antenna underlay terminals is analysed. Although both outage probability and symbol error probability are common performance measures, outage probability is selected here because it characterizes the probability of the data loss and deep fading in wireless links [27], and is independent of signal modulation techniques (see Section 2.1.2). On the other hand, zero-forcing is necessarily sub-optimal because the interference temperature limit is not exploited. That is, the zero-forcing beamforming coefficients are computed to make the secondary-terminal-to-primary interference (I_{S2P}) identical to zero. However, in fact, the primary receiver can tolerate $I_{S2P} \leq I_{th}$, where I_{th} is the interference temperature limit. But, outage analysis of zero-forcing demonstrates the effectiveness of this type of beamforming in addressing the bi-directional interferences and thus improving the reliability of underlay two-way relay networks.

2. To develop optimal transmitter/receiver beamforming algorithms for multiple antenna underlay terminals. As mentioned before, the ZFB-MRT/MRC algo-

rithm is sub-optimal and thus its capability in improving the reliability is limited because it does not utilize the fact that the primary nodes have some interference tolerance (interference temperature limit). Exploiting this fact provides us with more degrees of freedom in deriving the beamforming vectors. Therefore, optimal transmitter/receiver beamforming algorithms are required to exploit the interference temperature limit and thus to improve the reliability of underlay two-way relay networks.

3. To develop optimal distributed beamforming algorithms for cooperative single antenna underlay relays. Although optimal transmitter/receiver beamforming will be investigated for multi-antenna terminals, equipping multiple antennas in wireless devices are sometimes difficult due to the size and the cost constraints [28, 29]. Alternatively, multiple spatially-separated cooperative single-antenna relays can act as a distributed beamformer. Therefore, optimal distributed beamforming algorithms are required in such a context to mitigate the bi-directional interferences and to improve the reliability and capacity.

Significance: Although several cognitive wireless standards, such as IEEE 802.22, ECMA 392, IEEE 802.15.4g and IEEE 802.11af, have been developed, they all reuse the vacant TV bands via the interweave mode [12]. Alternatively, the use of the underlay mode has been suggested [30] because it can reuse not only vacant radio bands, but also some occupied radio bands. Thus, it has more potential in relieving the spectrum congestion and spectrum under-utilization. Currently, it achieves short-range high data rate with extremely low transmit power in ultra wideband systems [6, 31]. But those systems are not suitable for communications over large areas such as a cellular network. Therefore, integrating beamforming and relaying with underlay cognitive networks is currently receiving significant research interest [32–70]. Thus, the proposed transmitter/receiver and relay design in this thesis could significantly contribute to the realization of underlay networks to relieve spectrum congestion and under-utilization.

1.3 Thesis Outline and Contributions

Outline: Chapter 2 introduces the related basic concepts, techniques, and related previous researches. Chapters 3 to 5 present the three major contributions of this thesis. Chapter 6 provides conclusions and future research directions.

Contributions: This thesis investigates beamforming and relaying in underlay networks to address the bi-directional (S2P and P2S) interference issues and thus to improve the system performance, focusing on two amplify-and-forward (AF) relay configurations: (1) multi-antenna terminals and one single-antenna two-way relay; and (2) single-antenna terminals and $K \geq 1$ single-antenna two-way relays. Specific contributions are listed as follows.

- The outage probabilities of sub-optimal beamforming algorithms are derived [71] (Chapter 3). Specifically, mathematically tractable end-to-end (E2E) SINRs are formulated based on a fixed-gain relay, and thereby the closed-form exact and asymptotic high transmit power and interference temperature limit region E2E outage probabilities are derived considering both path loss and small-scale fading effects, when ZFB-MRT/MRC are employed at the two terminals. It has been found that only the location of the relay significantly impacts the outage. And as the secondary transmit power $P_s \to \infty$, a diversity of order zero or $(\min(M_1, M_2) - 1)$, where M_j $(j = 1, 2)$ is the number of antennas at the two secondary terminals, respectively, is achieved if the interference temperature limit I_{th} is finite or if the ratio $\frac{I_{th}}{P_s}$ is a constant. Besides, simulation results show that beamforming is effective in addressing the bi-directional interference issues in underlay two-way relay networks and improving the reliability. This promotes us to investigate the optimization of beamforming vectors and power allocations in Chapters 4 and 5.

- Transmitter/receiver designs are developed for the first configuration to improve the reliability assuming perfect knowledge of the channel gains [72] (Chapter 4). Specifically, the optimal receiving (Rx) beamforming vectors are derived first in closed-form and proven to be independent of the transmit powers and transmitting (Tx) beamforming vectors. Then the optimal and

low-complexity sub-optimal Tx beamforming vectors and transmit powers are developed, which can improve the achievable SINR by as much as 20 dB.

- Joint transmitter and relay designs are developed for the second configurataion to improve the reliability assuming partial knowledge of the channel gains [73] (Chapter 5). Specifically, the optimal relay gain and transmitter powers are developed through numerical computations when there is only one relay. Since in this case, no beamforming is performed, the phase distortion in the signal introduced by the complex channel gain is not explored. Therefore, the achievable SINR is very limited, e.g., lower than 0 dB regardless of the interference temperature limit. Then, for $K > 1$ relays, the optimal and low-complexity sub-optimal transmitter powers and relay gains, which form the distributed beamforming vector, are developed. And simulation results show that they can improve the achievable SINR by 10 dB or more.

Overall, the thesis results demonstrate how beamforming and relaying address the bi-directional interference problems in underlay secondary networks and thus pave the way to improve the performance of secondary networks.

$\sim$

Chapter 2

Background

The first part of this chapter reviews wireless channels, outage probability, multiple antenna networks, beamforming algorithms, relay networks and cognitive modes. The second part reviews algorithmic complexity, interior-point algorithms and semi-definite relaxation (SDR).

2.1 Wireless communications

Wireless communications use electromagnetic signals for transmission of data, voice, video and other information. Most critical technical challenges of wireless communications are:

1. Multi-path propagation (i.e. multiple radio signals reaches the receiving antenna through multiple paths due to reflections, refractions, and other effects);

2. Spectrum limitations (wireless bandwidth is limited, as discussed in Section 1.1);

3. Energy limitations (portable handsets are battery operated).

The above challenges are the classical ones where only primary networks exist. The context in this thesis is somewhat different and includes the co-existence of primary and secondary networks. Thus, interference issues dominate the overall network reliability and design.

Before dealing with these interference issues, we introduce background material on wireless channels, outage probability, multiple antenna networks, beamforming,

relay networks and cognitive modes.

2.1.1 Wireless Channels

Wireless channels refer to the medium between the transmitter and the receiver, which introduce random variations in both the amplitude and phase of the transmitted signal. The fundamental effects of wireless channels include large-scale fading and small-scale fading [74]. These effects are modelled as a complex channel coefficient/gain $h \in \mathbb{C}$. The knowledge of h is referred to as channel state information (CSI). With this channel gain h, the baseband received signal, without including interference signals, is typically represented as,

$$y = hs + w, \tag{2.1}$$

where $s \in \mathbb{C}$ is the transmitted signal, and $w \in \mathbb{C}$ is the additive white Gaussian noise (AWGN). AWGN is an additive thermal noise, which has uniform power across the frequency band.

The large-scale and small-scale fading effects are embodied in the average of the inverse power ($\mathbb{E}\left\{\frac{1}{|h|^2}\right\}$) over larger time scales (seconds) and the instantaneous envelop ($|h|$) over small time scales (milliseconds) of the complex channel gain h in (2.1) [74].

Large-scale Fading and Small-scale Fading

Large-scale fading, including path loss and shadowing, causes slow signal changes in outdoor environments. While path loss refers to the signal power attenuation due to the increase in the distance between the transmitter and receiver, shadowing is the power attenuation due to the obstacles interposed between the transmitter and receiver, which is modelled by a random variable superposed on the path loss model. If the AWGN component in (2.1) is neglected, then the large-scale fading effect including both path loss and shadowing, or equivalently the average of the inverse power ($\mathbb{E}\left\{\frac{1}{|h|^2}\right\}$) over larger time scales (seconds) can be modelled by the log-distance model (2.2) [74].

$$\mathbb{E}\left\{\frac{1}{|h|^2}\right\}_{\mathrm{dB}} = L_{\mathrm{dB}} = \left(\frac{P_T}{P_R}\right)_{\mathrm{dB}} = L(d_0)_{\mathrm{dB}} + 10n\log_{10}\left(\frac{d}{d_0}\right) + X, \tag{2.2}$$

where L is the loss of the average received power ($P_R = \mathbb{E}\{|y|^2\}$), for a given transmitted power ($P_T = \mathbb{E}\{|x|^2\}$), d_0 is the reference distance, n is the path loss exponent, $L(d_0)_{\mathrm{dB}}$ is the path loss at the reference distance, and $X \sim \mathcal{N}(0, \sigma_X^2)$ is the shadowing random variable, both X and σ_X are in decibel scale. Note that, the sum of the first two terms in (2.2) is the path loss effect, which is the average of the power loss, or equivalently $\mathbb{E}\left\{\frac{1}{|h|^2}\right\}$, over all times and thus is only related to the distance between the transmitter and receiver.

In contrast to large-scale fading, small-scale fading refers to changes in the signal due to reflections and scatters in indoor, macrocellular and microcellular outdoor environments. These reflections and scatters result in multiple copies of the transmitted signal arriving at the receiver. Those copies may interfere constructively or destructively, which results in the distortion in both amplitude and phase in the received signal. Commonly used statistical models to characterize such fadings include Rayleigh and Rician models. The Rayleigh fading model is suitable for channels without a dominant line-of-sight component. Here, the real and imaginary parts of the complex channel gain h in (2.1) has independent Gaussian distribution with zero mean and equal variance. And its envelope $|h|$ follows the Rayleigh distribution with the probability density function (PDF) given by [75],

$$f_{|h|}(x) = \frac{2x}{\Omega} e^{-\frac{x^2}{\Omega}},\ 0 \le x \le \infty, \tag{2.3}$$

where Ω is the average envelop power. The Rician fading model fits well when there exists a dominant line-of-sight component. In this case, the real and imaginary parts of the complex channel gain h in (2.1) are independent $\mathcal{N}(a, b)$-distributed. Then, its envelope $|h|$ has the Rician distribution with the PDF given by [75],

$$f_{|h|}(x) = \frac{x}{b} e^{-\frac{x^2+2a^2}{2b}} I_0\left(\frac{\sqrt{2}ax}{b}\right),\ 0 \le x \le \infty, \tag{2.4}$$

where $I_0(\cdot)$ is the modified Bessel function of the first kind [148, Eq. (8.406.3)].

Channel Estimation

Since wireless channel introduces random variations to the transmitted signal, the CSI, e.g., h in (2.1), is often required to recover the desired signal at the receiver. This can be obtained through channel estimation processes, such as pilot-based channel estimation [76–83]. In pilot-based channel estimation, transmitter inserts pilots, which are pre-designed known symbols, into specific time and frequency locations of the signal. The receiver uses the pilot symbols to extract CSI via various estimators, such as maximum likelihood (ML) estimator [80] and minimum-mean-square-error (MMSE) estimator [81–83].

2.1.2 Outage Probability

As a result of the channel fading effect, the received signal may fall below certain threshold required for satisfactory performance. This event is called outage. Therefore, outage probability is a popular performance measure of wireless communications [25, 84–93]. To determine the outage probability, the received signal model, which includes the desired signal, interference and noise, must be considered. and can be generically represented as,

$$y(t) = hx(t) + h_1 s(t) + \omega(t) \tag{2.5}$$

where $h = \beta e^{j\phi}$ and $h_1 = \beta_1 e^{j\phi_1}$ are the complex fading channel gains, $x(t)$ and $s(t)$ are the desired and interference signals, respectively, and $\omega(t)$ is the zero-mean AWGN with power N_0. Based on this model, the instantaneous SINR (γ) is defined as,

$$\gamma = \frac{|\beta|^2 P_s}{|\beta_1|^2 P_i + N_0}. \tag{2.6}$$

where $P_s \triangleq |x(t)|^2$ and $P_i \triangleq |s(t)|^2$. When the SINR (γ) is below a predefined threshold (γ_{th}), the system is said to be in outage [94]. Therefore, the outage probability is defined as,

$$P_{out} = \Pr[\gamma \leq \gamma_{th}] = \int_0^{\gamma_{th}} p(\gamma) \mathrm{d}\gamma, \tag{2.7}$$

where $p(\gamma)$ is the PDF of the received SINR (γ).

Beside outage probability, other performance measures for wireless communications include Shannon capacity (also known as ergodic capacity) and average symbol error probability. Shannon capacity (C) gives the maximum data rate that can be transmitted over the channel with any arbitrarily small error probability, while given a modulation technique, average symbol error probability is the probability that a symbol of data is received with error averaged over the distribution of the received SINR [27]. Then, the Shannon capacity (C) and the average symbol error probability ($\bar{P}_s$) for the signal model (2.5) are calculated as [27],

$$C = \int_0^\infty B \log_2(1+\gamma) p(\gamma) \mathrm{d}\gamma, \tag{2.8}$$

$$\bar{P}_s = \int_0^\infty P_s(\gamma) p(\gamma) \mathrm{d}\gamma, \tag{2.9}$$

where B is the bandwidth, and $P_s(\gamma)$ is the symbol error probability in AWGN with SINR γ.

From (2.7), (2.8) and (2.9), it is clear that all these performance measures require the PDF of the received SINR. And outage probability is selected in the thesis because:

1. It characterizes the probability of data loss in fading channels [27];

2. It is only related to the distribution of the received SINR, and is independent of the modulation techniques and the bandwidth.

2.1.3 Multiple Antenna Networks

Multiple antenna networks consist of nodes that use multiple antennas for transmission and/or reception. An example of a multiple antenna link in a flat-fading channel is shown in Fig. 2.1, where the transmitter is equipped with $m \geq 1$ antennas and the receiver is equipped with $n \geq 1$ antennas. Then, the received signal vector $\boldsymbol{y} \in \mathbb{C}^{n\times 1}$ is given as,

$$\boldsymbol{y} = \boldsymbol{H}\boldsymbol{x} + \boldsymbol{w}, \tag{2.10}$$

where $\boldsymbol{x} \in \mathbb{C}^{m\times 1}$ is the transmitted signal vector, $\boldsymbol{H} \in \mathbb{C}^{n\times m}$ denotes the Rayleigh fading channel matrix with independent and identically distributed (i.i.d) elements

$h_{ij} \sim \mathcal{CN}(0,\,1)$ $(i = 1, 2, ..., n;\;\; j = 1, 2, ..., m)$, where $\mathcal{CN}(0,\,1)$ is the complex Gaussian distribution with zero mean and unit variance, and $\boldsymbol{w} \in \mathbb{C}^{n\times 1}$ is the AWGN vector with i.i.d $\mathcal{CN}(0,\,\sigma^2)$ distributed elements.

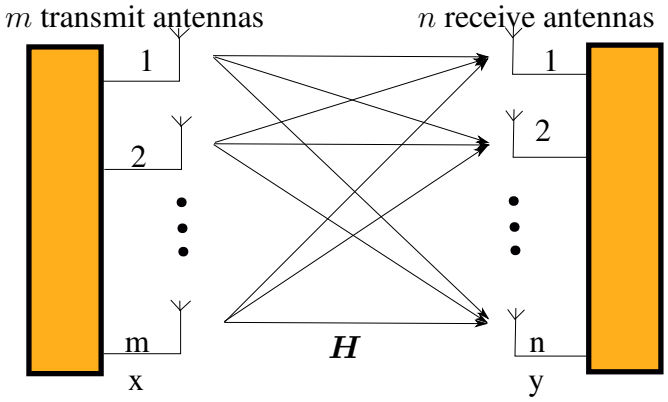

Figure 2.1: Multiple-Input Multiple-Output (MIMO) Link

Since multiple antenna nodes can transmit a symbol vector $\boldsymbol{x}$ (2.10), instead of one single symbol at a time, $\boldsymbol{x}$ can be appropriately designed to mitigate wireless channel impairments and resource constraints, thereby achieving spatial diversity gain, spatial multiplexing gain and interference reduction [95].

- Spatial diversity gain is achieved by transmitting a single data stream over multiple MIMO links, resulting in several observations of the same transmitted signal at the receiver. Appropriately combining these multiple observations may result in improved reliability.

- Spatial multiplexing refers to splitting a high-rate data signal into multiple independent low-rate streams and then transmitting each stream from a different transmit antenna. By doing this, the wireless data rate at higher signal-to-noise ratios (SNRs) is improved. This increase is called the spatial multiplexing gain. Accordingly, the channel capacity (C) for the system shown in Fig. 2.1 is proportional to the smaller number of transmit antennas and receive antennas, $C = \min(m, n) \log_2 \text{SNR}$ bits/s/Hz, if a linear receiver is used [96]. In this case, the spatial multiplexing gain is $\min(m, n)$.

- Interference reduction is achieved by exploiting the spatial dimensions to separate signals for different nodes sharing time and frequency resources, and results in improved reliability. One potential solution to interference reduction is beamforming.

2.1.4 Beamforming Algorithms

Originally, beamforming involved changing the antenna directions physically to radiate or receive greater energy in a target direction while attenuating energy in other directions [17, 97]. In those earliest beamforming, the antenna dish and feed operate as a spatial integrator [17] to form a "beam", where the frontal energy of the antenna is constructively summed while the energy from other directions are destructively added.

Currently, with the development of smart antennas [98], signal processing (or beamforming) algorithms are used to create the desired gain pattern while keeping antennas fixed. These algorithms generate a set of coefficients (called beamforming vector) to weigh the signal samples before transmission or after reception. Such linear or non-linear beamforming algorithms can thus be employed at multi-antenna nodes during transmitting or receiving (Figs. 2.2 and 2.3).

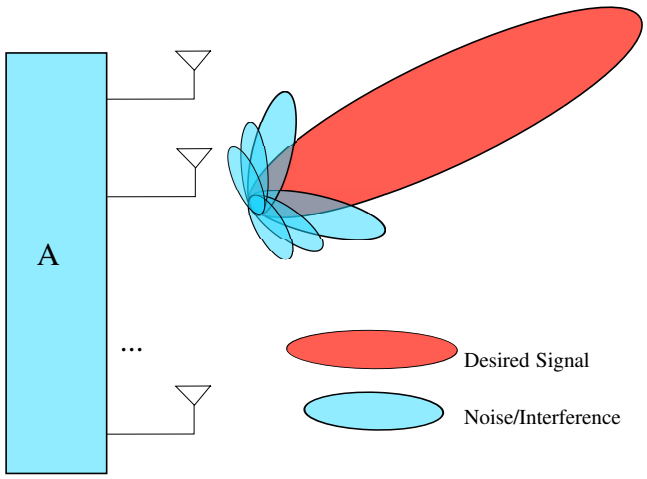

Figure 2.2: Tx Beamforming

In Fig. 2.2, the transmitter A, equipped with $m > 1$ antennas, uses Tx beamforming to transmit a signal vector $\boldsymbol{x} \in \mathbb{C}^{m\times 1}$ through channel $\boldsymbol{H} \in \mathbb{C}^{n\times m}$. With

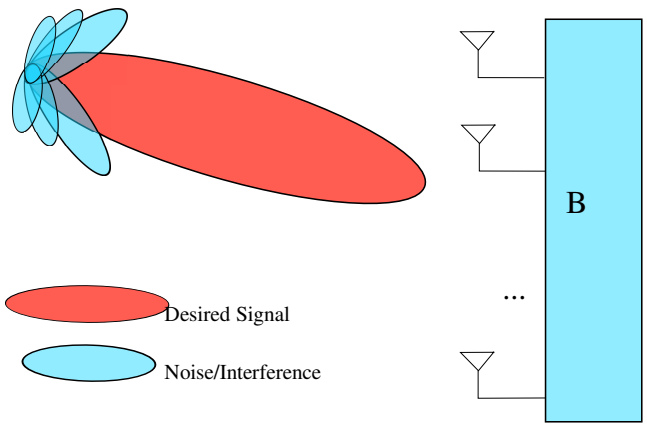

Figure 2.3: Rx Beamforming

linear Tx beamforming, the signal $\boldsymbol{y}$ received at the destination is given as,

$$\boldsymbol{y} = \boldsymbol{H}\boldsymbol{B}_{tx}\boldsymbol{x} + \boldsymbol{n}, \tag{2.11}$$

where $\boldsymbol{B}_{tx} \in \mathbb{C}^{m\times m}$ is the Tx beamforming matrix, and $\boldsymbol{n} \in \mathbb{C}^{n\times 1}$ is the AWGN vector.

In Fig. 2.3, the receiver B applies Rx beamforming to its received signal $\boldsymbol{y} \in \mathbb{C}^{n\times 1}$ to recover the desired signal $\boldsymbol{x} \in \mathbb{C}^{m\times 1}$. The resulting signal $\hat{\boldsymbol{y}}$ is given as,

$$\hat{\boldsymbol{y}} = \boldsymbol{B}_{rx}(\boldsymbol{H}\boldsymbol{x} + \boldsymbol{n}), \tag{2.12}$$

where $\boldsymbol{B}_{rx} \in \mathbb{C}^{m\times n}$ is the Rx beamforming matrix, $\boldsymbol{H} \in \mathbb{C}^{n\times m}$ and $\boldsymbol{n} \in \mathbb{C}^{n\times 1}$ are the complex channel matrix and the AWGN vector, respectively.

Both matrices $\boldsymbol{B}_{tx}$ and $\boldsymbol{B}_{rx}$ can be generated via different beamforming algorithms. Given the availability of CSI, zero-forcing beamforming (ZFB), maximal-ratio combining/transmission (MRC/MRT), and combined ZFB and MRC/MRT (ZFB-MRC/MRT) are of great interest and popular due to their simplicity in implementation.

Zero-forcing beamforming (ZFB)

When done at the transmitter, ZFB is also known as channel inversion [99, 100], and the beamforming matrix $\boldsymbol{B}_{tx}$ in (2.11) is given as [75],

$$\boldsymbol{B}_{tx} = \alpha\boldsymbol{H}^H(\boldsymbol{H}\boldsymbol{H}^H)^{-1}, \tag{2.13}$$

where α is a scale factor to satisfy the power constraint.

Accordingly, when applied at the receiver side, $\boldsymbol{B}_{rx}$ is given as,

$$\boldsymbol{B}_{rx} = (\boldsymbol{H}^H \boldsymbol{H})^{-1} \boldsymbol{H}^H. \tag{2.14}$$

While conventional ZFB ((2.13) and (2.14)) eliminates only the interference signals, to further mitigate the background noise, regularized zero-forcing beamforming was developed in [99,100]. And the corresponding Tx beamforming matrix $\boldsymbol{B}_{tx}$ is calculated as [74],

$$\boldsymbol{B}_{tx} = \alpha \boldsymbol{H}^H (\boldsymbol{H}\boldsymbol{H}^H + \beta \boldsymbol{I})^{-1}, \tag{2.15}$$

where α is a scale factor to satisfy the power constraint, and β is the regularizing factor determined by both the transmit power and noise power.

Maximal-ratio combining/transmission (MRC/MRT)

MRC/MRT are widely investigated in MIMO systems [47, 91, 101–110] because it can maximize the received signal-to-noise ratio (SNR) [75, 111].

MRC, at the receiver side, is one of the most popular diversity-combining methods, where multiple received signals are weighted and linearly combined to maximize the SNR [75]. It computes the Rx beamforming matrix $\boldsymbol{B}_{rx}$ as,

$$\boldsymbol{B}_{rx} = \boldsymbol{H}^H. \tag{2.16}$$

Similar to MRC, the transmitter can weigh different signal components to precancel the effect of the wireless channel and thus to maximize the received SNR [111]. This is known as MRT, and the Tx beamforming matrix $\boldsymbol{B}_{tx}$ is given as,

$$\boldsymbol{B}_{tx} = \boldsymbol{H}^H. \tag{2.17}$$

ZFB and MRT/MRC (ZFB-MRT/MRC)

Combined ZFB and MRC (ZFB-MRC) is often used at the receiver in interference MIMO scenarios (Fig. 2.4) because it is capable of mitigating the interference signals while maximizing the desired signal power. An example of such a network is shown in Fig. 2.4, where there is a N_A-antenna transmitter A sending message to

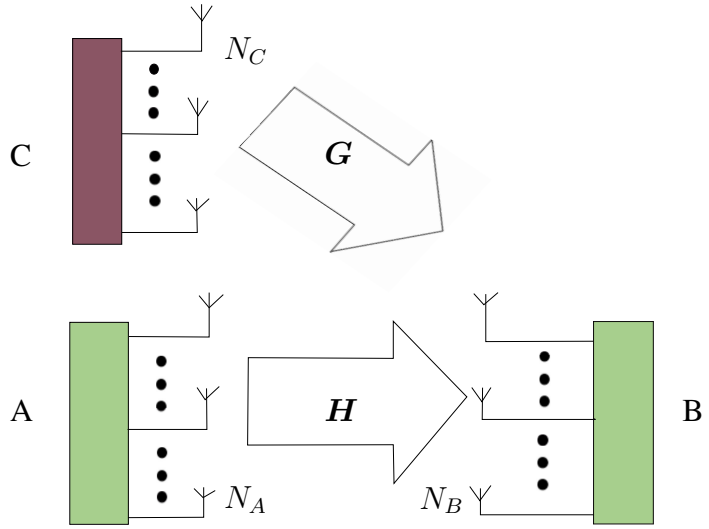

Figure 2.4: MIMO Network with Interference

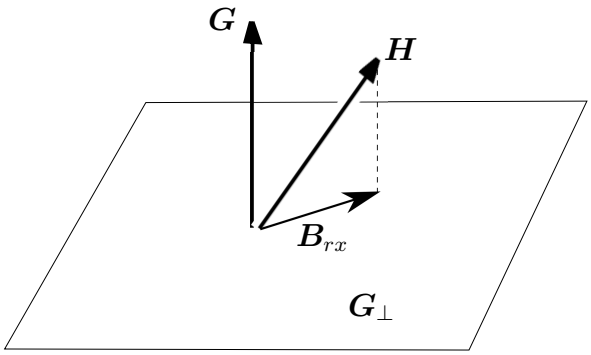

Figure 2.5: Explanation of ZFB-MRC

the N_B-antenna receiver B through the flat fading MIMO channel $\boldsymbol{H} \in \mathbb{C}^{N_B \times N_A}$. Concurrently, the interference generated by an N_C-antenna transmitter C is received at B via the flat fading MIMO channel $\boldsymbol{G} \in \mathbb{C}^{N_B \times N_C}$.

In such a system, the receiver B can apply ZFB-MRC to nullify the interference from C and to maximize the signal power from A. To achieve these dual goals, the Rx beamforming matrix should be chosen as the projection of the signal channel $\boldsymbol{H}$ to the subspace $\boldsymbol{G}_{\perp}$, which is orthogonal to the interference channel $\boldsymbol{G}$ [112, 113], as shown in Fig. 2.5. Therefore, the Rx beamforming matrix $\boldsymbol{B}_{rx}$ is calculated via,

$$\boldsymbol{B}_{rx} = \boldsymbol{G}_{\perp}\boldsymbol{H}^{H}. \tag{2.18}$$

Similar processes can be applied at the transmitter to nullify interference signals to other users while maximizing the signal power at the target user. This is called

ZFB-MRT and its corresponding Tx beamforming matrix is selected as,

$$\boldsymbol{B}_{tx} = \boldsymbol{H}^H \boldsymbol{G}_\perp, \tag{2.19}$$

where $\boldsymbol{H}$ is the matrix of the channels to the target user and $\boldsymbol{G}$ is the interference channel matrix.

Since ZFB-MRT/MRC can nullify the interferences and also maximize the desired signal power, they are employed at the two multi-antenna secondary terminals in our study (Chapters 3 and 4) as sub-optimal beamforming algorithms.

Distributed Beamforming

While the preceding beamforming algorithms are often applied at co-located multiple antennas in a single node, distributed beamforming is applied at spatially separated single-antenna nodes, e.g., a set of $K > 1$ single-antenna relays act as a distributed beamformer.

Consider a one-way multi-relay network, as shown in Fig. 2.6, consisting of one source A, one destination B, and multiple AF relays. All the nodes are equipped with one single-antenna. Let $\boldsymbol{h}_s \in \mathbb{C}^{K\times 1}$ and $\boldsymbol{h}_d \in \mathbb{C}^{1\times K}$ be the flat fading channel vectors, with the ith element denoting the complex channel gain from the source A to the ith ($i = 1, 2, ..., K$) relay and from the ith ($i = 1, 2, ..., K$) relay to the destination B, respectively. Usually, the ith relay can obtain h_{s_i} and h_{d_i} through channel estimation processes [80–83].

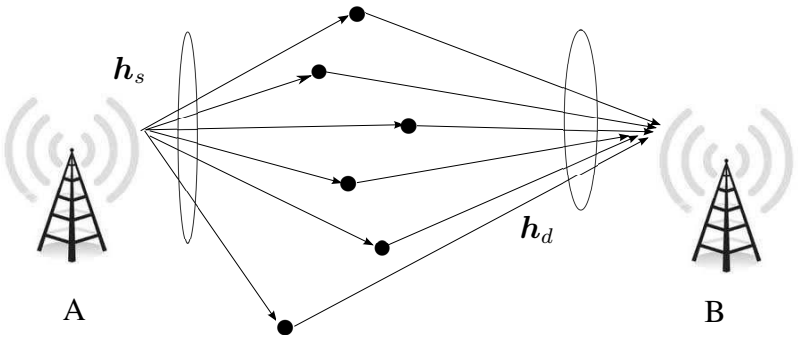

Figure 2.6: One-Way Multi-Relay Network

In such a network, signal transmission from A to B requires two consecutive time slots: (1) A broadcasts to relays in the first slot, and (2) every relay multiplies

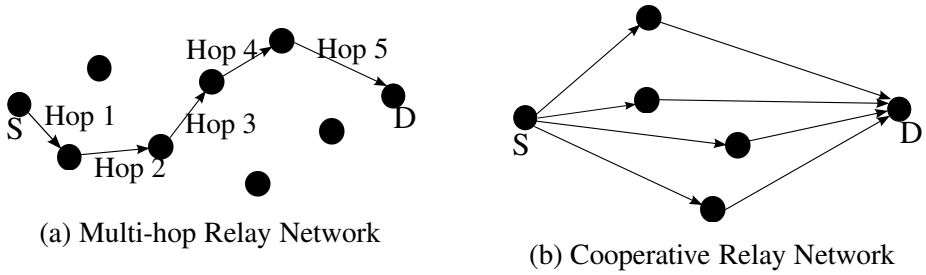

(a) Multi-hop Relay Network

(b) Cooperative Relay Network

Figure 2.7: Relay Networks

its received signal with a relay gain $\omega_i \in \mathbb{C}$ ($i = 1, 2, ..., K$) and forwards the resultant to the destination B simultaneously in the second slot. Although each relay is equipped with only one antenna, all the antennas together form a virtual antenna array. Therefore, the set of gains ω_i ($i = 1, 2, ..., K$) are the beamforming coefficients. If the relays can communicate CSI (h_{s_i} and h_{d_i}) and their received signals to each other, preceding beamforming algorithms can be applied here. Otherwise, distributed beamforming is employed with the optimum ω_i ($i = 1, 2, ..., K$) given as, [74]

$$\omega_i = \beta \frac{h_{s_i}^* h_{d_i}^*}{1 + P_s|h_{s_i}|^2 + P_i|h_{d_i}|^2}, \tag{2.20}$$

where P_s and P_i are the transmit power of the source and the ith relay, respectively, and β is a scale factor to fulfil the power constraint. Such distributed beamforming in this spatially-separated relays are studied in Chapter 5, where the underlay network is a peer-to-peer network (see Section 5.2).

2.1.5 Relay Networks

Although beamforming can mitigate interference, it might not be capable of enlarging the coverage due to the restrictions on the transmit power of secondary nodes. A solution is to use intermediate nodes (relays) to forward the signal hop-by-hop. The basic relay configuration consists of a source node (S), a destination node (D), and one or several intermediate nodes (relays). Direct S to D transmissions may not be possible because: (1) the S-D distance is greater than the transmission range, (2) fading and shadowing in the S-D link is excessive. In this context, two types of relaying may be used.

1. Multi-hop Relaying (Fig. 2.7(a)), where the message is forwarded by a set of

relays hop-by-hop to enlarge the communication coverage area.

2. Cooperative Relaying (Fig. 2.7(b)), where the message from S is repeated by multiple relays simultaneously and D receives multiple copies of the message.

In both types, relay nodes process their received signal from the previous hop and forward the resultant to the next hop. Two widely used relaying algorithms are Amplify-and-Forward (AF) relaying and Decode-and-Forward (DF) relaying [74].

AF v.s. DF

In Fig. 2.7(b), the received signal at a relay node is represented as,

$$r = h_{sr}x_s + n_r \tag{2.21}$$

where $x_s \in \mathbb{C}$ is the transmitted signal with $|x_s|^2 = P$, $n_r \in \mathbb{C}$ is the zero-mean AWGN with variance N_0, and $h_{sr} \in \mathbb{C}$ is the complex source-to-relay channel gain. This signal r will first be processed at the relay and then forwarded to the destination. To process the signal, various schemes are available, e.g., AF and DF [74].

- **Amplify-and-Forward**: the relay node only multiplies its received noisy signal r with a coefficient/gain β, which is chosen to comply with some constraint, such as the power constraint P_r. Therefore, the coefficient β is calculated from $\beta^2|r|^2 \leq P_r$, if the instant channel gain h_{sr} is known, and β is given by,

$$\beta = \sqrt{\frac{P_r}{P|h_{sr}|^2 + N_0}}, \tag{2.22}$$

  which is also called CSI-assisted gain [114]. But if the instant channel gain h_{sr} is not known and only the average power of the channel gain $\mathbb{E}\{|h_{sr}|^2\}$ is available, the relay gain β should be selected such that the average power $\beta^2\mathbb{E}\{|r|^2\}$ does not exceed P_r. Therefore, the relay gain is given as,

$$\beta = \sqrt{\frac{P_r}{P\mathbb{E}\{|h_{sr}|^2\} + N_0}}. \tag{2.23}$$

  In this case, the relay is called fixed-gain relay [115].

- **Decode-and-Forward**: the relay node decodes r and outputs $\hat{x}_s$, then re-encodes $\hat{x}_s$, and forwards the resultant to the destination. This decoding and re-encoding process can be denoted by $\mathcal{Q}(r)$, where $\mathcal{Q}(\bullet)$ denotes the decoding and re-encoding function.

Although AF relaying has the disadvantage of amplifying noise, it has the advantage of low processing complexity compared to DF relaying and also avoids error propagation to the destination. Therefore, this thesis is limited to AF relaying. However, the beamforming algorithms developed may be extended to DF cases.

One-Way v.s. Two-Way Relaying

Consider a relay network consisting of two transceivers (A and B) and one relay. All nodes work in the half-duplex mode, where the node can transmit and receive, but does only one of them at a time [116]. The use of half-duplex nodes however presents an inefficiency. Suppose A and B are not directly linked, but exchange information only through the relay (R). Therefore, this exchange requires four time slots for a one-way relay and only two time slots for a two-way relay (Fig. 2.8).

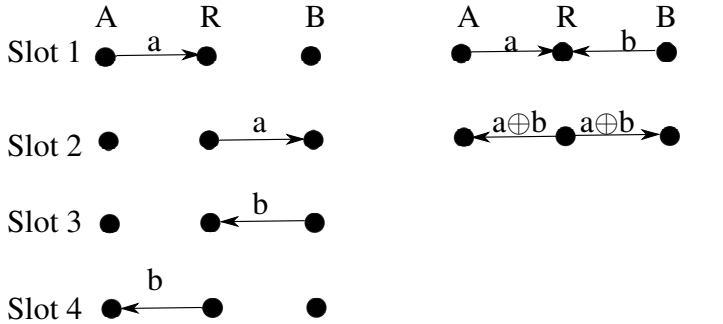

(a) One-Way Relay (b) Two-Way Relay

Figure 2.8: One-Way and Two-Way Relay Protocols

Thus, while the conventional one-way relay requires four time slots for mutual information exchange, direct exchange between two nodes A and B without a relay requires only two time slots. This increase in the transmission time (Fig. 2.8(a)) is referred to as a spectral efficiency loss. This loss arises due to the fact that the relay can only operate in the half-duplex mode.

One method to reduce this loss is to use full-duplex nodes, which can transmit and receive simultaneously [116]. These are not commercialized yet, but under research and development now [117]. Another way to compensate for this spectral efficiency loss is a two-way relay (Fig. 2.8(b)) [76], which requires only two time slots for mutual information exchange. This is achieved by using network coding, which works as follows. In the first time slot, A and B transmit simultaneously and the relay receives the combination of the messages from A and B. Then in the second time slot, the relay broadcasts this combination, and knowing CSI and the message sent by themselves, A and B can recover their desired message from the relayed signal [74]. In this case not only resources but also messages are shared between nodes.

In this thesis, we focus on a two-hop relay network to allow bi-directional information exchange (S$\rightarrow$D and D$\rightarrow$S) to exploit the spectral efficiency of two-way relays because it can provide nearly twice spectral efficiency as conventional one-way relay [76].

2.1.6 Cognitive Modes

As mentioned before, secondary nodes can access the licensed spectrum via one of the three modes: (1) interweave, (2) overlay, and (3) underlay. They are briefly described and compared next.

Interweave [74]

This mode allows secondary nodes to transmit only when primary nodes are not transmitting, which results in temporarily unused licensed spectrum bands. They are known as spectrum holes (if any). Those spectrum holes must be detected by secondary nodes, such as using the energy detection method [160]. Also, they must be ready to stop transmissions if a primary node resumes transmissions. Therefore, interweave mode implies that the primary receivers have zero interference tolerance, and no interference issues exist in this mode since secondary and primary nodes will not transmit simultaneously.

Overlay [74]

This mode requires secondary nodes to act as relays to assist primary's transmission. In return, they can transmit their own signals as long as the interference on primary receivers is under the interference temperature limit. Because secondary nodes must allocate some energy to relay primary signals, the energy left for their own transmission is reduced. Moreover, secondary nodes must adjust their transmit powers to comply with the interference temperature limit. Consequently, secondary capacity, coverage and reliability are affected.

Underlay [74]

In the underlay mode, secondary nodes are allowed to transmit simultaneously with primary nodes as long as its interference on primary receivers is under the interference temperature limit. To comply with this S2P interference constraint, channel gains between primary and secondary nodes are required, which can be obtained via some appropriate channel estimation processes [118, 119].

Compared with interweave and overlay, the underlay mode has the following advantages.

- Underlay nodes have lower operation complexity compared to overlay nodes because underlay nodes adjust their transmissions only to comply with the interference temperature limit, while overlay nodes must adjust their transmissions both to comply with the interference temperature limit and to cooperate with primary nodes;
- Underlay nodes have any-time access to the licensed spectrum because they can transmit even if primary nodes are transmitting.

To further quantify performance differences, we next compare the three modes in terms of capacity measured in bits/s/Hz under certain assumptions.

Comparison of cognitive modes

It has been shown that the underlay mode has a lower outage probability than the interweave mode, e.g., 10^{-2} and 10^{-1}, respectively, in [120], and can provide com-

parable data rates as the overlay mode, where the secondary node uses DF scheme to forward the primary information [121]. However, the underlay mode considered in [120] used a wide spectrum band, and a comparison of these three modes has not been done. Therefore, a quick comparison is provided here based on the following assumptions.

We assume both the primary and secondary networks consist of only one single-antenna half-duplex transmitter-receiver pair. Timing synchronization between the primary and secondary nodes is perfect. Channels are non-fading with AWGN levels of N_0. Since in the interweave mode, the secondary transmitter is allowed to transmit only when the primary transmitter is not transmitting, we denote κ as the probability that the primary transmitter is idle. Then, at a given time, if the primary transmitter is idle, the secondary transmitter can transmit with its maximum available power no matter under which mode it works. But, if the primary transmitter is transmitting, the secondary transmitter can transmit only under the overlay or underlay mode and its transmit power must be adjusted to comply with the interference temperature limit.

With those assumptions, when there are secondary transmissions, the primary data rate is reduced to,

$$R_1 = \log_2(1 + \frac{P_p}{P_s + N_0}), \tag{2.24}$$

where P_p and P_s are the primary and secondary transmit powers, respectively. However, the performance penalty of the primary network must be kept within the acceptable bounds. Therefore, the primary data rate must be kept above the minimum primary data rate, which is given as [121],

$$R_1^{min} = \rho \log_2(1 + \frac{P_p}{N_0}), \tag{2.25}$$

where ρ is the minimum ratio. This minimum primary data rate is used to calculate the maximum secondary transmit power, which is the smaller one of the maximum available transmit power and the interference temperature limit in this case.

The capacity of the secondary network, which is computed via $C = \log_2(1 + \text{SINR})\text{bits/s/Hz}$ is chosen as the performance comparison metric. Details of calculating the capacity for each mode are discussed in Appendix A. Fig. 2.9 plots the

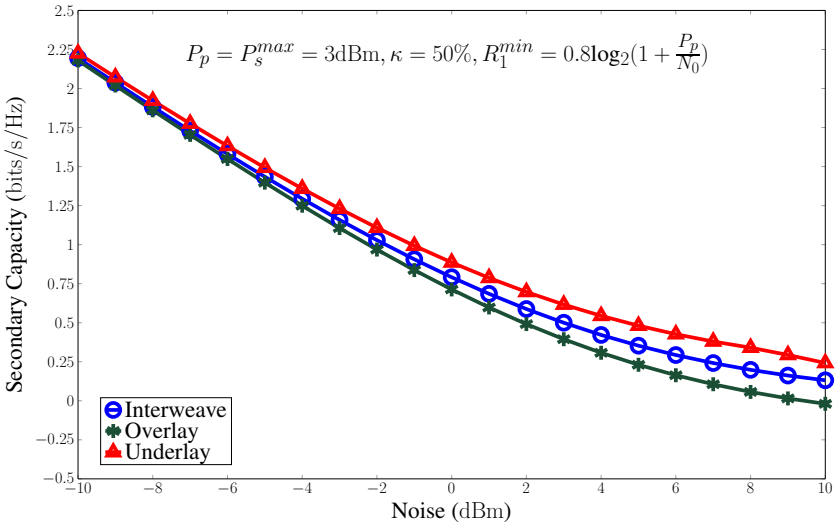

Figure 2.9: Secondary Capacity of Interweave, Overlay, and Underlay Modes

capacities of the three cognitive modes as functions of the noise power N_0. The primary transmit power (P_p) and the maximum available secondary transmit power (P_s^{max}) are both set to 3 dBm. And the idle probability κ and the minimum ratio ρ are set to 50% and 0.8, respectively. Clearly, subject to the assumptions made above, the underlay cognitive mode has the highest capacity. Therefore, the motivation to investigate the underlay cognitive networks is clear.

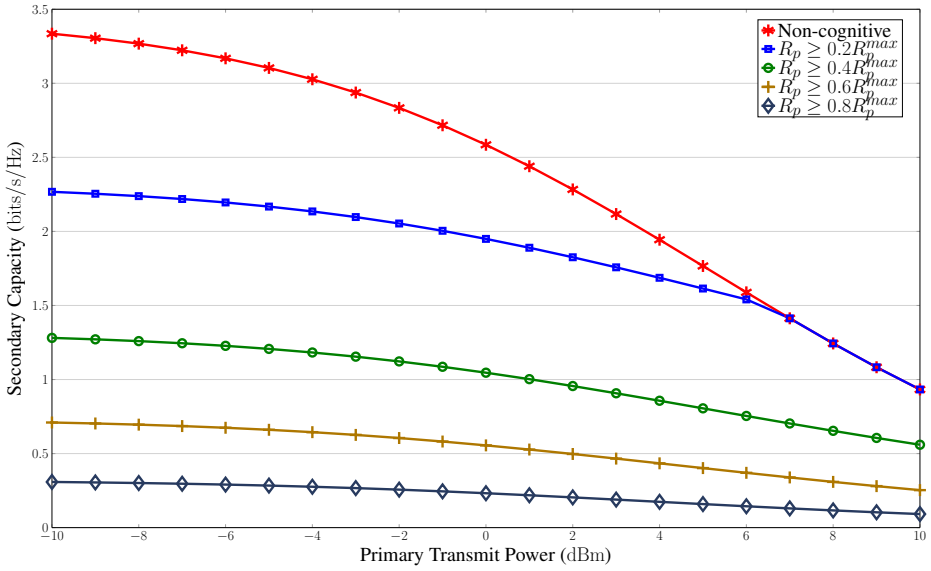

Figure 2.10: Secondary Capacity of Underlay Mode

Although the underlay mode has the benefits of any-time spectrum accesses and low-complexity operation, its performance is highly impacted by the interference due to the primary transmissions and the low transmit power due to the interference temperature limit. The resulting performance degradation in terms of capacity, based on the assumptions made above, is shown in Fig. 2.10, where $\kappa = 0$ and the capacity is computed by $C = \log_2(1 + \frac{P_s}{P_p+N_0})\text{bits/s/Hz}$. The secondary transmit power (P_s) is determined by the smaller one of its maximum value ($10\,\text{dBm}$) and the interference temperature limit, which is calculated from R_1^{min}, where $\rho \in \{0, 0.2, 0.4, 0.6, 0.8\}$. When $\rho = 0$, the primary network acts just as an interference source and no constraint on the S2P interference exists. Clearly, with larger ρ, or equivalently smaller interference temperature limit, and larger P_p, the underlay capacity degrades more. Thus, significant performance penalty on the underlay network occurs due to the primary interference and the interference temperature limit. Therefore, interference mitigation techniques, such as relaying and beamforming, are needed.

2.2 Algorithms

Since this thesis develops optimal transmitting/receiving and relaying designs, related optimization algorithms are introduced in this section, including the concept of complexity, interior-point algorithms and semidefinite relaxation (SDR).

2.2.1 Complexity

Complexity of an algorithm is a measure of resources, such as energy and size of silicon chip area, required. It is often expressed in terms of floating-point operations [122]. Typical operations include addition, subtraction, multiplication and division [123]. For wireless communications, computational time is crucial because of the need for low latency [111]. Therefore, low-complexity, i.e., less running time and energy, algorithms are preferable for wireless communications. In this thesis, running time is selected as the complexity measure of an algorithm.

The running time of an algorithm is the number of primitive operations [124],

given a particular input. It is usually estimated in worst-case scenarios and in the asymptotic sense. Therefore, given an input of size n, the running time of an algorithm is presented by $\mathcal{O}(f(n))$, which refers to the set of functions satisfying

$$\mathcal{O}(f(n)) = \{g(n) : \exists c, n_0 > 0, \text{ such that } 0 \leq g(n) \leq cf(n), \ \forall n \geq n_0\}. \quad (2.26)$$

For example, $\mathcal{O}(n)$ means that the running time is asymptotically no worse than cn.

2.2.2 Interior-Point Algorithms

In this section, we review interior-point (IP) algorithms, which are widely used to solve convex optimization problems with both equality and inequality constraints. The generic problem is expressed as,

$$\begin{aligned} \text{(P-2.1)} \quad \text{minimize} \quad & f_0(\boldsymbol{x}) \\ \text{subject to} \quad & f_i(\boldsymbol{x}) \leq 0, \ i = 1, \ ..., \ m \\ & \boldsymbol{A}\boldsymbol{x} = \boldsymbol{b}, \end{aligned}$$

where $f_0, \ ... \ f_m : \boldsymbol{C}^n \rightarrow \boldsymbol{C}$ are convex and twice continuously differentiable, $\boldsymbol{A} \in \boldsymbol{C}^{p \times n}$, and $\boldsymbol{b} \in \boldsymbol{C}^{p \times 1}$. Given this problem is solvable, the IP algorithms work as follows [125].

First, (P-2.1) is converted into an equivalent unconstrained problem. To this end, Lagrange multipliers $\boldsymbol{\lambda} = [\lambda_1, \lambda_2, ..., \lambda_p]^T$ and logarithmic barrier functions $-(1/t)\text{log}(-f_i(\boldsymbol{x}))$ ($i = 1, \ 2, \ ..., \ m$) are used to incorporate the equality and inequality constraints into the objective function, where t is the penalty parameter. Consequently, the following unconstrained optimization problem is obtained,

$$\text{(P-2.2)} \quad \text{minimize} \quad f_0(\boldsymbol{x}) + \boldsymbol{\lambda}^T(\boldsymbol{A}\boldsymbol{x} - \boldsymbol{b}) + \sum_{i=1}^{m} -(1/t)\text{log}(-f_i(\boldsymbol{x})).$$

Clearly, (P-2.2) is only an approximation of (P-2.1) and the approximation accuracy increases as the penalty t increases. Therefore, the basic idea behind interior-point algorithms is to solve a sequence of unconstrained optimization problems as (P-2.2) iteratively and increasing t by $\mu > 1$ at each iteration until the approximation accuracy threshold ϵ is achieved ($m/t < \epsilon$). The solution of the previous iteration is used as the initial point of the current one [125]. The main steps are given

in IP Algorithm. To realize the IP algorithms, various mathematical methods are developed, and their running time is given as $\mathcal{O}(\max(k,n)^4 n^{1/2}\log(1/\epsilon))$ [126], where n is the length of $\boldsymbol{x}$, $k = m + p$ with m being the number of inequality constraints and p being the number of equality constraints (e.g., the length of $\boldsymbol{b}$).

Algorithm IP Algorithm: Interior-Point Algorithm

Input: strictly feasible $\boldsymbol{x}$, $t := t^{(0)}$, $\mu > 1$, accuracy threshold $\epsilon > 0$

while $m/t \geq \epsilon$ **do**
  Compute $\boldsymbol{x}^\star(t)$ by solving (P-2.2), starting at $\boldsymbol{x}$;
  $\boldsymbol{x} := \boldsymbol{x}^\star(t)$;
  $t := \mu t$;
end

2.2.3 Semidefinite Relaxation

While interior-point algorithms handle convex problems, semidefinite relaxation (SDR) [126] is powerful for non-convex optimization problems, particularly non-convex quadratically constrained quadratic programs (QCQPs) in the form as,

$$\begin{aligned} \text{(P-2.3)} \quad \text{minimize} \quad & \boldsymbol{x}^H \boldsymbol{C} \boldsymbol{x} \\ \text{subject to} \quad & \boldsymbol{x}^H \boldsymbol{G}_i \boldsymbol{x} \geq g_i,\ i = 1,\ ...,\ m \\ & \boldsymbol{x}^H \boldsymbol{F}_i \boldsymbol{x} = f_i,\ i = 1,\ ...,\ p \\ & \boldsymbol{x}^H \boldsymbol{L}_i \boldsymbol{x} \leq l_i,\ i = 1,\ ...,\ q \end{aligned}$$

where $\boldsymbol{C}$, $\boldsymbol{G}_i$, $\boldsymbol{F}_i$, and $\boldsymbol{L}_i$ are general Hermitian matrices. Because (P-2.3) is non-convex, it is very difficult to solve, which means that it can not be solved in polynomial time, or equivalently the running time (2.26) required to solve this problem is not a polynomial expression of the problem size [126]. However, an approximation technique can be used to solve this problem by first converting (P-2.3) to an

equivalent problem in the form as,

$$\begin{aligned}
\text{(P-2.4)} \quad \text{minimize} \quad & \text{Tr}(\boldsymbol{C}\boldsymbol{X}) \\
\text{subject to} \quad & \text{Tr}(\boldsymbol{G}_i\boldsymbol{X}) \geq g_i,\ i = 1,\ ...,\ m \\
& \text{Tr}(\boldsymbol{F}_i\boldsymbol{X}) = f_i,\ i = 1,\ ...,\ p \\
& \text{Tr}(\boldsymbol{L}_i\boldsymbol{X}) \leq l_i,\ i = 1,\ ...,\ q \\
& \boldsymbol{X} \succeq \boldsymbol{0},\ \text{rank}(\boldsymbol{X}) = 1
\end{aligned}$$

where $\boldsymbol{X} = \boldsymbol{x}\boldsymbol{x}^H$. Although (P-2.4) is still nonconvex, it becomes convex when the constraint $\text{rank}(\boldsymbol{X}) = 1$ is dropped. Therefore, (P-2.4) is approximated by (P-2.5), which is called SDR.

$$\begin{aligned}
\text{(P-2.5)} \quad \text{minimize} \quad & \text{Tr}(\boldsymbol{C}\boldsymbol{X}) \\
\text{subject to} \quad & \text{Tr}(\boldsymbol{G}_i\boldsymbol{X}) \geq g_i,\ i = 1,\ ...,\ m \\
& \text{Tr}(\boldsymbol{F}_i\boldsymbol{X}) = f_i,\ i = 1,\ ...,\ p \\
& \text{Tr}(\boldsymbol{L}_i\boldsymbol{X}) \leq l_i,\ i = 1,\ ...,\ q \\
& \boldsymbol{X} \succeq \boldsymbol{0}
\end{aligned}$$

Note that (P-2.5) can be solved by an interior-point algorithm. Let $\boldsymbol{X}^\star$ be the optimal solution to (P-2.5). If $\text{rank}(\boldsymbol{X}^\star) = 1$, then there must be a $\boldsymbol{x}^\star$ such that $\boldsymbol{X}^\star = \boldsymbol{x}^\star\boldsymbol{x}^{\star H}$, and $\boldsymbol{x}^\star$ is the optimal solution to (P-2.3). Otherwise, we must extract a $\boldsymbol{x}^\star$, which is feasible to (P-2.3), from $\boldsymbol{X}^\star$ [126]. One widely used method to extract $\boldsymbol{x}^\star$ is called eigenvalue approximation [126], which works as follows. First, decomposite $\boldsymbol{X}^\star$ by eigenvalues $\lambda_1 \geq \lambda_2 \geq ...\lambda_r$, where $r = \text{rank}(\boldsymbol{X}^\star)$. Then, choose λ_1 and its corresponding eigenvector $\boldsymbol{q}_1$ to build $\tilde{\boldsymbol{x}} = \sqrt{\lambda_1}\boldsymbol{q}_1$ as the solution to (P-2.3) if it is feasible. Otherwise, map $\tilde{\boldsymbol{x}}$ to its "nearby" feasible point to (P-2.3) as the solution.

Note that, it has been shown in [126,127] that if (P-2.5) has only two constraints, it always has a rank-1 solution, $\text{rank}\{\boldsymbol{X}_j^\star\} = 1$, whenever (P-2.5) is feasible.

2.3 Prior Related Research

As mentioned before, cognitive networks are susceptible to the bidirectional (P2S and S2P) interference signals. To deal with the S2P interference, power allocation, i.e. adjusting the power levels at various nodes, has been studied [128, 129], and various beamforming algorithms have been developed [32–40] based on the following criteria: 1) the minimization of the transmit power; 2) the minimization of the interference to primary nodes; 3) the maximization of the worse received SNR at the secondary nodes; and 4) the minimization of a weighted sum of S2P interference and minimum SNR.

Although beamforming is capable of mitigating interferences in underlay networks, the coverage area does not increase, which is due to low transmit power. To address this problem, underlay relaying has been introduced [41–70, 113, 130–133, 161]. Among them, [47, 51–70, 132] analysed the outage performance for different relaying and beamforming algorithms. [51–68] focused on relay selection strategies, while [47, 69, 70, 132] studied beamforming in underlay one-way DF relay networks, where Rx beamforming was investigated in [47, 132] and distributed beamforming was analysed in [69, 70].

Besides analysis of outage performance, transmit design problem in AF relay networks, e.g., beamforming and power allocation, which has been extensively investigated [134–145] for conventional non-cognitive cases, has been studied recently [41, 41–50, 162] for cognitive networks. Of these, [41–45, 47, 48] studied beamforming in one-way relay networks, while [46, 49, 50] considered two-way relays.

Note that, most of those previous researches focused on one-way relays and only on the S2P interferences, while neglected the P2S interference. Therefore, this thesis considers both interferences and focuses on two-way relaying.

2.4 Conclusion

This chapter reviewed related topics, including wireless channels, outage probability, multiple antenna networks, different beamforming algorithms, relaying schemes

and protocols, and the cognitive modes. Complexity, interior-point algorithms, and semidefinite relaxation, were discussed. And some of the related previous research was also reviewed.

$\sim$

Chapter 3

Outage Analysis of ZFB-MRT/MRC Underlay Two-Way Relay Systems

As mentioned before, this thesis explores beamforming and two-way relaying techniques to mitigate the bi-directional interferences and thus to enhance coverage, reliability and capacity of the underlay networks. Thus, the performance of underlay beamforming and two-way relay networks must be characterized. Specifically, this chapter studies the outage performance of ZFB-MRT/MRC for two multi-antenna terminals and one single-antenna AF fixed-gain relay node. Although the ZFB-MRT/MRC scheme can completely nullify some S2P and P2S interference signals, it does not exploit the interference temperature limit, or equivalently, it does not use the fact that the primary receiver can tolerate interference as much as the interference temperature limit. However, it offers mathematical tractability and the resulting analysis yields important insights. Therefore, considering both path loss effect and small-scale fading, the closed-form exact and asymptotic E2E outage probabilities are derived first[1]. Then, the two-way outage probability, which is the probability of failure in either communication direction, is analysed via simulations.

3.1 Introduction

Although underlay networks can reduce spectrum congestion by reusing the licensed spectrum bands simultaneously with primary nodes, they usually have reduced coverage range and limited data rate due to the interference constraints. How-

[1] *A version of this chapter has been accepted for publication in IEEE Commun. Lett. (2015).*

ever, the coverage can be enhanced by introducing relays, and the interference signals can be mitigated by using beamforming if the underlay nodes are equipped with multiple antennas. Therefore, this chapter analyses the outage performance of beamforming in underlay two-way relay networks of multi-antenna terminals.

3.1.1 Prior Related Research

Outage probabilities of underlay relay networks have been extensively investigated recently in [47, 51–70, 132, 161], where only one-way relaying was considered. With various relay selection strategies, the outage probabilities were characterized for DF relaying [51–61] and AF relaying [62–68], respectively.

However, the performance analysis of beamforming in underlay relay systems has only been studied in [47, 69, 70, 132]. With multi-antenna secondary receivers, the performance of Rx beamforming was studied in [47,132]. With multiple cooperative relays, distributed beamforming was investigated in [69, 70]. It is worthwhile to mention that all of theses studies were limited to DF single-antenna one-way relay and neglected the impact of the P2S interference.

3.1.2 Motivation and Contribution

To the best of our knowledge, the performance of beamforming for underlay two-way AF relay networks considering both S2P and P2S interferences has not yet been analysed previously. Therefore, this chapter will fill this gap. Specifically, the outage performance of ZFB-MRT/MRC for two multi-antenna terminals (SU_1 and SU_2) and one single-antenna fixed-gain relay (R) (Fig. 3.1) is analysed.

The relay is limited to one single-antenna and fixed-gain because multiple antennas in some relays may be difficult due to the size and the cost constraints [28,29] and fixed gain provides us with mathematically tractable SINR expression. On the other hand, although for underlay networks, ZFB-MRT/MRC is necessarily sub-optimal because the interference temperature limit is not exploited (that is, ZFB-MRT computes the beamforming vector to make the interference at the primary receiver I_{S2P} identical to zero; however, the primary receiver can tolerate interference $I_{S2} \leq I_{th}$), it is employed here due to its mathematical tractability.

In this configuration (Fig. 3.1), two-time slots are required for mutual information exchange between SU_1 and SU_2. Although, the SU_j-to-primary and primary-to-SU_j ($j = 1, 2$) interference signals are mitigated via ZFB-MRT and ZFB-MRC, respectively, the primary-to-R interference in time slot one will propagate to SU_1 and SU_2 in time slot two. All these effects are considered in our outage analysis. To be more specific, the contributions of this chapter can be enumerated as follows.

1. Assuming both path loss effect and small-scale fading, the exact and asymptotic E2E outage probabilities are derived in closed-form considering the P2S interference residual and the S2P interference constraint [71].

2. It has been found that the distances between the relay and primary/secondary terminals are critical to the outage, while the distances between the primary and secondary terminals do not affect the outage at all.

3. In high secondary transmit power region, with ZFB-MRT/MRC, the diversity order is zero if the interference temperature limit is fixed. However, if the interference temperature limit is proportional to the secondary transmit power, a diversity of order $\min(M_1, M_2) - 1$ is achieved, where M_1 and M_2 are the number of antennas equipped at the two secondary terminals, respectively.

4. The effectiveness of beamforming in addressing the interferences and improving the reliability of underlay two-way relay networks are shown via simulation results. For instance, the outage probabilities could be as low as 10^{-4} if the two secondary terminals are equipped with 16 antennas and the locations between the relay and the primary nodes are 1.5 times of the locations between the relay and the secondary terminals.

5. Simulation results of two-way outage probabilities also show the similarity between cognitive and non-cognitive two-way relay networks. Both of their two-way outage probabilities are determined by the weakest link [146].

This chapter is organized as follows. Section 3.2 introduces the details of the system configuration and signal flow. Section 3.3 derives the closed-form exact and

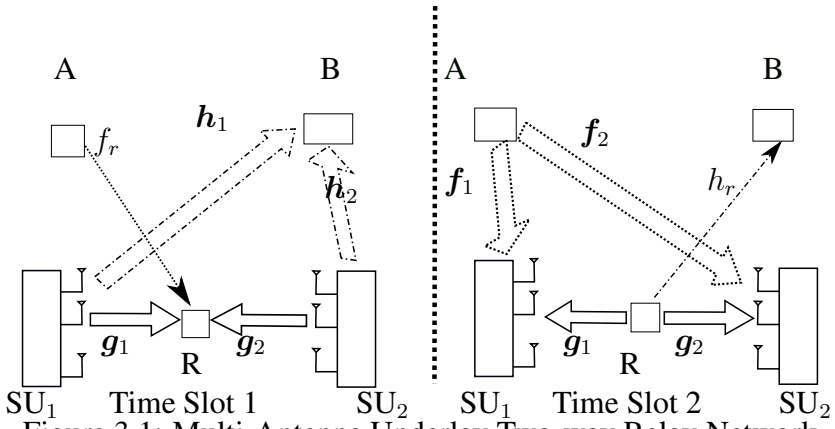

Figure 3.1: Multi-Antenna Underlay Two-way Relay Network

asymptotic E2E probabilities and verifies them via simulations. Section 3.4 analyses the two-way outage probabilities via simulations. And Section 3.5 concludes this chapter.

3.2 System Configuration and Signal Flow

System Configuration

In our underlay two-way relay set-up (Fig. 3.1), the two secondary terminals SU_j are equipped with $M_j \geq 2$ antennas ($j = 1, 2$), respectively, and the AF relay R is equipped with only one antenna. In real applications, these two secondary terminals could be two wireless access points in two separate homes or two microcell base stations. And they are connected temporally by the relay, which is a single-antenna mobile device, such as a personal digital assistant (PDA). The primary network is modelled as one transmitter (A) and receiver (B). All the nodes are half-duplex nodes. And perfect time synchronization is assumed between the primary and secondary networks, which was also adopted in [47, 70]. Thus, our results characterize the maximum interference power scenario.

Both path loss effect and small-scale fading are assumed throughout this chapter. Consider any two nodes x and y with n_x and n_y antennas at a distance $d_{\text{x,y}}$ in Fig. 3.1. The channel from x to y is thus denoted by a $\mathbb{C}^{n_y \times n_x}$ matrix with

independent and identical distributed $\mathcal{CN}(0,\ \lambda_{\mathrm{x,y}})$ entries, where $\lambda_{\mathrm{x,y}}$ accounts for the path loss effect and satisfies $\lambda_{\mathrm{x,y}} \propto d_{\mathrm{x,y}}^{-\omega}$, where ω is the path loss exponent. Based on these, vectors $\boldsymbol{g}_j \in \mathbb{C}^{M_j \times 1}$, $\boldsymbol{h}_j \in \mathbb{C}^{M_j \times 1}$ and $\boldsymbol{f}_j \in \mathbb{C}^{M_j \times 1}$ ($j = 1,\ 2$) are the reciprocal $\mathrm{SU}_j \leftrightarrow$R channel, the $\mathrm{SU}_j \rightarrow$B and A$\rightarrow\mathrm{SU}_j$ interference channels with $g_{j_i} \sim \mathcal{CN}(\mathbf{0},\ \lambda_{\mathrm{SU}_j,\mathrm{R}})$, $h_{j_i} \sim \mathcal{CN}(\mathbf{0},\ \lambda_{\mathrm{SU}_j,\mathrm{B}})$ and $f_{j_i} \sim \mathcal{CN}(\mathbf{0},\ \lambda_{\mathrm{A,SU}_j})$ ($i = 1, 2, ..., M_j$), respectively. $h_r \sim \mathcal{CN}(0,\ \lambda_{\mathrm{R,B}})$ and $f_r \sim \mathcal{CN}(0,\ \lambda_{\mathrm{A,R}})$ are the R$\rightarrow$B and A$\rightarrow$R interference channels, respectively. In order to simplify the representations in the following analysis, we define $\lambda_0 = \lambda_{\mathrm{A,R}}$, $\lambda_j = \lambda_{\mathrm{SU}_j,\mathrm{R}}$ ($j = 1,\ 2$), and $\lambda_3 = \lambda_{\mathrm{R,B}}$.

Because full CSI requirement, e.g., all the secondary-to-secondary (S2S), P2S and S2P channels, necessitates a large overhead, we assume that every secondary node x$\in\{\mathrm{SU}_1,\ \mathrm{SU}_2,$ and R$\}$ obtains CSI only of channels involving itself, e.g., x$\rightarrow$B, A$\rightarrow$x, x$\rightarrow$R/SU_j (if x=SU_j/R, $j = 1, 2$), via a suitable channel estimation process [118]. With this assumption, SU_j can calculate its own beamforming vectors. We also assume that R calculates its relay gain G and feeds it back to SU_j ($j = 1, 2$).

Without loss of generality, zero-mean complex AWGN with N_0 variance at every receiving node and unit symbol power are assumed as well. The notations, I_{th}, P_s and P_p are used to denote the interference temperature limit, and the transmit powers at SU_j ($j = 1,\ 2$) and A, respectively.

Signal Flow

Since the two-way relay requires two consecutive time slots, in time slot one, SU_j ($j = 1, 2$) and A simultaneously transmit symbols s_j and $x^{(1)}$, respectively. Then, the signal y_r and interference signal $x_{int}^{(1)}$ received at R and B are then given as,

$$y_r = \sqrt{P_s}\boldsymbol{g}_1^T\boldsymbol{m}_1 s_1 + \sqrt{P_s}\boldsymbol{g}_2^T\boldsymbol{m}_2 s_2 + \sqrt{P_p} f_r x^{(1)} + n_r, \tag{3.1}$$

$$x_{int}^{(1)} = \sqrt{P_s}\boldsymbol{h}_1^T\boldsymbol{m}_1 s_1 + \sqrt{P_s}\boldsymbol{h}_2^T\boldsymbol{m}_2 s_2, \tag{3.2}$$

where $n_r \in \mathbb{C}$ is the AWGN component and $\boldsymbol{m}_j \in \mathbb{C}^{M_j \times 1}$ ($j = 1,\ 2$) are the normalized Tx beamforming vectors at SU_j, which is derived via ZFB-MRT. According to the principle of ZFB-MRT, $\boldsymbol{m}_j$ ($j = 1, 2$) is chosen as the projection of

the SU$_j$ $\rightarrow$R channel $\boldsymbol{g}_j$ onto the sub-space $\Phi_j = \boldsymbol{I} - \frac{\boldsymbol{h}_j^* \boldsymbol{h}_j^T}{\|\boldsymbol{h}_j\|^2}$, which is orthogonal to the SU$_j$ $\rightarrow$B interference channel $\boldsymbol{h}_j$. Therefore, it is computed as,

$$\boldsymbol{m}_j = \frac{\Phi_j \boldsymbol{g}_j^*}{\sqrt{\boldsymbol{g}_j^T \Phi_j \boldsymbol{g}_j^*}}, \tag{3.3}$$

where the denominator is the normalizing factor. Since with ZFB-MRT, the SU$_j$-to-B ($j = 1, 2$) interference signal is completely mitigated, e.g., $\boldsymbol{h}_j^T \boldsymbol{m}_j = 0$, it is guaranteed that the P2S interference in this time slot is under the interference temperature limit, $|x_{int}^{(1)}|^2 = 0 < I_{th}$.

In the second time slot, A transmits symbol $x^{(2)}$, and simultaneously R transmits Gy_r, where $G \in \mathbb{C}$ is the relay gain. Then the interference signal $x_{int}^{(2)}$ at B and the signal vector $\boldsymbol{y}_j$ received at SU$_j$ ($j = 1,\ 2$) are given as,

$$x_{int}^{(2)} = h_r G y_r, \tag{3.4}$$

$$\begin{aligned} \boldsymbol{y}_j = & \underbrace{\sqrt{P_s} G \boldsymbol{g}_j \boldsymbol{g}_j^T \boldsymbol{m}_j s_j}_{\text{Self-Interference}} + \underbrace{\sqrt{P_s} G \boldsymbol{g}_j \boldsymbol{g}_{\bar{j}}^T \boldsymbol{m}_{\bar{j}} s_{\bar{j}}}_{\text{Signal}} \\ & + \underbrace{\sqrt{P_p} G \boldsymbol{g}_j f_r x^{(1)} + \sqrt{P_p} \boldsymbol{f}_j x^{(2)}}_{\text{P2S Interference}} + \underbrace{G \boldsymbol{g}_j n_r + \boldsymbol{n}_j}_{\text{Noise}}, \end{aligned} \tag{3.5}$$

where $\boldsymbol{n}_j \in \mathbb{C}^{M_j \times 1}$ is the vector of AWGN at SU$_j$, and $\bar{j} = 1$, if $j = 2$, and vise versa.

Knowing G and $\boldsymbol{g}_j$ ($j = 1, 2$), SU$_j$ can eliminate the self-interference part $\sqrt{P_s} \boldsymbol{g}_j G \boldsymbol{g}_j^T \boldsymbol{m}_j s_j$ in its received signal y_j perfectly. After the self-interference cancellation and Rx beamforming, the resulting signal $\hat{y}_j$ is represented as,

$$\begin{aligned} \hat{y}_j = & \underbrace{\sqrt{P_s} G \boldsymbol{d}_j^T \boldsymbol{g}_j \boldsymbol{g}_{\bar{j}}^T \boldsymbol{m}_{\bar{j}} s_{\bar{j}}}_{\text{Signal}} + \underbrace{G \boldsymbol{d}_j^T \boldsymbol{g}_j n_r + \boldsymbol{d}_j^T \boldsymbol{n}_j}_{\text{Noise}} \\ & + \underbrace{\sqrt{P_p} G \boldsymbol{d}_j^T \boldsymbol{g}_j f_r x^{(1)} + \sqrt{P_p} \boldsymbol{d}_j^T \boldsymbol{f}_j x^{(2)}}_{\text{P2S Interference}} \end{aligned} \tag{3.6}$$

where $\boldsymbol{d}_j \in \mathbb{C}^{M_j \times 1}$ ($j = 1, 2$) are the normalized Rx beamforming vectors, which is calculated via ZFB-MRC as,

$$\boldsymbol{d}_j = \frac{\Psi_j \boldsymbol{g}_j^*}{\sqrt{\boldsymbol{g}_j^T \Psi_j \boldsymbol{g}_j^*}}, \tag{3.7}$$

where $\Psi_j = \boldsymbol{I} - \frac{\boldsymbol{f}_j^* \boldsymbol{f}_j^T}{\|\boldsymbol{f}_j\|^2}$ is the sub-space orthogonal to the A$\rightarrow$SU$_j$ interference channel $\boldsymbol{f}_j$ ($j = 1, 2$).

Although ZFB-MRC can nullify the A $\rightarrow$SU$_j$ ($j = 1, 2$) interferences completely, e.g., $\sqrt{P_p}\boldsymbol{d}_j^T \boldsymbol{f}_j x^{(2)} = 0$, the accumulated interference still exists, e.g., $\sqrt{P_p} G \boldsymbol{d}_j^T \boldsymbol{g}_j f_r x^{(1)}$. Therefore, it must be considered in performance analysis.

After substituting the beamforming vectors $\boldsymbol{m}_j$ and $\boldsymbol{d}_j$ into (3.6), the received SINR (S_j) at SU$_j$ ($j = 1, 2$) is represented as,

$$S_j = \frac{P_s \|\boldsymbol{g}_{\bar{j}}\|^2 \rho_{\boldsymbol{h}_{\bar{j}}} \|\boldsymbol{g}_j\|^2 \rho_{\boldsymbol{f}_j}}{\|\boldsymbol{g}_j\|^2 \rho_{\boldsymbol{f}_j} (P_p |f_r|^2 + N_0) + \frac{N_0}{|G|^2}} \tag{3.8}$$

where , $\rho_{\boldsymbol{h}_j} = 1 - \frac{|\boldsymbol{h}_j^T \boldsymbol{g}_j^*|^2}{\|\boldsymbol{h}_j\|^2 \|\boldsymbol{g}_j\|^2}$, $\rho_{\boldsymbol{f}_j} = 1 - \frac{|\boldsymbol{f}_j^T \boldsymbol{g}_j^*|^2}{\|\boldsymbol{f}_j\|^2 \|\boldsymbol{g}_j\|^2}$. Depending on how the relay gain G is calculated, CSI-assisted or fixed-gain, the received SINR may result in different representations.

With CSI-assisted relaying, SU$_j$ ($j = 1, 2$) are required to communicate $\boldsymbol{m}_j$ to the relay (R) such that R can adapt its relay gain G before each transmission. In this case, G should be chosen such that the R$\rightarrow$B interference is below the interference temperature limit I_{th}, e.g., $|x_{int}^{(2)}|^2 \leq I_{th}$. Therefore, the CSI-assisted relay gain $G_{\textbf{CSI-assisted}}$ must satisfy,

$$|G_{CSI-assisted}|^2 = \frac{I_{th}}{|h_r|^2 [P_s |\boldsymbol{g}_1^T \boldsymbol{m}_1|^2 + P_s |\boldsymbol{g}_2^T \boldsymbol{m}_2|^2 + P_p |f_r|^2 + N_0]}. \tag{3.9}$$

Substituting (3.9) into (3.8) results in the CSI-assisted SINR ($S_j^{\text{CSI-assisted}}$) as,

$$S_j^{\text{CSI-assisted}} = \frac{\frac{P_s \|\boldsymbol{g}_{\bar{j}}\|^2 \rho_{\boldsymbol{h}_{\bar{j}}}}{P_p |f_r|^2 + N_0} \frac{I_{th} \|\boldsymbol{g}_j\|^2 \rho_{\boldsymbol{f}_j}}{N_0 |h_r|^2}}{\frac{P_s (\|\boldsymbol{g}_1\|^2 \rho_{\boldsymbol{h}_1} + \|\boldsymbol{g}_2\|^2 \rho_{\boldsymbol{h}_2})}{P_p |f_r|^2 + N_0} + \frac{I_{th} \|\boldsymbol{g}_j\|^2 \rho_{\boldsymbol{f}_j}}{N_0 |h_r|^2} + 1}. \tag{3.10}$$

With fixed-gain relaying, SU$_j$ ($j = 1, 2$) is required to send only the average ($\mathbb{E}\{|\boldsymbol{g}_j^T \boldsymbol{m}_j|^2\}$) to R, which has the benefit of reduced overhead compared with CSI-assisted relaying since such averages are more static. In this case, the fixed relay gain $G_{\text{fixed-gain}}$ should be chosen such that $\mathbb{E}\{|x_{int}^{(2)}|^2\} \leq I_{th}$, which implies that,

$$|G_{\text{fixed-gain}}|^2 = \frac{I_{th}}{\mathbb{E}\{|h_r|^2\} [P_s \mathbb{E}\{|\boldsymbol{g}_1^T \boldsymbol{m}_1|^2\} + P_s \mathbb{E}\{|\boldsymbol{g}_2^T \boldsymbol{m}_2|^2\} + P_p \mathbb{E}\{|f_r|^2\} + N_0]}. \tag{3.11}$$

Accordingly, by substituting (3.11) into (3.8), the fixed-gain SINR ($S_j^{\text{fixed-gain}}$) is obtained as (3.12), where $\gamma_{jR} = \bar{\gamma} \|\boldsymbol{g}_j\|^2 \rho_{\boldsymbol{h}_j}$, $\gamma_{Rj} = \bar{\gamma} \|\boldsymbol{g}_j\|^2 \rho_{\boldsymbol{f}_j}$, $\gamma_3 = \gamma_0 |f_r|^2$, $C = \frac{\bar{\gamma}}{|G_{\text{fixed}}|^2}$, $\bar{\gamma} = \frac{P}{N_0}$, and $\gamma_0 = \frac{P_p}{N_0}$.

$$S_j^{\text{fixed-gain}} = \frac{\gamma_{\bar{j}R}\gamma_{Rj}}{\gamma_{Rj}(\gamma_3+1)+C}. \tag{3.12}$$

Besides the benefit of reduced overhead, the fixed-gain relaying also provide us with mathematically tractable SINRs ((3.12)), while the CSI-assisted relaying results in mathematically intractable SINRs ((3.10)). Therefore, the following outage analysis focuses on the fixed-gain case. However, our numerical comparisons for both cases are also provided. For simplicity, we use G and S_j to represent $G_{\text{fixed-gain}}$ and $S_j^{\text{fixed-gain}}$, respectively, hereafter.

3.3 E2E Outage Probability Analysis

In this section, the closed-form exact and asymptotic E2E outage probabilities based on fixed-gain relaying is derived. The asymptotic outage probabilities are in the sense of $P_s \to \infty$ and $I_{th} \to \infty$, respectively.

3.3.1 Exact E2E Outage Probability

To analyse the exact E2E outage probability, we start with characterizing the statistics of γ_{jR} and γ_{Rj} ($j = 1,\ 2$) in (3.12). And the following theorem is obtained.

Theorem 3. 1. *The random variables γ_{jR} and γ_{Rj} ($j = 1,\ 2$) are Gamma$(M_j - 1, \bar{\gamma}\lambda_j)$ distributed.*

Proof. We start with deriving the distribution of $\gamma_{jR} = \bar{\gamma}\|\boldsymbol{g}_j\|^2\rho_{\boldsymbol{h}_j}$ ($j = 1, 2$). To find its cumulative distribution function (CDF), the CDFs and PDFs of $\|\boldsymbol{g}_j\|^2$ and $\rho_{\boldsymbol{h}_j}$ ($j = 1, 2$) must be obtained first.

To find the CDF of $\rho_{\boldsymbol{h}_j}$ ($j = 1, 2$), we first define $\hat{\boldsymbol{h}}_j = \frac{\boldsymbol{h}_j}{\sqrt{\lambda_{SU_j,B}}}$ and $\hat{\boldsymbol{g}}_j = \frac{\boldsymbol{g}_j}{\sqrt{\lambda_j}}$ ($j = 1,\ 2$). Both $\hat{\boldsymbol{h}}_j$ and $\hat{\boldsymbol{g}}_j$ are thus $\mathcal{CN}(0,\ 1)$ distributed and $\rho_{\boldsymbol{h}_j}$ remains unchanged when $\boldsymbol{h}_j$ and $\boldsymbol{g}_j$ are replaced by $\sqrt{\lambda_{SU_j,B}}\hat{\boldsymbol{h}}_j$ and $\sqrt{\lambda_j}\hat{\boldsymbol{g}}_j$, respectively. It has been proven in [147] that the random variable $X = \frac{|\hat{\boldsymbol{h}}_j^T\hat{\boldsymbol{g}}_j^*|^2}{\|\hat{\boldsymbol{h}}_j\|^2\|\hat{\boldsymbol{g}}_j\|^2}$ is Beta$(1,\ M_j-1)$ distributed and is independent from both $\hat{\boldsymbol{g}}_j$ and $\hat{\boldsymbol{h}}_j$ because X is the normalized correlation between $\hat{\boldsymbol{g}}_j$ and a uniformly distributed variable $\boldsymbol{v} = \frac{\hat{\boldsymbol{h}}_j}{\|\hat{\boldsymbol{h}}_j\|}$. Since the Beta distribution has the property that if $X \sim$ Beta(α, β), then $1-X \sim$ Beta(β, α),

$\rho_{\boldsymbol{h}_j} = 1 - X$ is Beta$(M_j - 1,\, 1)$-distributed, whose CDF $F_{\rho_{\boldsymbol{h}_j}}(\rho)$ and PDF $f_{\rho_{\boldsymbol{h}_j}}(\rho)$ are given as,

$$F_{\rho_{\boldsymbol{h}_j}}(\rho) = \frac{B(\rho; M_j - 1, 1)}{B(M_j - 1, 1)}, \tag{3.13}$$

$$f_{\rho_{\boldsymbol{h}_j}}(\rho) = \frac{\rho^(M_j - 2)}{B(M_j - 1, 2)}, \tag{3.14}$$

where $0 < \rho < 1$, $B(\cdot, \cdot)$ is the Beta function, and $B(\cdot; \cdot, \cdot)$ is the incomplete Beta function.

On the other hand, the random variable $Y_j = \|\boldsymbol{g}_j\|^2$ is a sum of M_j absolute square $\mathcal{CN}(0,\, \lambda_j)$ terms and as such is Gamma$(M_j,\, \lambda_j)$ distributed, whose CDF $F_Y(y)$ and PDF $f_Y(y)$ are given as,

$$F_Y(y) = P(M_j, \frac{y}{\lambda_j}), \tag{3.15}$$

$$f_Y(y) = \frac{y^{M_j - 1} e^{-\frac{y}{\lambda_j}}}{\lambda_j^{M_j} \Gamma(M_j)}, \tag{3.16}$$

where $y > 0$, $\Gamma(\cdot)$ is the Gamma function, and $P(\cdot, \cdot)$ is the regularized lower incomplete Gamma function. Then by expanding $P(s, x) = 1 - \sum_{i=1}^{s} \frac{x^{s-i} e^{-x}}{(s-i)!}$, given s is a positive integer, the CDF of γ_{jR} ($j = 1,\, 2$) is derived as,

$$\begin{aligned}
F_{\gamma_{jR}}(\gamma) &= \int_0^{\infty} F_{\rho_{\boldsymbol{h}_j}}\left(\frac{\gamma}{\bar{\gamma} y}\right) f_{Y_j}(y) \mathrm{d}y \\
&= \int_0^{\frac{\gamma}{\bar{\gamma}}} f_{Y_j}(y) \mathrm{d}y + \int_{\frac{\gamma}{\bar{\gamma}}}^{\infty} (\frac{\gamma}{\bar{\gamma} y})^{M_j - 1} \frac{y^{M_j - 1} e^{-\frac{y}{\lambda_j}}}{\int_0^{\infty} t^{M_j - 1} e^{-t} dt \lambda_j^{M_j}} \mathrm{d}y \\
&= P(M_j, \frac{\gamma}{\bar{\gamma} \lambda_j}) + \frac{\gamma^{M_j - 1} e^{-\frac{\gamma}{\bar{\gamma} \lambda_j}}}{(\bar{\gamma} \lambda_j)^{M_j - 1} \Gamma(M_j)} \\
&= 1 - \sum_{i=1}^{M_j} \frac{\gamma^{M_j - i} e^{-\frac{\gamma}{\bar{\gamma} \lambda_j}}}{(\bar{\gamma} \lambda_j)^{M_j - i} (M_j - i)!} + \frac{\gamma^{M_j - 1} e^{-\frac{\gamma}{\bar{\gamma} \lambda_j}}}{(\bar{\gamma} \lambda_j)^{M_j - 1} \Gamma(M_j)} \\
&= 1 - \sum_{i=1}^{M_j - 1} \frac{\gamma^{M_j - 1 - i} e^{-\frac{\gamma}{\bar{\gamma} \lambda_j}}}{(\bar{\gamma} \lambda_j)^{M_j - 1 - i} (M_j - 1 - i)!} \\
&= P(M_j - 1, \frac{\gamma}{\bar{\gamma} \lambda_j})
\end{aligned} \tag{3.17}$$

Therefore, γ_{jR} is Gamma$(M_j - 1, \bar{\gamma} \lambda_j)$-distributed. The proof for γ_{Rj} is analogous and omitted here. □

Using the statistics of γ_{jR} and γ_{Rj} ($j = 1, 2$), we then derive the exact E2E outage probability (P_j^{out}, $j = 1, 2$) in Theorem 3. 2.

Theorem 3. 2. *Given $\gamma_{th} > 0$ as the minimum SINR required at SU_j, the E2E outage probability $P_j^{out}(\gamma_{th}) = Pr[S_j \leq \gamma_{th}]$ at SU$_j$ ($j = 1, 2$) is given by,*

$$P_j^{out}(\gamma_{th}) = 1 - 2\sum_{i=2}^{M_{\bar{j}}}\sum_{k=0}^{M_{\bar{j}}-i}\sum_{l=0}^{k}\frac{e^{-\frac{\gamma_{th}}{\bar{\gamma}\lambda_{\bar{j}}}}\left(\frac{\gamma_{th}}{\lambda_{\bar{j}}}\right)^{\frac{M_1+M_2-i+k-1}{2}}}{(M_j-2)!(M_{\bar{j}}-i-k)!(k-l)!} \times \frac{\left(\frac{C}{\lambda_j}\right)^{\frac{M_1+M_2-i-k-1}{2}}(\gamma_0\lambda_0)^l}{\bar{\gamma}^{(M_1+M_2-i-l-2)}\left(\frac{\gamma_{th}\gamma_0\lambda_0}{\lambda_{\bar{j}}}+\bar{\gamma}\right)^{l+1}}\mathcal{K}_{M_j-M_{\bar{j}}+i+k-1}\left(2\sqrt{\frac{C\gamma_{th}}{\bar{\gamma}^2\lambda_1\lambda_2}}\right) \tag{3.18}$$

Proof. To derive the E2E outage probabilities P_j^{out} ($j = 1, 2$) is equivalent to characterize the statistics of the random variable S_j. Therefore, without loss of generality, we derive the CDF $F_{S_1}(\gamma)$ ($\gamma > 0$) of S_1 here since the CDF of S_2 can be obtained similarly.

In Theorem 1, we have proven that γ_{jR} and γ_{Rj} ($j = 1, 2$) are identically distributed. Although given a j ($j = 1, 2$), they are correlated because both of them contain the term $\|\boldsymbol{g}_j\|^2$, they will not appear in S_j simultaneously. For instance, S_1 only contains γ_{2R} and γ_{R1}. Therefore, we simplify the notation as $\gamma_1 = \gamma_{R1}$ and $\gamma_2 = \gamma_{2R}$ here.

On the other hand, since $f_r \sim \mathcal{CN}(0, \lambda_0)$, γ_3 follows the Exp($\frac{1}{\gamma_0\lambda_0}$) distribution, whose CDF $F_{\gamma_3}(\gamma)$ and PDF $f_{\gamma_3}(\gamma)$ are given as,

$$F_{\gamma_3}(\gamma) = 1 - e^{-\frac{\gamma}{\gamma_0\lambda_0}}, \qquad f_{\gamma_3}(\gamma) = \frac{1}{\gamma_0\lambda_0}e^{-\frac{\gamma}{\gamma_0\lambda_0}}, \tag{3.19}$$

where $\gamma > 0$. Knowing both the CDFs and PDFs of γ_j ($j = 1, 2, 3$), $F_{S_1}(\gamma)$ is derived via (3.20).

$$F_{S_1}(\gamma) = \int_0^\infty\int_0^\infty F_{\gamma_2}\left(\left(\gamma_3 + 1 + \frac{C}{\gamma_1}\right)\gamma\right) f_{\gamma_3}(\gamma_3)f_{\gamma_1}(\gamma_1)\mathrm{d}\gamma_3\mathrm{d}\gamma_1 \tag{3.20}$$

By replacing $F_{\gamma_2}\left(\left(\gamma_3 + 1 + \frac{C}{\gamma_1}\right)\gamma\right)$ in (3.20) with the expansion $P(s, x) = 1 -$

$e^{-x}\sum_{t=0}^{s-1}\frac{x^t}{t!}$, given s is a positive integer, we obtain (3.21),

$$\begin{aligned}
F_{S_1}(\gamma) =& 1-\sum_{i=2}^{M_2}\int_0^{\infty}\int_0^{\infty}\frac{e^{-(\gamma_3+1+\frac{C}{\gamma_1})\frac{\gamma}{\lambda_2\bar{\gamma}}}(\frac{\gamma}{\bar{\gamma}\lambda_2})^{M_2-i}\gamma_1^{M_1-2}}{(M_1-2)!(M_2-i)!(\bar{\gamma}\lambda_1)^{M_1-1}\gamma_0\lambda_0}\\
&\times\left(\gamma_3+1+\frac{C}{\gamma_1}\right)^{M_2-i}e^{-\frac{\gamma_3}{\gamma_0\lambda_0}}e^{-\frac{\gamma_1}{\bar{\gamma}\lambda_1}}\mathrm{d}\gamma_3\mathrm{d}\gamma_1\\
=& 1-\sum_{i=2}^{M_2}\sum_{k=0}^{M_2-i}\sum_{l=0}^{k}\binom{M_2-i}{k}\binom{k}{l}\frac{(\frac{\gamma}{\bar{\gamma}\lambda_2})^{M_2-i}e^{-\frac{\gamma}{\bar{\gamma}\lambda_2}}C^{M_2-i-k}}{\gamma_0\lambda_0(\bar{\gamma}\lambda_1)^{M_1-1}(M_1-2)!(M_2-i)!}\\
&\times\int_0^{\infty}\gamma_3^l e^{-\gamma_3(\frac{\gamma}{\bar{\gamma}\lambda_2}+\frac{1}{\gamma_0\lambda_0})}\mathrm{d}\gamma_3\int_0^{\infty}\gamma_1^{M_1-M_2+i+k-2}e^{-(\frac{\gamma C}{\bar{\gamma}\lambda_2\gamma_1}+\frac{\gamma_1}{\bar{\gamma}\lambda_1})}\mathrm{d}\gamma_1\\
=& 1-2\sum_{i=2}^{M_2}\sum_{k=0}^{M_2-i}\sum_{l=0}^{k}\frac{e^{-\frac{\gamma_{th}}{\bar{\gamma}\lambda_2}}(\frac{\gamma_{th}}{\lambda_2})^{\frac{M_1+M_2-i+k-1}{2}}}{(M_1-2)!(M_2-i-k)!(k-l)!}\\
&\times\frac{(\frac{C}{\lambda_1})^{\frac{M_1+M_2-i-k-1}{2}}(\gamma_0\lambda_0)^l}{\bar{\gamma}^{(M_1+M_2-i-l-2)}(\frac{\gamma_{th}\gamma_0\lambda_0}{\lambda_2}+\bar{\gamma})^{l+1}}\mathcal{K}_{M_j-M_{\bar{j}}+i+k-1}\left(2\sqrt{\frac{C\gamma_{th}}{\bar{\gamma}^2\lambda_1\lambda_2}}\right)
\end{aligned}\tag{3.21}$$

where the second equality follows the use of the Binomial expansion, and the third equality follows [148, Eq. (3.351.3)] and [148, Eq.(3.471.9)]. □

Note that (3.18) includes only λ_i ($i=0,1,2,3$), which is determined by the distances between the relay (R) and all the other nodes in the system (SU_1, SU_2, A, and B). Therefore, we can claim that only the location of the relay impacts the outage.

3.3.2 Fixed Relay Gain

According to (3.11), it is clear that only the amplitude of the relay gain $|G|$ matters. Therefore, we assume that the relay gain G is positive real-valued. Then, to calculate the fixed relay gain G from (3.11), $\mathbb{E}\{|\boldsymbol{g}_j^T\boldsymbol{m}_j|^2\}$ ($j=1,2$) must be calculated first, which is equivalent to $\mathbb{E}\{\|\boldsymbol{g}_j\|^2\rho_{\boldsymbol{h}_j}\}$ from (3.22) by substituting $\boldsymbol{m}_j$, $\rho_{\boldsymbol{h}_j}$, and Φ_j ($j=1,\,2$).

$$
\begin{aligned}
|\boldsymbol{g}_j^T \boldsymbol{m}_j|^2 &= \frac{|\boldsymbol{g}_j^T \Phi_j \boldsymbol{g}_j^*|^2}{\boldsymbol{g}_j^T \Phi_j \boldsymbol{g}_j^*} \\
&= \boldsymbol{g}_j^T \Phi_j \boldsymbol{g}_j^* \\
&= \|\boldsymbol{g}_j\|^2 - \frac{\boldsymbol{g}_j^T \boldsymbol{h}_j^* \boldsymbol{h}_j^T \boldsymbol{g}_j^*}{\|\boldsymbol{h}_j\|^2} \\
&= \|\boldsymbol{g}_j\|^2 (1 - \frac{|\boldsymbol{h}_j^T \boldsymbol{g}_j^*|^2}{\|\boldsymbol{h}_j\|^2 \|\boldsymbol{g}_j\|^2}) \\
&= \|\boldsymbol{g}_j\|^2 \rho_{\boldsymbol{h}_j}. \qquad (3.22)
\end{aligned}
$$

Since it has been proven in Theorem 3. 1 that $\rho_{\boldsymbol{h}_j}$ ($j = 1,\ 2$) is Beta distributed with parameter $M_j - 1$ and 1, and independent from both $\boldsymbol{g}_j$ and $\boldsymbol{h}_j$, it is true that $\mathbb{E}\{\|\boldsymbol{g}_j\|^2 \rho_{\boldsymbol{h}_j}\} = \mathbb{E}\{\|\boldsymbol{g}_j\|^2\}\mathbb{E}\{\rho_{\boldsymbol{h}_j}\}$ and $\mathbb{E}\{\rho_{\boldsymbol{h}_j}\} = \frac{M_j - 1}{M_j}$. Secondly, because $\|\boldsymbol{g}_j\|^2 \sim$ Gamma$(M_j,\ \lambda_j)$ $(j = 1, 2)$, $h_r \sim \mathcal{CN}(0,\ \lambda_3)$ and $f_r \sim \mathcal{CN}(0,\ \lambda_0)$, we have $\mathbb{E}\{|h_r|^2\} = \lambda_3$, $\mathbb{E}\{|f_r|^2\} = \lambda_0$ and $\mathbb{E}\{\|\boldsymbol{g}_j\|^2\} = M_j \lambda_j$ $(j = 1,\ 2)$. Substituting all these into (3.11), we obtain the fixed relay gain as,

$$
\begin{aligned}
G &= \sqrt{\frac{I_{th}}{\mathbb{E}\{|h_r|^2\}[P_s \mathbb{E}\{|\boldsymbol{g}_1^T \boldsymbol{m}_1|^2\} + P_s \mathbb{E}\{|\boldsymbol{g}_2^T \boldsymbol{m}_2|^2\} + P_p \mathbb{E}\{|f_r|^2\} + N_0]}} \\
&= \sqrt{\frac{I_{th}}{\lambda_3[P_s \lambda_1 (M_1 - 1) + P_s \lambda_2 (M_2 - 1) + P_p \lambda_0 + N_0]}}. \qquad (3.23)
\end{aligned}
$$

3.3.3 Asymptotic E2E Outage Probability with $I_{th} \to \infty$

In this section, we derive the asymptotic E2E outage probability in high interference temperature limit region ($I_{th} \to \infty$), in which case the underlay network is equivalent to a conventional two-way relay network with the primary A being an interference source. In this case, all the secondary nodes can transmit unconstrained.

To derive the asymptotic E2E outage probability in such a scenario, the expansion (3.24) of $\mathcal{K}_\nu(z)$ is required.

$$
\begin{aligned}
\mathcal{K}_\nu(z) = \frac{1}{2}(\frac{1}{2}z)^{-\nu} \sum_{p=0}^{\nu-1} \frac{(\nu - p - 1)!}{p!} \left(-\frac{1}{4}z^2\right)^p + (-1)^{\nu+1} \\
\times \left(\frac{z}{2}\right)^\nu \sum_{p=0}^{\infty} \frac{\left(\frac{z^2}{4}\right)^p \left[\ln\left(\frac{z}{2}\right) - \frac{1}{2}\psi(p+1) - \frac{1}{2}\psi(\nu + p + 1)\right]}{p!(\nu + k)!} \qquad (3.24)
\end{aligned}
$$

where $\psi(x)$ is the diagamma function. Since in (3.18), the order ν of $\mathcal{K}_\nu(\cdot)$ is given by $(M_j-1)-(M_{\bar{j}}-i-k)$, there are three possible cases to consider: (1)$(M_j-1)-(M_{\bar{j}}-i-k)<0$, (2)$(M_j-1)-(M_{\bar{j}}-i-k)=0$, and (3)$(M_j-1)-(M_{\bar{j}}-i-k)>0$. For the first two cases, we find that, if $I_{th}\to\infty$, $\mathcal{K}_{M_j-M_{\bar{j}}+i+k-1}(\cdot)=0$ by substituting $C=\frac{\bar{\gamma}}{G^2}$ and (3.23) into (3.24) and using the $\mathcal{K}_\nu(z)=\mathcal{K}_{-\nu}(z)$ property of $\mathcal{K}_\nu(z)$. For case (3), the second term in (3.24) converges to zero with $I_{th}\to\infty$, and only the first term left, where the non-zero terms are only when $M_{\bar{j}}-i-k=0$ and $p=0$.

Therefore, combining all these three cases, the asymptotic E2E outage probability with $I_{th}\to\infty$ is given as,

$$P_j^{out}(\gamma_{th};I_{th}\to\infty)=1-\sum_{i=2}^{M_{\bar{j}}}\sum_{l=0}^{M_{\bar{j}}-i}\frac{e^{-\frac{\gamma_{th}N_0}{P_s\lambda_{\bar{j}}}}(N_0\gamma_{th})^{M_{\bar{j}}-i}(\gamma_0\lambda_0)^l}{\lambda_{\bar{j}}^{M_{\bar{j}}-i}P_s^{M_{\bar{j}}-i}(\frac{P_p\lambda_0\gamma_{th}}{P_s\lambda_{\bar{j}}}+1)^{(l+1)}(M_{\bar{j}}-i-l)!}, \quad (3.25)$$

where $j=1,2$. According to (3.25), it is clear that as $I_{th}\to\infty$, the E2E outage probability will converge to a constant. Therefore, the diversity order is zero in this case.

3.3.4 Asymptotic E2E Outage Probability with $P_s\to\infty$

In this section, we derive the asymptotic E2E outage probabilities in high transmit power region ($P_s\to\infty$) for two cases: (1) when I_{th} is fixed and (2) $I_{th}=aP_s$, $a>0$. To simplify the notations in this section, we define $\alpha_1=\frac{\lambda_3}{I_{th}}[\lambda_1(M_1-1)+\lambda_2(M_2-1)]$, $\alpha_2=\frac{\lambda_3}{I_{th}}(P_p\lambda_0+N_0)$, and $b=\frac{\gamma_{th}N_0}{\lambda_1\lambda_2}(\alpha_1+\frac{\alpha_2}{P_s})$.

(1) Fixed I_{th}

In this case, to derive the asymptotic E2E outage probability, we first substitute (3.23) into (3.18). By doing this, we found that, the non-zero term in the sums in (3.18) is when $k=0$ due to the fact that with $P_s\to\infty$, $\left(\alpha_1+\frac{\alpha_2}{P_s}\right)\to\alpha_1$, $\left(e^{-\frac{N_0\gamma_{th}}{\lambda_{\bar{j}}P_s}}\right)\to 1$, $\left[(\frac{P_p\lambda_0\gamma_{th}}{\lambda_{\bar{j}}P_s}+1)^{(l+1)}\right]\to 1$. Therefore, we obtain the asymptotic

E2E outage probability $P_j^{out}(\gamma_{th}; P_s \to \infty)$ $(j = 1, 2)$ as,

$$P_j^{out}(\gamma_{th}; P_s \to \infty) = 1 - 2\sum_{i=2}^{M_{\bar{j}}} \frac{\left(\frac{\alpha_1 \gamma_{th} N_0}{I_{th}\lambda_1\lambda_2}\right)^{\frac{M_j + M_{\bar{j}} - i - 1}{2}}}{(M_j - 2)!(M_{\bar{j}} - i)!} \mathcal{K}_{M_j - M_{\bar{j}} + i - 1}\left(2\sqrt{\frac{\alpha_1 N_0 \gamma_{th}}{I_{th}\lambda_1\lambda_2}}\right) \tag{3.26}$$

Obviously, with fixed I_{th} the E2E outage probability converges to a constant ((3.26)) in the high P_s region. Therefore, the diversity order is zero in this case.

(2) $I_{th} = aP_s$

In this case, we obtain the asymptotic E2E outage probability $P_j^{out}(\gamma_{th}; \frac{I_{th}}{P_s} = a, P_s \to \infty)$ $(j = 1, 2)$ in the following theorem.

Theorem 3. 3. *If* $\frac{I_{th}}{P_s} = a > 0$, *(*$\min\{M_1, M_2\} - 1$*) diversity can be achieved in high transmit power region (*$P_s \to \infty$*), and the corresponding asymptotic E2E outage probability is given by,*

$$P_j^{out}(\gamma_{th}; \frac{I_{th}}{P_s} = a, P_s \to \infty) = \phi(M_1, M_2)\left(\frac{b_1}{P_s}\right)^{\min(M_1, M_2) - 1}, \tag{3.27}$$

where $b_1 = \frac{N_0 \gamma_{th} \alpha_1}{a\lambda_1\lambda_2}$ *and* $\phi(M_1, M_2)$ *is given in* (3.28).

$$\phi(M_1, M_2) = \begin{cases} -\sum_{i=1}^{M_{\bar{j}}} \frac{(-1)^{i-1}(M_j - M_{\bar{j}} - 1)!}{(M_{\bar{j}} - i)!(M_j - 2)!(i-1)!} & \text{if } M_j > M_{\bar{j}} \\ -\sum_{i=1}^{M_{\bar{j}}} \frac{(-1)^{i}[\ln\left(\frac{b_1}{P_s}\right) - \psi(1) - \psi(i)]}{(M_{\bar{j}} - i)!(M_j - 2)!(i-1)!} & \text{if } M_j = M_{\bar{j}} \\ -\sum_{i=1}^{M_{\bar{j}}} \varphi(i) & \text{if } M_j < M_{\bar{j}} \end{cases} \tag{3.28}$$

$$\varphi(i) = \begin{cases} \frac{(-1)^{M_j - M_{\bar{j}} + i}[\ln\left(\frac{b_1}{P_s}\right) - \psi(1) - \psi(M_j - M_{\bar{j}} + i)]}{(M_j - 1)!(M_{\bar{j}} - i)!(M_j - M_{\bar{j}} + i - 1)!} & \text{if } M_j - 1 > M_{\bar{j}} - i \\ \frac{2\psi(1) - \ln\left(\frac{b_1}{P_s}\right)}{(M_j - 1)!(M_{\bar{j}} - i)!} & \text{if } M_j - 1 = M_{\bar{j}} - i \\ \frac{(M_{\bar{j}} - M_j - i)!}{(M_j - 2)!(M_{\bar{j}} - i)!} & \text{if } M_j - 1 < M_{\bar{j}} - i \end{cases}$$

Proof. Without loss of generality, the outage probability at SU_1 is used here. We first substitute $I_{th} = aP_s$ into (3.26), which results in,

$$P_1^{out}(\gamma_{th}) = 1 - 2\sum_{i=2}^{M_2} \frac{(\frac{b_1}{P_s})^{\frac{M_1 + M_2 - i - 1}{2}}}{(M_1 - 2)!(M_2 - i)!} \mathcal{K}_{M_1 - M_2 + i - 1}\left(2\sqrt{\frac{b_1}{P_s}}\right). \tag{3.29}$$

To derive $P_1^{out}(\gamma_{th}; \frac{I_{th}}{P_s} = a, P_s \to \infty)$ from (3.29), the expansion (3.24) of $\mathcal{K}_\nu(\cdot)$ is also required. Besides, we also need to consider three cases: (1) $M_1 > M_2$, (2)$M_1 = M_2$, and (3)$M_1 < M_2$.

Case (1): If $M_1 = M_2$, $M_1 - 1 - M_2 + i > 0$ always holds. Therefore, after applying (3.24), the lowest term of $\frac{1}{P_s}$ is given by $(M_2 - 1)$ when the index p in the second term of (3.24) is zero.

Case (2): If $M_1 > M_2$, $M_1 - 1 - M_2 + i > 0$ still always holds, and the lowest term of $\frac{1}{P_s}$ is given by $(M_2 - 1)$ when the index p in the first term of (3.24) takes value of $i - 1$.

Case (3): If $M_1 < M_2$, there are two possible cases depending on the value of the index i in (3.29): (a)$M_1 - 1 - M_2 + i \geq 0$ and (b) $M_1 - 1 - M_2 + i < 0$. For case (a), the lowest term of $\frac{1}{P_s}$ is given by $(M_1 - 1)$ with the index p in the second term of (3.24) being zero. For case (b), using the $\mathcal{K}_v(\cdot) = \mathcal{K}_{-v}(\cdot)$ property, the lowest term of $\frac{1}{P_s}$ is given by $(M_2 - 1)$ with the index p in the first term of (3.24) being $i - 1$.

Therefore, Theorem 3. 3 is obtained by collecting all the analysis for the three cases above. □

Comparatively, in this case, the underlay setup is equivalent to the conventional two-way relay networks consisting of two multi-antenna terminals and one single-antenna fixed gain AF relay [84]. In [84], MRT/MRC are applied at the two terminals to exploit the channel $\boldsymbol{g}_j$ $(j = 1, 2)$ and a diversity of order $\min(M_1, M_2)$ is achieved in high transmit power region. But in our study, ZFB-MRT/MRC applied at the two terminals will cause the diversity loss since only part of $\boldsymbol{g}_j$ $(j = 1, 2)$, which is orthogonal to the interference channels $\boldsymbol{h}_j$ and $\boldsymbol{f}_j$ $(j = 1, 2)$ is exploited. Therefore, in our study the diversity order is $\min(M_1, M_2) - 1$. In other words, the orthogonality requirement to enforce ZFB results in a small loss of degrees of freedom.

3.3.5 Results and Discussions

This section provides numerical results to validate the preceding analysis. The parameters N_0 and P_p are set to $0\,\text{dBm}$ and $10\,\text{dBm}$, respectively. And the path loss exponent ω is set to 3.5. In order to show the impact of the distance between

the relay and the primary nodes, we also assume that $d_{\mathrm{SU}_j,\mathrm{R}} = d$ $(j = 1, 2)$ and $d_{\mathrm{A,R}} = d_{\mathrm{R,B}} = d_1$.

Figs. 3.2 and 3.3 show the E2E outage probabilities as a function of the transmit power P_s with $d_1 = d$ and $d_1 = 1.5d$ for $M_1 = M_2 = 16$ and $M_1 = 8, M_2 = 16$, respectively. For comparisons, simulation results of CSI-Assisted gain are provided as well, where R adapts its relay gain via (3.9). It is shown that fixed gain outperforms CSI-Assisted gain. This is because with CSI-Assisted gain, the relay gain is chosen such that the interference power at B below I_{th} in each transmission, while fixed gain considers the average interference power. It is also shown that when R is located further ($d_1 = 1.5d$) from A and B, lower outage is achieved.

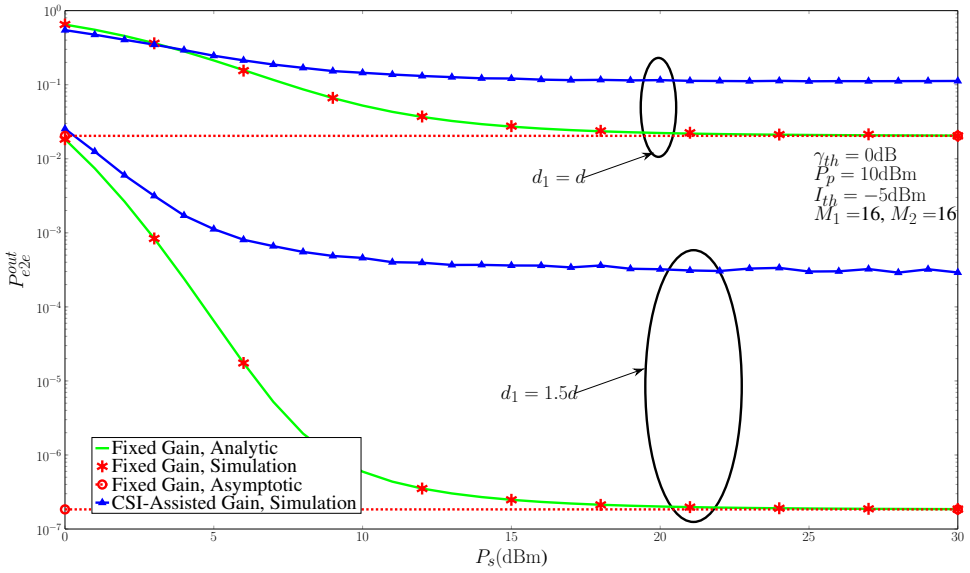

Figure 3.2: P_{e2e}^{out} v.s. P_s with $I_{th} = -5$ dBm, $M_1 = M_2 = 16$

Figs. 3.2 and 3.3 also show that employing ZFB-MRT/MRC, the E2E outage probabilities of underlay two-way relay networks can be lower than 10^{-4} with fixed-gain relays, 16 antennas at both secondary terminals and $d_1 = 1.5d$, respectively. Therefore, this shows the effectiveness of beamforming in addressing the bi-directional interference issues and improving the reliability of under two-way relay networks.

Another observation from Fig. 3.3 is that when $P_s < 20$ dBm, the E2E outage probability along the direction from the node with more antennas to the one with less antennas, e.g., $\mathrm{SU}_2 \rightarrow \mathrm{SU}_1$, outperforms the other direction. Therefore, we

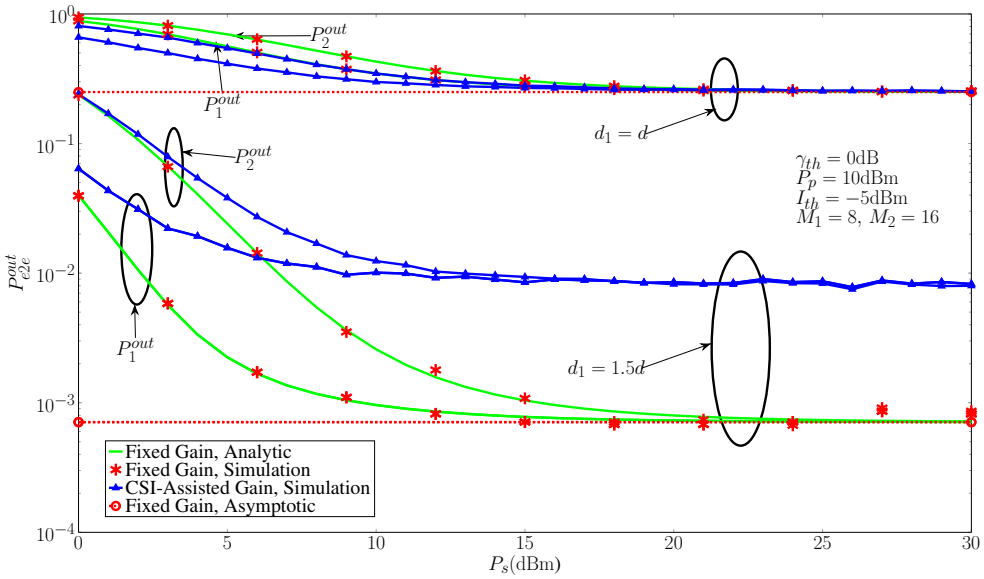

Figure 3.3: P_{e2e}^{out} v.s. P_s with $I_{th} = -5$ dBm,$M_1 = 8, M_2 = 16$

claim that equipping more antennas at the transmitter benefit more than equipping more antennas at the receiver. This is reasonable due to the following reason. Since ZFB-MRC nullifies the A-to-SU$_j$ ($j = 1, 2$) interferences in the second time slot, the outage performance is dominated by the ratio of the signal power to the A-to-R interference power in the first time slot. And with ZFB-MRT, the secondary terminals can transmit with their maximum power since the SU$_j$-to-B ($j = 1, 2$) interferences are nullified and thus with more antennas at the transmitter, higher signal-to-interference-ratio at the relay is achieved. However, when increasing P_s, the outage probabilities along both directions converge to the same outage floor.

Fig. 3.4 plots the E2E outage probabilities as functions of I_{th} for $M_1 = M_2 = 8$ and $M_1 = 8,\ M_2 = 16$, respectively. Note that, when $I_{th} \leq 10$ dBm, equipping more antennas at the receiver results in lower outage probability, e.g., P_2^{out} in $M_1 = 8, M_2 = 16$ outperforms P_2^{out} in $M_1 = M_2 = 8$. However, with increasing I_{th}, the outage probabilities at SU$_2$s in both setups converge to the same outage probability floor since both SU$_1$s are equipped with 8 antennas.

Fig. 3.5 verifies Theorem 3. 3 with I_{th} set as $0.001P_s$. Note that, the E2E outage probabilities at SU$_1$ and SU$_2$ overlap in both symmetric ($M_1 = M_2 = 8$) and asymmetric ($M_1 = 8,\ M_2 = 16$) systems.

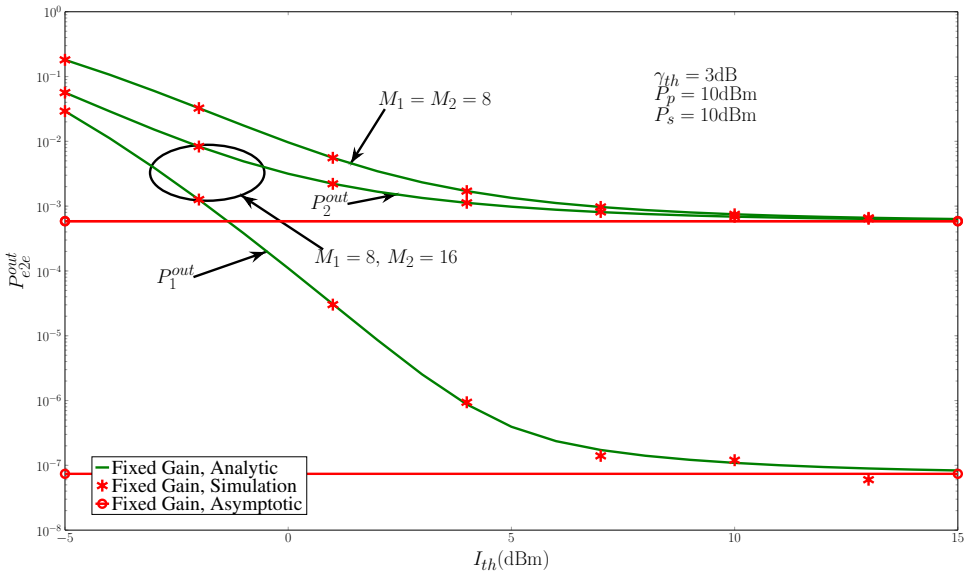

Figure 3.4: P_{e2e}^{out} v.s. I_{th} with $d_1 = 1.5d$ and $P_s = 10\,\text{dBm}$

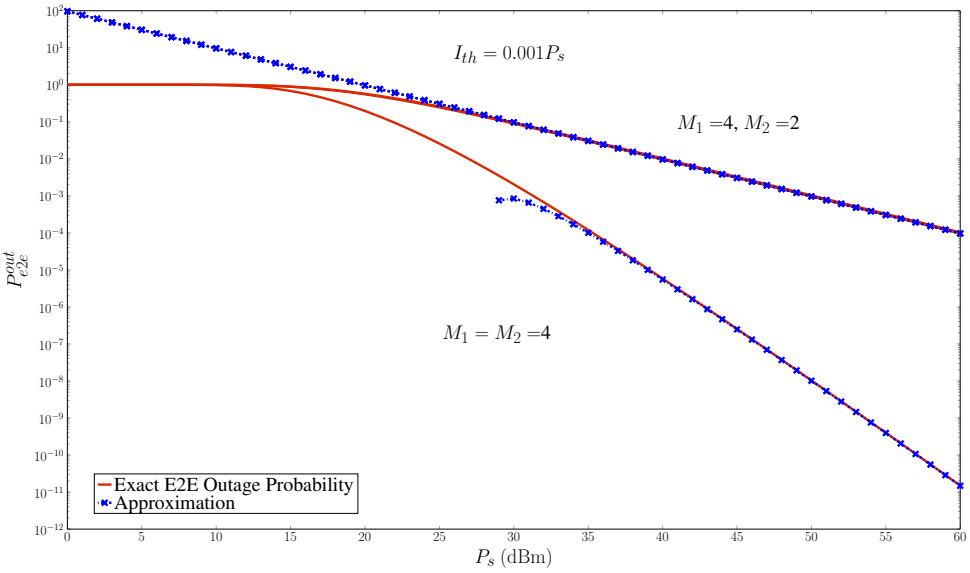

Figure 3.5: P_{e2e}^{out} v.s. P_s with $d_1 = 1.5d$ and $I_{th} = 0.001P_s$

3.4 Two-way Outage Probability

Since the secondary terminals SU_1 and SU_2 exchange information simultaneously via two-way relay, the successful transmission requires that both SU_1 and SU_2 can receive information from each other successfully. Therefore, we define the two-way outage probability ($P_{two-way}^{out}$) as the probability that the minimum of the two SINRs at the two secondary nodes is below the threshold (γ_{th}).

$$P_{two-way}^{out} = \Pr[\min(S_1,\, S_2) \leq \gamma_{th}] \tag{3.30}$$

According to (3.12), S_1 and S_2 are dependent via $\|\boldsymbol{g}_1\|^2$, $\|\boldsymbol{g}_2\|^2$, and γ_3. Moreover, each of S_1 and S_2 includes independent variables $\rho_{\boldsymbol{h}_j}$ and $\rho_{\boldsymbol{f}_j}$ ($j = 1,\, 2$). Thus, $P_{two-way}^{out}$ appears mathematical intractable. Therefore, only simulation results are given in the following section.

3.4.1 Simulation Results and Discussions

This section provides simulation results to analyse the two-way outage probability in the underlay two-way relay network Fig. 3.1. Similar to Section 3.3.5, the parameters N_0 and P_p are set to $0\,$dBm and $10\,$dBm, respectively. And the two-way outage probabilities are obtained through 10^{10} channel realizations.

Fig. 3.6 shows the outage probability as functions of the transmit power (P_s) with the interference temperature limit I_{th} set to $3\,$dBm under symmetric ($M_1 = M_2 = 8$) and asymmetric ($M_1 = 8$, $M_2 = 16$) system configurations, respectively. For comparison, the E2E outage probabilities at the two secondary terminals are shown as well.

Similar to the E2E outage probabilities, with the transmit power (P_s) being large enough, e.g., over $20\,$dBm, the two-way outage probability converges to a constant due to the impact of the interference constraint. Moreover, as shown in Fig. 3.6, it overlaps the E2E outage probabilities in symmetric system configurations. In asymmetric system configurations, it coincides with the communication along the direction from the terminal with less antennas to the terminal with more antennas, e.g., along the $SU_1 \rightarrow SU_2$ direction, which is the worse one between the two directions. Therefore, cognitive two-way relay networks is similar to conventional

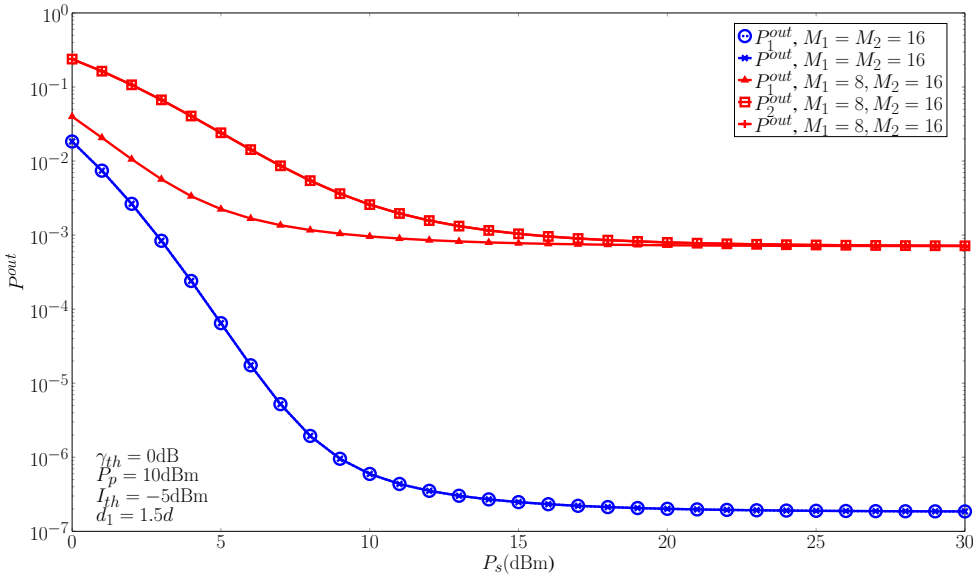

Figure 3.6: Two-way Outage Probability v.s. P_s with $I_{th} = -5$ dBm

cognitive two-way relay networks in the sense that the two-way outage probability is determined by the E2E outage probability of the weakest communication link [146]. This suggests us to develop beamforming algorithms to maximize the worse SINR in the next two chapters.

Fig. 3.7 shows the two-way outage probability as functions of the interference temperature limit (I_{th}) with the transmit power P_s set to 3 dBm, 10 dBm, and 20 dBm, respectively. Simulations are run with both symmetric ($M_1 = M_2 = 8$) and asymmetric ($M_1 = 8$, $M_2 = 16$) system configurations.

Note that, as shown in Fig. 3.7, with the same transmit power (P_s), in low interference temperature limit region, e.g., $I_{th} \leq 5$ dBm, the two-way outage probability with $M_1 = 8$, $M_2 = 16$ outperforms that with $M_1 = M_2 = 8$. However, these two two-way outage probabilities converge together as the interference temperature limit (I_{th}) increases. This means that, equipping more antennas at one secondary terminal only benefits in low interference temperature limit region.

3.5 Conclusion

This chapter characterized the outage performance of ZFB-MRT/MRC in underlay two-way relay networks when both path loss effect and small-scale fading were

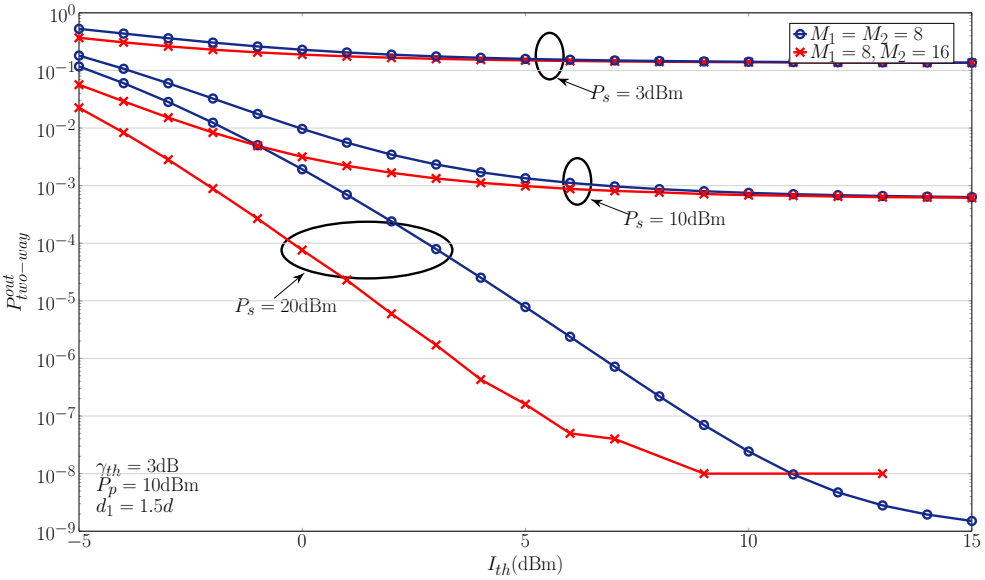

Figure 3.7: Two-way Outage Probability v.s. I_{th}

taken into consideration. While eliminating the SU$_j$ $\rightarrow$B and A$\rightarrow$SU$_j$ ($j = 1, 2,$) interferences completely, ZFB-MRT/MRC does not use the fact that the primary receiver can tolerate interference as much as the interference temperature limit. Therefore, it is not an optimal underlay beamforming algorithm. However, by investigating its outage performance, the following insights are obtained.

1. The location of the relay significantly impacts the outage. Therefore, the choice of relocation for the relays from the primary nodes is highly beneficial. Thus, if relay selection is possible from a pool of available nodes, which have the same distance from the underlay terminals, the node with the longest distance from the primary nodes should be selected.

2. With $I_{th} \rightarrow \infty$ and fixed P_s or $P_s \rightarrow \infty$ and fixed I_{th}, the diversity order is zero. But if $\frac{I_{th}}{P_s}$ is fixed, a diversity of order $(\min(M_1, M_2) - 1)$, where M_j ($j = 1, 2$) is the number of antennas at the secondary terminal SU$_j$, is achieved when $P_s \rightarrow \infty$.

3. Simulation results showed that even with sub-optimal beamforming, ZFB-MRT/MRC, the E2E outage probabilities of underlay two-way relay networks can be lower than 10^{-3} and 10^{-4} for CSI-assisted and fixed-gain re-

lays, respectively. Therefore, beamforming is effective in addressing the bi-directional interference issues and improving the reliability of under two-way relay networks.

4. Simulation results also showed that cognitive two-way relay networks are similar to conventional non-cognitive two-way relay networks in the sense that the two-way outage probability is determined by the E2E outage probability of the weakest communication link [146]. This promotes us to develop beamforming algorithms to maximize the worse SINR in the next two chapters.

$\sim$

Chapter 4

Cognitive Beamforming in Underlay Two-Way Relay Networks with Multi-Antenna Terminals

Chapter 3 has shown that for an underlay two-way relay and two multi-antenna terminals, sub-optimal beamforming (ZFB-MRT/MRC) improves outage probabilities, e.g., as low as 10^{-3} with a CSI-assisted relay and 10^{-4} with a fixed-gain relay. Thus, even better performance can be expected from optimal beamforming algorithms. Therefore, this chapter develops optimal transmitter/receiver design, e.g., transmit powers, and Tx and Rx beamforming vectors at the two secondary terminals to improve the outage performance and the reliability and capacity considering both P2S and S2P interferences. The Rx beamforming vectors are found in closed-form, while the transmit powers and Tx beamforming vectors are derived by the proposed optimal algorithm (JTBPA). To reduce the computational complexity, the use of sub-optimal Tx beamforming algorithms, MRT and ZFB-MRT, are proposed, and the transmit powers are optimized to partially recover the performance losses due to the use of sub-optimal beamforming vectors[1].

4.1 Introduction

Although it has been shown in Chapter 3 that, with ZFB-MRT/MRC, the outage probabilities of underlay two-way relay networks can be improved, this improve-

[1] *A version of this chapter has been submitted to IEEE Trans. Cognitive Commun. and Network (2015).*

ment is limited due to not exploiting the interference temperature limit. That is, the weighting coefficients of ZFB-MRT are computed to make the S2P interference (I_{S2P}) identical to zero. However, the primary receiver can tolerate $I_{S2P} \leq I_{th}$. Therefore, more sophisticated optimal beamforming algorithms are needed to further improve the outage probabilities and thus the reliabilities of underlay two-way relay networks.

4.1.1 Prior Related Research

As mentioned before, underlay networks suffer from the bi-directional (S2P and P2S) interferences, and thus their communication coverage range is shortened and the capacity is degraded. To address the S2P interferences, power allocation, i.e. adjusting the power levels at various nodes, has been studied in [128, 129], and various beamforming algorithms have been studied extensively based on different criteria [32–40]. For a single secondary transmitter-receiver pair, optimal beamforming vectors were derived by using a rotation matrix to maximize the received SINR [35], and by using a bi-section search and an interior-point algorithm to maximize the energy efficiency [40]. For a secondary network consisting of one secondary base station and multiple secondary receivers, beamforming algorithms were developed in [32–34, 36–38]. [32] derived orthogonal beamforming vectors by the Gram-Schmidt algorithm, while [33, 34] generated the optimal beamforming vectors by using an interior-point algorithm to maximize the number of nodes served under the QoS constraint [33], and to maximize the worse received SINR at multiple secondary receivers [34]. [37] also developed the optimal beamforming vectors by using an interior-point algorithm for: 1) the minimization of the transmit power; 2) the minimization of the interference to primary nodes; 3) the maximization of the worse received SNR at the secondary nodes; and 4) the minimization of a weighted sum of interference and minimum SNR. [36] derived the optimal beamforming vectors through a convex optimization based on the Karush-Tuhn-Tucker conditions to maximize the sum rate of the secondary receivers. [38] derived the optimal beamforming vectors by using the uplink-downlink duality and the subgradient method to maximize the worse SINR of some secondary nodes under the

QoS constraints of other secondary nodes. Besides, beamforming in secondary networks consisting of multiple secondary base stations was investigated in [39] via the generalized Benders decomposition to minimize the overall transmit power. It is worth to mention that, most of the studies did not consider the P2S interference.

Then, to both enlarge the limited coverage and mitigate the S2P interferences, both beamforming and AF relaying were studied in [41–47]. Beamforming at the multi-antenna secondary base station and the one-way relay was studied to maximize the data rate [41]. Distributed beamforming via multiple cooperative single-antenna AF relay nodes were investigated in [42–46]. Of these, [42–45] maximized the received SNR or minimized the interference at the primary receivers for one-way relays and [46] considered two-way relays. A sub-optimal beamforming, MRT, for an underlay multi-antenna transmitter-receiver pair and a single-antenna one-way relay node was studied in [47]. However, all these studies neglected the P2S interferences as well.

4.1.2 Motivation and Contribution

Since previous research treated one-way relays and neglected the P2S interferences, the performance improvements with two-way relay and optimal beamforming have not been determined. Thus, this chapter investigates beamforming considering both P2S and S2P interferences in an underlay two-way relay network of two multi-antenna secondary terminals (SU_1 and SU_2) and a single-antenna half-duplex two-way AF relay. Particularly, cognitive beamforming vectors and transmit powers for SU_1 and SU_2 are developed to maximize the worse of the two received SINRs at SU_1 and SU_2. This worse SINR maximization is selected here as the criterion because it determines the two-way outage probability [146]. And the cognitive beamforming involves both Tx beamforming and Rx beamforming. The contributions of this chapter are listed as follows.

1. The closed-form optimal Rx beamforming vectors are derived to mitigate the primary-to-SU_j ($j = 1, 2$) interferences [72].

2. The optimal transmit powers and Tx beamforming vectors are jointly derived

by our proposed bi-section search based optimal algorithm (JTBPA) [72]. In each iteration, JTBPA equivalently converts the non-convex NP-hard feasibility problem into two interference minimization problems, which can be solved by semidefinite relaxation (SDR).

3. To reduce the computational complexity required by JTBPA, optimal power allocation is developed when two low-complexity sub-optimal Tx beamforming algorithms, MRT and ZFB-MRT, are employed [72].

4. An assessment of the relative merits of the algorithms proposed in this chapter is provided through extensive simulation and numerical results. For instance, JTBPA increases the achievable SINR by as mush as $20\,\text{dB}$ compared with no Tx beamforming and equal power allocation (EPA). Moreover, ZFB-MRT with and without optimal power allocation has only $1\,\text{dB}$ and $2\,\text{dB}$ gap from JTBPA, respectively, while their required running time is only 1% of that required by JTBPA.

This chapter is organized as follows. Section 4.2 introduces the details of the system configuration and signal flow, then formulates the optimization problem. Section 4.3 derives the optimal Rx beamforming vectors and relay gain. Section 4.4 develops the optimal Tx beamforming and power allocation algorithm (JTBPA) and the optimal power allocation for sub-optimal Tx beamforming algorithms. Section 4.5 conducts simulations to assess our proposed algorithms. And Section 4.6 concludes this chapter.

4.2 System Configuration, Signal Flow and Problem Formulation

System Configuration

The same system configuration in Chapter 3 is adopted in this chapter (Fig. 4.1), where the secondary network consisting of one single-antenna AF relay node (R) and two multi-antenna terminals (SU_1 and SU_2) coexists with the primary network

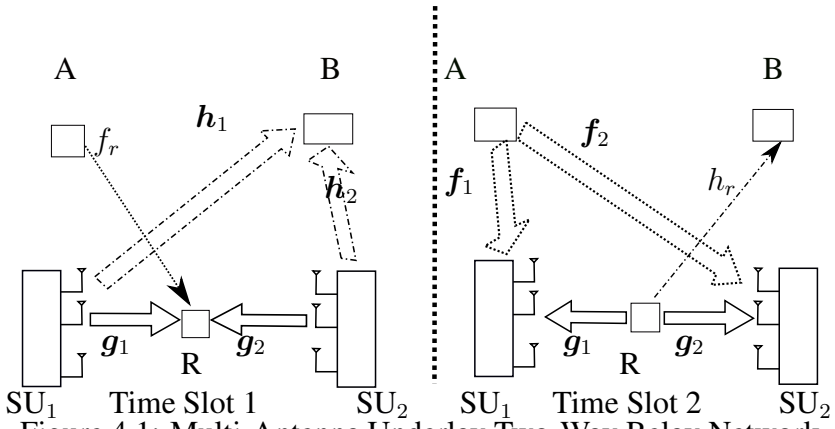

Figure 4.1: Multi-Antenna Underlay Two-Way Relay Network

of one single-antenna transmitter-receiver pair (A-B). SU_1 and SU_2 are equipped with M_1 and M_2 antennas, respectively. All nodes are half-duplex.

We assume flat fading and identically and independently $\mathcal{CN}(0,1)$-distributed channel coefficients. This chapter uses the following notations. $\boldsymbol{g}_j \in \mathbb{C}^{M_j \times 1}$ ($j = 1, 2$) are the reciprocal channels between SU_j and the relay R. $\boldsymbol{h}_j \in \mathbb{C}^{M_j \times 1}$ ($j = 1,\ 2$) and $\boldsymbol{h}_r \in \mathbb{C}$ are the interference channels from SU_j and R to B, respectively. $\boldsymbol{f}_j \in \mathbb{C}^{M_j \times 1}$ ($j = 1,\ 2$) and $f_r \in \mathbb{C}$ are the interference channels form A to SU_j and R, respectively.

We assume that the instantaneous CSI of all the channels is perfectly known at every node. This perfect CSI assumption may be realized by involving a central control device and has also been adopted in [42–45]. This device collects CSIs, which are obtained through an appropriate channel estimation scheme [118, 119] at nodes in Fig. 4.1, and then broadcasts them out before each round of mutual information exchange between SU_1 and SU_2, e.g., every $4\,\mu$s (the symbol duration in WLAN networks) [158]. The overhead for this CSI collection and broadcast process in real applications increases linearly with the number of antennas and the required updating rate. The updating rate may be reduced if the nodes are not mobile. It also depends on how the CSI is collected and broadcast. For instance, if the estimated CSIs are directly communicated, the overhead will depend on the accuracy required to represent the complex channel gains. But if a codebook [159],

which is a table of quantized CSIs and each CSI associated with a reference number, is used and shared between nodes in the system, the central control device only collects and broadcasts this reference number and thus the overhead will be reduced. Under this perfect CSI assumption, both SU_j ($j = 1, 2$) and the relay R can calculate all the transmit parameters, such as the beamforming vectors, transmit powers and relay gain.

Moreover, AWGN noise of zero mean and σ^2 variance are assumed at every receiving node, and unit symbol power is assumed as well. As in [47, 69, 132], perfect time synchronization is assumed between the primary and secondary networks, which will lead to the maximum interference power.

Signal Flow

When using the two-slot two-way relay (Fig. 4.1), SU_j ($j = 1, 2$) transmits the signal $\sqrt{P_j}\boldsymbol{m}_j s_j$ to the relay R in the first time slot, where P_j is the transmit power, s_j is the symbol to be transmitted, and $\boldsymbol{m}_j \in \mathbb{C}^{M_j \times 1}$, $\|\boldsymbol{m}_j\|^2 = 1$, is the normalized Tx beamforming vector. Simultaneously, A transmits $x^{(1)}$ to B with transmit power P_P. Therefore, the signal y_r and the interference $x_{int}^{(1)}$ received at the relay R and B are given as,

$$y_r = \sqrt{P_1}\boldsymbol{g}_1^T\boldsymbol{m}_1 s_1 + \sqrt{P_2}\boldsymbol{g}_2^T\boldsymbol{m}_2 s_2 + \sqrt{P_p} f_r x^{(1)} + n_r, \tag{4.1}$$

$$x_{int}^{(1)} = \sqrt{P_1}\boldsymbol{h}_1^T\boldsymbol{m}_1 s_1 + \sqrt{P_2}\boldsymbol{h}_2^T\boldsymbol{m}_2 s_2, \tag{4.2}$$

where $n_r \in \mathbb{C}$ is the AWGN at the relay.

In the second time slot, A transmits $x^{(2)}$ to B with transmit power P_P. Meanwhile, the relay R multiplies its received signal y_r with a complex relay gain $Ge^{j\theta}$ and broadcasts the resultant. Since only the signal power levels are considered, e.g., SINR and interference power at B, the phase θ component in the relay gain is irrelevant (see (4.6) and (4.8)). For this reason, we set $\theta = 0$ and model the relay gain as a positive real-valued scale G. Then the interference signal $x_{int}^{(2)}$ at B and the

signal vector $\boldsymbol{y}_j$ ($j = 1,\ 2$) received at SU$_j$ are given as,

$$x_{int}^{(2)} = h_r G y_r, \tag{4.3}$$

$$\begin{aligned}\boldsymbol{y}_j = &\underbrace{\sqrt{P_j} G \boldsymbol{g}_j \boldsymbol{g}_j^T \boldsymbol{m}_j s_j}_{\text{Self-Interference}} + \underbrace{\sqrt{P_{\bar{j}}} G \boldsymbol{g}_j \boldsymbol{g}_{\bar{j}}^T \boldsymbol{m}_{\bar{j}} s_{\bar{j}}}_{\text{Signal}} \\ &+ \underbrace{\sqrt{P_p} G \boldsymbol{g}_j f_r x^{(1)} + \sqrt{P_p} \boldsymbol{f}_j x^{(2)}}_{\text{P2S Interference}} + \underbrace{G \boldsymbol{g}_j n_r + \boldsymbol{n}_j}_{\text{Noise}},\end{aligned} \tag{4.4}$$

where $\boldsymbol{n}_j \in \mathbb{C}^{M_j \times 1}$ is the AWGN vector at SU$_j$, and $\bar{j} = 1$, if $j = 2$, and vise versa.

Knowing $\boldsymbol{g}_j$, $\boldsymbol{m}_j$ and G, SU$_j$ ($j = 1,\ 2$) can subtract the self-interference part $\sqrt{P_j} G \boldsymbol{g}_j \boldsymbol{g}_j^T \boldsymbol{m}_j s_j$ from (4.4) perfectly and then apply the Rx beamforming. Therefore, after the self-interference cancellation and Rx beamforming, the resulting signal $\hat{y}_j$ is represented as,

$$\begin{aligned}\hat{y}_j = &\underbrace{\sqrt{P_{\bar{j}}} G \boldsymbol{d}_j^T \boldsymbol{g}_j \boldsymbol{g}_{\bar{j}}^T \boldsymbol{m}_{\bar{j}} s_{\bar{j}}}_{\text{Signal}} + \underbrace{\sqrt{P_p} G \boldsymbol{d}_j^T \boldsymbol{g}_j f_r x^{(1)} + \sqrt{P_p} \boldsymbol{d}_j^T \boldsymbol{f}_j x^{(2)}}_{\text{P2S Interference}} \\ &+ \underbrace{G \boldsymbol{d}_j^T \boldsymbol{g}_j n_r + \boldsymbol{d}_j^T \boldsymbol{n}_j}_{\text{Noise}},\end{aligned} \tag{4.5}$$

where $\boldsymbol{d}_j \in \mathbb{C}^{M_j \times 1}$ ($j = 1,\ 2$) is the Rx beamforming vector satisfying $\|\boldsymbol{d}_j\|^2 = 1$.

Then, from (4.5), the instantaneous SINR at SU$_j$ ($j = 1,\ 2$) can be calculated as,

$$\text{SINR}_j = \frac{P_{\bar{j}} G^2 \boldsymbol{d}_j^H \boldsymbol{G}_j \boldsymbol{d}_j \boldsymbol{m}_{\bar{j}}^H \boldsymbol{G}_{\bar{j}} \boldsymbol{m}_{\bar{j}}}{\boldsymbol{d}_j^H (G^2 \Delta \boldsymbol{G}_j + \boldsymbol{F}_j) \boldsymbol{d}_j}, \tag{4.6}$$

where $\boldsymbol{G}_j = \boldsymbol{g}_j^* \boldsymbol{g}_j^T$, $\Delta = P_p |f_r|^2 + \sigma^2$, and $\boldsymbol{F}_j = P_p \boldsymbol{f}_j^* \boldsymbol{f}_j^T + \sigma^2 \boldsymbol{I}_{M_j}$. And from (4.2) and (4.3), the interference powers at B in time slot 1 and 2 are calculated as,

$$P_I^{(1)} = P_1 \boldsymbol{m}_1^H \boldsymbol{H}_1 \boldsymbol{m}_1 + P_2 \boldsymbol{m}_2^H \boldsymbol{H}_2 \boldsymbol{m}_2, \tag{4.7}$$

$$P_I^{(2)} = |h_r|^2 G^2 (P_1 \boldsymbol{m}_1^H \boldsymbol{G}_1 \boldsymbol{m}_1 + P_2 \boldsymbol{m}_2^H \boldsymbol{G}_2 \boldsymbol{m}_2 + \Delta), \tag{4.8}$$

where $\boldsymbol{H}_j = \boldsymbol{h}_j^* \boldsymbol{h}_j^T$ ($j = 1,\ 2$).

Problem Formulation

As mentioned in Section 4.1, we aim at deriving the relay gain G, transmit powers P_j ($j = 1, 2$), Tx beamforming vectors $\boldsymbol{m}_j$ ($j = 1, 2$) and Rx beamforming vectors $\boldsymbol{d}_j$ ($j = 1, 2$) to maximize the worse SINR at the two terminals. Recall that, since

the secondary nodes work in the underlay mode, their interference received at B ($P_I^{(1)}$ and $P_I^{(2)}$) must be lower than the interference temperature limit (I_{th}). Meanwhile, we restrict the transmit powers P_j ($j = 1, 2$) under their maximum values P_j^{max}. Putting all these conditions together, the optimization problem is formulated as,

$$\begin{aligned}
\text{(P-4.1)} \quad \max_{P_j, G, \boldsymbol{m}_j, \boldsymbol{d}_j} \quad & \min\{\text{SINR}_1, \text{SINR}_2\} \\
\text{s. t.} \quad & \|\boldsymbol{m}_j\|^2 = 1,\ \|\boldsymbol{d}_j\|^2 = 1, && \text{(4.9a)} \\
& P_1 \le P_1^{max},\ P_2 \le P_2^{max}, && \text{(4.9b)} \\
& P_I^{(1)} \le I_{th},\ P_I^{(2)} \le I_{th}, && \text{(4.9c)} \\
& j = 1, 2.
\end{aligned}$$

There are two ways to implement this in a practical setup. First, SU_1 or SU_2 can solve (P-4.1) using our proposed algorithms and then broadcast the results to the relay and the other terminal. This method, however, will introduce additional overhead, time delay and quantization errors when sending the complex beamforming vectors. Second, all the nodes, the relay R and the terminals SU_j ($j = 1, 2$), individually solve (P-4.1) prior to a data exchange session (e.g., $4\,\mu$s in WLAN networks) [158].

4.3 Optimal Relay Gain and Rx Beamforming Vectors

In this section, we derive the optimal relay gain G and Rx beamforming vectors $\boldsymbol{d}_j$ ($d = 1, 2$) as follows. Since among the constraints (4.9a)-(4.9c), only $P_I^{(2)} \le I_{th}$ depends on the relay gain G, when the optimal value of (P-4.1) is achieved, $P_I^{(2)} = I_{th}$ must hold. Because otherwise, if (P-4.1) achieves its optimal value SINR^o and $P_I^{(2)} < I_{th}$, we can always find a $\hat{G} > G$ such that $P_I^{(2)} = I_{th}$, and this $\hat{G}$ will increase both SINR_1 and SINR_2, which will leads to a worse SINR $\min(\text{SINR}_1,\text{SINR}_2)$ larger than SINR^o. Therefore, G should be chosen as,

$$G = \sqrt{\frac{I_{th}}{|h_r|^2(P_1 \boldsymbol{m}_1^H \boldsymbol{G}_1 \boldsymbol{m}_1 + P_2 \boldsymbol{m}_2^H \boldsymbol{G}_2 \boldsymbol{m}_2 + \Delta)}}. \tag{4.10}$$

Then if we substitute (4.10) into (4.6), SINR$_j$ ($j = 1, 2$) can be reformulated as,

$$\text{SINR}_j = \frac{P_{jR}\gamma_{Rj}}{P_{1R} + P_{2R} + (\gamma_{Rj} + 1)\Delta}, \tag{4.11}$$

where $P_{jR} = P_j \boldsymbol{m}_j^H \boldsymbol{G}_j \boldsymbol{m}_j$, and $\gamma_{Rj} = \frac{I_{th}\boldsymbol{d}_j^H \boldsymbol{G}_j \boldsymbol{d}_j}{|h_r|^2 \boldsymbol{d}_j^H \boldsymbol{F}_j \boldsymbol{d}_j}$ ($j = 1, 2$) are the signal powers from SU$_j$ to R and the SINR from R to SU$_j$, respectively. Then, the following lemma is obtained.

Lemma 4. 1. *SINR$_j$ in* (4.11) *increases with the increase in* γ_{Rj}.

Proof. See Appendix B.1 for proof. □

Lemma 4.1 implies that the optimal value of (P-4.1) is achieved when γ_{Rj} ($d = 1, 2$), which is determined by $\boldsymbol{d}_j$ only, achieves its maximum value. Thus, the Rx beamforming vectors $\boldsymbol{d}_j$ ($j = 1, 2$) should be chosen to maximize γ_{Rj}. It is known that the generalized Rayleigh-Ritz ratio in the form as $\frac{\boldsymbol{d}_j^H \boldsymbol{G}_j \boldsymbol{d}_j}{\boldsymbol{d}_j^H \boldsymbol{F}_j \boldsymbol{d}_j}$ is maximized when $\boldsymbol{d}_j$ is computed via (4.12) by exploiting the definition of $\boldsymbol{G}_j$ [149]. Apparently, according to (4.12), the selection of the Rx beamforming vectors ($\boldsymbol{d}_j$, $j = 1, 2$) is independent of the selection of P_j and $\boldsymbol{m}_j$ ($j = 1, 2$). Once $\boldsymbol{d}_j$ ($j = 1, 2$) is determined, the Sherman-Morrison formula [150] can be applied to compute the maximum value γ_{Rj}^{max} as (4.13).

$$\boldsymbol{d}_j = \frac{(P_p \boldsymbol{f}_j^* \boldsymbol{f}_j^T + \sigma^2 I_{M_j})^{-1} \boldsymbol{g}_j^*}{|(P_p \boldsymbol{f}_j^* \boldsymbol{f}_j^T + \sigma^2 I_{M_j})^{-1} \boldsymbol{g}_j^*|}. \tag{4.12}$$

$$\gamma_{Rj}^{max} = \frac{I_{th}}{|h_r|^2}(\|\boldsymbol{g}_j\|^2 - \frac{P_p |\boldsymbol{f}_j^T \boldsymbol{g}_j^*|^2}{\sigma^2(\sigma^2 + P_p \|\boldsymbol{f}_j\|^2)}) \tag{4.13}$$

For simplicity, we denote γ_{Rj}^{max} in (4.13) as γ_j ($j = 1, 2$) hereafter and reformulate (P-4.1) into,

$$\text{(P-4.2)} \quad \max_{P_1, P_2, \boldsymbol{m}_1, \boldsymbol{m}_2} \quad \min\{\frac{\gamma_1 P_{2R}}{P_{1R} + P_{2R} + (\gamma_1 + 1)\Delta}, \frac{\gamma_2 P_{1R}}{P_{1R} + P_{2R} + (\gamma_2 + 1)\Delta}\}$$

$$\text{s. t.} \quad \|\boldsymbol{m}_j\|^2 = 1,\ j = 1,\ 2, \tag{4.14a}$$

$$P_1 \leq P_1^{max},\ P_2 \leq P_2^{max}, \tag{4.14b}$$

$$P_1 \boldsymbol{m}_1^H \boldsymbol{H}_1 \boldsymbol{m}_1 + P_2 \boldsymbol{m}_2^H \boldsymbol{H}_2 \boldsymbol{m}_2 \leq I_{th}. \tag{4.14c}$$

which is an optimization problem with regard to the transmit powers $P_j (j = 1, 2)$ and Tx beamforming vector $\boldsymbol{m}_j$ $(j = 1, 2)$. The solution to (P-4.2) will be developed in the next section.

4.4 Tx Beamforming and Power Allocation

In this section, we first develop the optimal algorithm (JTBPA) for (P-4.2) to jointly derive the optimal Tx beamforming vectors $\boldsymbol{m}_j$ and transmit powers P_j $(j = 1, 2)$. Then, to reduce the high computational complexity, we also propose to use low-complexity, sub-optimal Tx beamforming algorithms ZFB-MRT and MRT. In this case, $\boldsymbol{m}_j$ $(j = 1, 2)$ has closed-form solution and we then optimize P_j $(j = 1, 2)$ to partially mitigate the performance losses due to the suboptimal $\boldsymbol{m}_j$ $(j = 1, 2)$.

4.4.1 Optimal Joint Tx Beamforming and Power Allocation

Since (P-4.2) is a non-convex optimization problem, we start with the following lemma, which helps us to find the optimal Tx beamforming vectors and power allocation.

Lemma 4. 2. *There exists an optimal solution* $(P_1^o,\ P_2^o,\ \boldsymbol{m}_1^o,\ \boldsymbol{m}_2^o)$ *to (P-4.2) such that the corresponding optimal SINRs at the two terminals satisfying* $SINR_1^o = SINR_2^o$.

Proof. See Appendix B.2 for proof. □

By applying Lemma 4.2, (P-4.2) is reformulated to an equivalent problem,

$$\text{(P-4.3)} \quad \max_{P_1,\, P_2,\, \boldsymbol{m}_1,\, \boldsymbol{m}_2} \quad \frac{\gamma_1 P_{2R} - \gamma_2 P_{1R}}{(\gamma_1 - \gamma_2)\Delta}$$

$$\text{s. t.} \quad \|\boldsymbol{m}_j\|^2 = 1,\ j = 1,\ 2, \tag{4.15a}$$

$$P_1 \le P_1^{max},\ P_2 \le P_2^{max}, \tag{4.15b}$$

$$P_1 \boldsymbol{m}_1^H \boldsymbol{H}_1 \boldsymbol{m}_1 + P_2 \boldsymbol{m}_2^H \boldsymbol{H}_2 \boldsymbol{m}_2 \le I_{th}, \tag{4.15c}$$

$$\Phi(P_{1R}, P_{2R}) = 0, \tag{4.15d}$$

where

$$\Phi(P_{1R}, P_{2R}) = \gamma_1 P_{2R}^2 - \gamma_2 P_{1R}^2 + (\gamma_1 - \gamma_2) P_{1R} P_{2R} + \gamma_1(\gamma_2 + 1)\Delta P_{2R} - \gamma_2(\gamma_1 + 1)\Delta P_{1R}. \tag{4.16}$$

Notice that, (P-4.3) is a QCQP with quadratic equality constraint, which is generally non-convex and NP-hard [126]. And to solve (P-4.3), three cases need to be considered: (1) $\gamma_1 > \gamma_2$, (2) $\gamma_1 = \gamma_2$ and (3) $\gamma_1 < \gamma_2$. Since $\gamma_1 = \gamma_2$ is a zero-probability event, we neglect this case here, and focus on the other two cases.

CASE 1: $\gamma_1 > \gamma_2$

In this case, ($P_1,\ P_2,\ \boldsymbol{m}_1,\ \boldsymbol{m}_2$) should be chosen such that (P_{1R}, P_{2R}) satisfies both $\gamma_1 P_{2R} - \gamma_2 P_{1R} > 0$ and $\Phi(P_{1R},\ P_{2R}) = 0$. Clearly, $\Phi(P_{1R},\ P_{2R}) = 0$ is a hyperbolic curve passing the origin point $(P_{1R},\ P_{2R}) = (0,\ 0)$, and it is easy to prove that the points $(P_{1R},\ P_{2R})$ on this hyperbolic curve $\Phi(P_{1R},\ P_{2R}) = 0$ always satisfies $\gamma_1 P_{2R} - \gamma_2 P_{1R} > 0$ when $P_{jR} > 0$ ($j = 1,\ 2$). Therefore, given $\gamma_1 > \gamma_2$, there must exist a solution ($P_1,\ P_2,\ \boldsymbol{m}_1,\ \boldsymbol{m}_2$) such that $\Phi(P_{1R},\ P_{2R}) = 0$ and the optimal value of (P-4.3) is achieved.

CASE 2: $\gamma_1 < \gamma_2$

With the similar analysis as in CASE 1, the same conclusion can be obtain, given $\gamma_1 < \gamma_2$.

Therefore, there must exist an optimal ($P_1,\ P_2,\ \boldsymbol{m}_1,\ \boldsymbol{m}_2$) such that the corresponding (P_{1R}, P_{2R}) is on the hyperbolic curve $\Phi(P_{1R},\ P_{2R}) = 0$. Therefore, we propose a bi-section search based optimal algorithm (JTBPA) to jointly find the optimal Tx beamforming vectors $\boldsymbol{m}_j$ and transmit powers P_j ($j = 1, 2$). This bi-section search is performed in the range $[t_{low}, t_{up}]$, where t_{low} and t_{up} are the lower

and upper bounds to the optimal value of (P-4.3). The lower bound t_{low} could be simply chosen as zero since the SINR should always be positive, while the upper bound t_{up} could be chosen as the optimal value of (P-4.4), which drops the constraint (4.15c) in (P-4.3) and maximizes the objective function with regard to P_{jR} ($j = 1,\ 2$).

$$\text{(P-4.4)} \quad \max_{P_{1R},\, P_{2R}} \quad \frac{\gamma_1 P_{2R} - \gamma_2 P_{1R}}{(\gamma_1 - \gamma_2)\Delta}$$

$$\text{s.t.} \quad P_{1R} \leq P_1^{max}\text{Tr}(\boldsymbol{G}_1), \tag{4.17a}$$

$$P_{2R} \leq P_2^{max}\text{Tr}(\boldsymbol{G}_2), \tag{4.17b}$$

$$\Phi(P_{1R}, P_{2R}) = 0 \tag{4.17c}$$

In (P-4.4), the first two constraints result from the fact that the maximum value of $P_{jR} = P_j \boldsymbol{m}_j^H \boldsymbol{G}_j \boldsymbol{m}_j$ ($j = 1,\ 2$) equals to the multiplication of P_j^{max} and the principle eigenvalue of $\boldsymbol{G}_j$, which is $\text{Tr}(\boldsymbol{G}_j)$ according to the definition of $\boldsymbol{G}_j$. It is worth mentioning that the objective function $\frac{\gamma_1 P_{2R} - \gamma_2 P_{1R}}{(\gamma_1 - \gamma_2)\Delta}$ of (P-4.4) implies that $(P_{1R},\ P_{2R})$ should be located as far from the line $P_{2R} = \frac{\gamma_2}{\gamma_1} P_{1R}$ as possible. On the other hand, to satisfy the constraint (4.17c), $(P_{1R},\ P_{2R})$ should be on the hyperbolic curve $\Phi(P_{1R},\ P_{2R}) = 0$ as well. Since when $P_{1R} \geq 0$ and $P_{2R} \geq 0$, $\Phi(P_{1R}, P_{2R}) = 0$ monotonically increases and has only one cross point with $P_{2R} = \frac{\gamma_2}{\gamma_1} P_{1R}$ at $(0,\ 0)$, the distance from points $(P_{1R},\ P_{2R})$ on the hyperbolic curve to the line $P_{2R} = \frac{\gamma_2}{\gamma_1} P_{1R}$ increases with the increase in P_{1R}. Otherwise, $\Phi(P_{1R}, P_{2R}) = 0$ and $P_{2R} = \frac{\gamma_2}{\gamma_1} P_{1R}$ would have another cross point when $P_{1R} > 0$ and $P_{2R} > 0$. Therefore, let $(P_1^{max}\text{Tr}(\boldsymbol{G}_1),\ P_{2R}^{(1)})$ and $(P_{1R}^{(2)},\ P_2^{max}\text{Tr}(\boldsymbol{G}_2))$ be the cross points of $P_{1R} = P_1^{max}\text{Tr}(\boldsymbol{G}_1)$ and $P_{2R} = P_2^{max}\text{Tr}(\boldsymbol{G}_2)$ with $\Phi(P_{1R}, P_{2R}) = 0$, respectively, then the one satisfying both (4.17a) and (4.17b) must be the optimal solution to (P-4.4), which is Step 2 in JTBPA.

Once the initial range of the bi-section search is determined, at each iteration, given $\text{SINR}_1 = \text{SINR}_2 = t_{\text{mid}} = \frac{t_{up} + t_{low}}{2}$, $(P_{1R_{\text{mid}}},\ P_{2R_{\text{mid}}})$ is obtained by solving the equations $\frac{\gamma_1 P_{2R_{\text{mid}}} - \gamma_2 P_{1R_{\text{mid}}}}{(\gamma_1 - \gamma_2)\Delta} = t_{\text{mid}}$ and $\Phi(P_{1R},\ P_{2R}) = 0$. Once $(P_{1R_{\text{mid}}},\ P_{2R_{\text{mid}}})$ is determined, all we need to do is to check if there is a $(P_1,\ P_2,\ \boldsymbol{m}_1,\ \boldsymbol{m}_2)$ such that both $P_j \boldsymbol{m}_j^H \boldsymbol{G}_j \boldsymbol{m}_j = P_{jR_{\text{mid}}}$ ($j = 1, 2$), and $P_1 \boldsymbol{m}_1^H \boldsymbol{H}_1 \boldsymbol{m}_1 + P_2 \boldsymbol{m}_2^H \boldsymbol{H}_2 \boldsymbol{m}_2 \leq I_{th}$

Algorithm JTBPA: Optimal Joint Beamforming and Power Allocation

Input : $\boldsymbol{G}_1$, $\boldsymbol{G}_2$, $\boldsymbol{H}_1$, $\boldsymbol{H}_2$, $\boldsymbol{F}_1$, $\boldsymbol{F}_2$, Δ, h_r, I_{th}, P_1^{max}, P_2^{max}
Output: SINR, P_1, P_2, $\boldsymbol{m}_1$, $\boldsymbol{m}_2$, $\boldsymbol{d}_1$, $\boldsymbol{d}_2$, G

Compute γ_j and $\boldsymbol{d}_j$, $(j = 1, 2)$ using (4.13) and (4.12), respectively;
Compute $(P_1^{max}\text{Tr}(\boldsymbol{G}_1),\ P_{2R}^{(1)})$ and $(P_{1R}^{(2)},\ P_2^{max}\text{Tr}(\boldsymbol{G}_2))$ being the cross points of $P_{1R} = P_1^{max}\text{Tr}(\boldsymbol{G}_1)$ and $P_{2R} = P_2^{max}\text{Tr}(\boldsymbol{G}_2)$ with $\Phi(P_{1R}, P_{2R}) = 0$ respectively. Chose the one satisfying both (4.17a) and (4.17b) as the solution to (P-4.4), compute its optimal value and set the result to t_{up};
$t_{\text{low}} = 0$, $t_{\text{mid}} = \frac{t_{\text{up}}+t_{\text{low}}}{2}$, $t_{\text{mid}}^{\text{old}} = Inf$;
while $|t_{\text{mid}} - t_{\text{mid}}^{\text{old}}| > \eta$ **do**
    $t_{\text{mid}}^{\text{old}} = t_{\text{mid}}$;
    Calculate $(P_{1R_{\text{mid}}},\ P_{2R_{\text{mid}}})$ such that both $\frac{\gamma_1 P_{2R_{\text{mid}}} - \gamma_2 P_{1R_{\text{mid}}}}{(\gamma_1-\gamma_2)\Delta} = t_{\text{mid}}$ and (4.15d) are satisfied;
    Find $\hat{\boldsymbol{m}}_j^H \boldsymbol{H}_j \hat{\boldsymbol{m}}_j$ and $\hat{\boldsymbol{m}}_j$ by solving (P-4.6) using SDR $(j = 1,\ 2)$;
    if $\hat{\boldsymbol{m}}_1^H \boldsymbol{H}_1 \hat{\boldsymbol{m}}_1 + \hat{\boldsymbol{m}}_2^H \boldsymbol{H}_2 \hat{\boldsymbol{m}}_2 \le I_{th}$ **then**
        $t_{\text{low}} = t_{\text{mid}}$;
        $P_j = \|\hat{\boldsymbol{m}}_j\|^2$, $\boldsymbol{m}_j = \frac{1}{\sqrt{P_j}}\hat{\boldsymbol{m}}_j$, $(j = 1,\ 2)$;
    else $t_{\text{up}} = t_{\text{mid}}$;
    end
    $t_{\text{mid}} = \frac{t_{\text{up}}+t_{\text{low}}}{2}$;
end
$G = \sqrt{\frac{I_{th}}{|h_r|^2(P_1 \boldsymbol{m}_1^H \boldsymbol{G}_1 \boldsymbol{m}_1 + P_2 \boldsymbol{m}_2^H \boldsymbol{G}_2 \boldsymbol{m}_2 + \Delta)}}$;
return SINR, P_1, P_2, $\boldsymbol{m}_1$, $\boldsymbol{m}_2$, $\boldsymbol{d}_1$, $\boldsymbol{d}_2$, G.

are satisfied. This is equivalent to solve the feasibility problem,

$$\begin{aligned}
\text{(P-4.5)} \quad \text{find} \quad & \hat{\boldsymbol{m}}_1,\, \hat{\boldsymbol{m}}_2 \\
\text{s.t.} \quad & \|\hat{\boldsymbol{m}}_j\|^2 \le P_j^{max},\, j=1,\,2, && \text{(4.18a)} \\
& \hat{\boldsymbol{m}}_1^H \boldsymbol{H}_1 \hat{\boldsymbol{m}}_1 + \hat{\boldsymbol{m}}_2^H \boldsymbol{H}_2 \hat{\boldsymbol{m}}_2 \le I_{th}, && \text{(4.18b)} \\
& \hat{\boldsymbol{m}}_j^H \boldsymbol{G}_j \hat{\boldsymbol{m}}_j = \gamma_{jR_{\text{mid}}},\, j=1,2, && \text{(4.18c)}
\end{aligned}$$

where $\hat{\boldsymbol{m}}_j = \sqrt{P_j}\boldsymbol{m}_j$ ($j=1,\,2$). If such a ($P_1,\,P_2,\,\boldsymbol{m}_1,\,\boldsymbol{m}_2$) can be found, t_{low} is updated to t_{mid}. Otherwise, t_{up} is updated to t_{mid}.

Note that (P-4.5) is still a NP-hard, non-convex feasibility problem since it contains both quadratic inequality and equality constraints [126]. However, we can convert it into two M_j-dimensional ($j=1,\,2$) interference minimization problems (P-4.6).

$$\begin{aligned}
\text{(P-4.6)} \quad \min_{\hat{\boldsymbol{m}}_j} \quad & \hat{\boldsymbol{m}}_j^H \boldsymbol{H}_j \hat{\boldsymbol{m}}_j \\
\text{s.t.} \quad & \|\hat{\boldsymbol{m}}_j\|^2 \le P_j^{max}, && \text{(4.19a)} \\
& \hat{\boldsymbol{m}}_j^H \boldsymbol{G}_j \hat{\boldsymbol{m}}_j = \gamma_{jR_{\text{mid}}}, && \text{(4.19b)} \\
& j=1,\,2,
\end{aligned}$$

where $\hat{\boldsymbol{m}}_j^H \boldsymbol{H}_j \hat{\boldsymbol{m}}_j$ ($j=1,2$) is the SU$_j$ $\rightarrow$B interference power in the first time slot. Then, if we define $\boldsymbol{X}_j = \hat{\boldsymbol{m}}_j \hat{\boldsymbol{m}}_j^H$ ($j=1,2$), (P-4.6) is equivalent to,

$$\begin{aligned}
\text{(P-4.7)} \quad \min_{\hat{\boldsymbol{m}}_j} \quad & \text{Tr}(\boldsymbol{H}_j \boldsymbol{X}_j) \\
\text{s.t.} \quad & \text{Tr}(\boldsymbol{X}_j) \le P_j^{max}, && \text{(4.20a)} \\
& \text{Tr}(\boldsymbol{G}_j \boldsymbol{X}_j) = \gamma_{jR_{\text{mid}}}, && \text{(4.20b)} \\
& \boldsymbol{X} \succeq \boldsymbol{0},\, \text{rank}\{\boldsymbol{X}\} = 1. && \text{(4.20c)}
\end{aligned}$$

which can be solved by SDR technique [126]. In SDR, the rank-1 constraint (4.20c) is dropped and the optimal solution $\boldsymbol{X}_j^\star$ to the resultant problem is found via interior-point algorithms [125]. Note that, it has been shown in [126, 127] that with only two constraints, the SDR of (P-4.7) always has a rank-1 solution, rank$\{\boldsymbol{X}_j^\star\} = 1$, whenever the optimization problem is feasible. Therefore, $\boldsymbol{X}_j^\star$ is also optimal to (P-4.7) and the optimal solution $\hat{\boldsymbol{m}}_j^\star$ to (P-4.6) can be extracted from $\boldsymbol{X}_j^\star$. Once

the optimal $\hat{\boldsymbol{m}}_j^H \boldsymbol{H}_j \hat{\boldsymbol{m}}_j$ ($j = 1, 2$) of (P-4.6) is found, we compare the sum of them with the interference temperature limit I_{th}. If $\hat{\boldsymbol{m}}_1^H \boldsymbol{H}_1 \hat{\boldsymbol{m}}_1 + \hat{\boldsymbol{m}}_2^H \boldsymbol{H}_2 \hat{\boldsymbol{m}}_2 \leq I_{th}$, it is equivalent to that (P-4.5) is feasible, otherwise (P-4.5) is not feasible.

4.4.2 Optimal Power Allocation with Different Tx Beamforming

Although JTBPA optimally computes P_j and $\boldsymbol{m}_j$ ($j = 1, 2$), the bi-section search and the use of SDR result in high computational complexity (see Table 4.1). Therefore, low-complexity alternatives are desirable. To this end, we use two widely-used, low-complexity Tx beamforming strategies (MRT and ZFB-MRT). These strategies yield closed-form matrix expressions for the beamforming vectors. Contingent upon their beamforming vectors, we will optimize the power allocation to partially compensate for the performance loss. Note that whilst such a two-stage solution is necessarily sub-optimal, significant complexity savings are possible.

MRT

According to the principle of MRT, the Tx beamforming vector $\boldsymbol{m}_j^{MRT}$ ($j = 1, 2$) is chosen as (4.21) to maximize the received signal power at the relay R.

$$\boldsymbol{m}_j^{MRT} = \frac{\boldsymbol{g}_j^*}{\|\boldsymbol{g}_j\|}. \tag{4.21}$$

ZFB-MRT

According to the principle of ZFB-MRT, we first find the sub-space $\Psi_j = I - \frac{\boldsymbol{h}_j^* \boldsymbol{h}_j^T}{\|\boldsymbol{h}_j\|^2}$ ($j = 1, 2$), which is orthogonal to the SU$_j$ $\rightarrow$B interference channels $\boldsymbol{h}_j$ ($j = 1, 2$), then project $\boldsymbol{g}_j$ onto Ψ_j ($j = 1, 2$). Thus, the Tx beamforming vector $\boldsymbol{m}_j^{ZFB-MRT}$ ($j = 1, 2$) is computed via,

$$\boldsymbol{m}_j^{ZFB-MRT} = \frac{\Psi_j \boldsymbol{g}_j^*}{\sqrt{\boldsymbol{g}_j^T \Psi_j \boldsymbol{g}_j^*}}, \tag{4.22}$$

Since the use of the sub-space Ψ_j ($j = 1, 2$) eliminates the interference from SU$_j$'s transmission to B, the interference constraint in the first time slot ((4.23b)) is always satisfied. In principle, this allows for an arbitrary increase in the transmit powers (P_j, $j = 1, 2$) at the terminals.

Optimal Power Allocation (OPA)

To derive the optimal power allocation (P_1, P_2), we can first substitute the sub-optimal Tx beamforming vectors $\boldsymbol{m}_j$ $(j = 1, 2)$, which are determined by either (4.21) or (4.22), into (P-4.3). Then, the optimal power allocation problem (P-4.8) is obtained.

$$\begin{aligned} \text{(P-4.8)} \quad \max_{P_1, P_2} \quad & \frac{P_2\gamma_1\tilde{P_{2R}} - P_1\gamma_2\tilde{P_{1R}}}{(\gamma_1 - \gamma_2)\Delta} \\ \text{s.t.} \quad & P_1 \le P_1^{max},\ P_2 \le P_2^{max}, && \text{(4.23a)} \\ & a_1P_1 + a_2P_2 \le I_{th}, && \text{(4.23b)} \\ & \Phi(P_1, P_2) = 0, && \text{(4.23c)} \end{aligned}$$

where $\tilde{P_{jR}} = \boldsymbol{m}_j^H \boldsymbol{G}_j \boldsymbol{m}_j$, $a_j = \boldsymbol{m}_j^H \boldsymbol{H}_j \boldsymbol{m}_j$ $(j = 1, 2)$, and

$$\begin{aligned} \Phi(P_1, P_2) =& \gamma_1\tilde{P_{2R}}^2P_2^2 - \gamma_2\tilde{P_{1R}}^2P_1^2 + (\gamma_1 - \gamma_2)\tilde{P_{1R}}\tilde{P_{2R}}P_1P_2 \\ & + \gamma_1(\gamma_2 + 1)\Delta\tilde{P_{2R}}P_2 - \gamma_2(\gamma_1 + 1)\Delta\tilde{P_{1R}}P_1. \end{aligned} \tag{4.24}$$

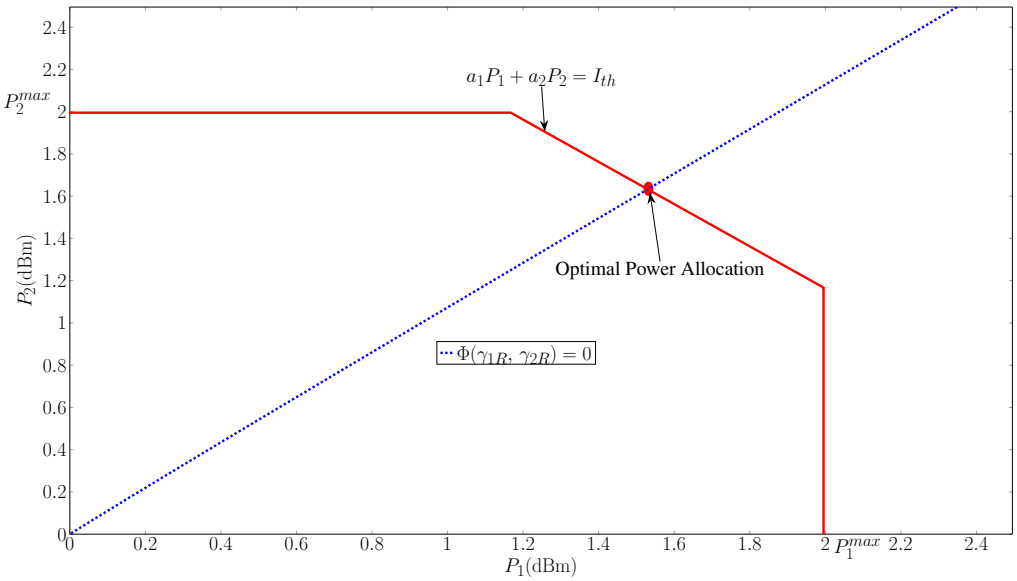

Figure 4.2: Optimal Power Allocation

It is easy to prove that with the optimal power allocation $(P_1,\ P_2)$, at least one of the three constraints (4.23a) and (4.23b) is satisfied with equality, because otherwise we can increase P_1 or P_2 to achieve a better solution. Consequently, the optimal power allocation $(P_1,\ P_2)$ lies on the red solid line in Fig. 4.2, which is

formed by (4.23a) and (4.23b). Therefore, the optimal power allocation $(P_1,\ P_2)$ must be the cross point of the red solid line and the hyperbolic curve $\Phi(P_1,\ P_2)=0$, and this cross point must be the one among (4.25a)–(4.25c) satisfying both (4.23a) and (4.23b). (4.25a)–(4.25c) are the cross points $(P_1^{(1)}, P_2^{(1)})$, $(P_1^{(2)}, P_2^{(2)})$ and $(P_1^{(3)}, P_2^{(3)})$ of $\Phi(P_1,\ P_2)=0$ with $P_1=P_1^{max}$, $P_2=P_2^{max}$, and $a_1P_1+a_2P_2=I_{th}$, respectively.

$$P_1^{(1)} = \frac{-\xi_1-\sqrt{\xi_1^2-4\zeta_1\varrho_1}}{2\zeta_1},\ P_2^{(1)}=P_2^{max}, \tag{4.25a}$$

$$P_1^{(2)} = P_1^{max},\ P_2^{(2)}=\frac{-\xi_2+\sqrt{\xi_2^2-4\zeta_2\varrho_2}}{2\zeta_2}, \tag{4.25b}$$

$$P_1^{(3)} = \frac{-\xi_3-\sqrt{\xi_3^2-4\zeta_3\varrho_3}}{2\zeta_3},\ P_2^{(3)}=\frac{I_{th}}{a_1}-\frac{a_1}{a_2}P_1^{(3)}, \tag{4.25c}$$

where
$$\begin{aligned}
\xi_1 &= (\gamma_1-\gamma_2)\tilde{P_{1R}}\tilde{P_{2R}}P_2^{max}-\gamma_2(\gamma_1+1)\Delta\tilde{P_{1R}},\\
\zeta_1 &= -\gamma_2\tilde{P_{1R}}^2,\\
\varrho_1 &= \gamma_1\tilde{P_{2R}}^2P_2^{max^2}+\gamma_1(\gamma_2+1)\Delta\tilde{P_{2R}}P_2^{max},\\
\xi_2 &= (\gamma_1-\gamma_2)\tilde{P_{1R}}\tilde{P_{2R}}P_1^{max}+\gamma_1(\gamma_2+1)\Delta\tilde{P_{2R}},\\
\zeta_2 &= \gamma_1\tilde{P_{2R}}^2,\\
\varrho_2 &= -\gamma_2\tilde{P_{1R}}^2P_1^{max^2}-\gamma_2(\gamma_1+1)\Delta\tilde{P_{1R}}P_1^{max},\\
\xi_3 &= -\frac{2I_{th}a_1\gamma_1\tilde{P_{2R}}^2}{a_2^2}+\frac{(\gamma_1-\gamma_2)\tilde{P_{1R}}I_{th}}{a_2}-\frac{\gamma_1(\gamma_2+1)\Delta\tilde{P_{2R}}a_1}{a_2}\\
&\quad -\gamma_2(\gamma_1+1)\Delta\tilde{P_{1R}},\\
\zeta_3 &= \frac{\gamma_1\tilde{P_{2R}}^2a_1^2}{a_2^2}-\gamma_2\tilde{P_{1R}}^2-\frac{(\gamma_1-\gamma_2)\tilde{P_{1R}}\tilde{P_{2R}}a_1}{a_2},\\
\varrho_3 &= \frac{\gamma_1\tilde{P_{2R}}^2I_{th}^2}{a_2^2}+\frac{\gamma_1(\gamma_2+1)\Delta\tilde{P_{2R}}I_{th}}{a_2}.
\end{aligned}$$

4.4.3 Complexity Analysis

This section analyses and compares the complexity of JTBPA and sub-optimal Tx beamforming with optimal power allocation in terms of running time. Since JTBPA does a bi-section search and applies SDR at each iteration, its running time can be estimated as follows. The worst-case total number of iterations required by the bi-section search is given as $\log_2(\frac{t_{\text{up}}-t_{\text{low}}}{\eta})$ [124], where t_{up} and t_{low} are the initial

upper and lower bounds of the bi-section search, respectively, and η is the stopping criteria. At each iteration, SDR requires running time of $\mathcal{O}(M_1^{4.5}\log(1/\epsilon))$ and $\mathcal{O}(M_2^{4.5}\log(1/\epsilon))$ to solve two interference minimization problems, respectively, given $\epsilon > 0$ being the approximation accuracy threshold required in the interior-point algorithm in SDR [126]. Therefore, the total running time of JTBPA is given as $\mathcal{O}(\log_2(\frac{t_{\text{up}}-t_{\text{low}}}{\eta})\log(1/\epsilon)\max(M_1, M_2)^{4.5})$.

For both MRT and ZFB-MRT, only matrix multiplication is utilized, which requires running time of $\mathcal{O}(M_j^2)$ to compute the Tx beamforming vectors $\boldsymbol{m}_j$ ($j = 1, 2$). Then, the optimal power is obtained through numerical calculations, which requires constant time. Therefore, the running time of MRT or ZFB-MRT with optimal power allocation is significantly lower than JTBPA. A clear comparison is shown in Table 4.1

Table 4.1: Comparison of Running Times

Algorithms	Running Times
JTBPA	$\mathcal{O}(\log_2(\frac{t_{\text{up}}-t_{\text{low}}}{\eta})\log(1/\epsilon)\max(M_1, M_2)^{4.5})$
MRR with Optimal Power	$\mathcal{O}(\max(M_1, M_2)^2)$
ZFB-MRT with Optimal Power	$\mathcal{O}(\max(M_1, M_2)^2)$

4.5 Results and Discussions

This section presents the simulation results to compare (1) JTBPA, (2) ZFB-MRT with optimal power allocation (ZFB-MRT-OPA), (3) ZFB-MRT with maximum power (ZFB-MRT-MP), (4) MRT with optimal power allocation (MRT-OPA), (5) Ideal and (6) equal power allocation (EPA). The Ideal case includes only the conventional two-way relay network (SU_1, SU_2 and R) without any interference constraints. In this case, MRC is the optimal RX beamforming strategy for SU_j ($j = 1, 2$) to receive signals in the second time slot because it maximizes the received signal power at SU_j. Then, in terms of Tx beamforming in the Ideal case, MRT is selected since it can maximize the $\text{SU}_j \rightarrow$R ($j = 1, 2$) signal in the first time slot. And the maximum available power are selected at both SU_j ($j = 1, 2$) and R. In the EPA case, $\boldsymbol{m}_j$ is set to $\frac{1}{\sqrt{M_j}}\mathbf{1}$ ($j = 1, 2$), where the denominator is the normalizing

factor, and P_j $(j = 1, 2)$ is set to P, where $P = \min(\frac{I_{th}}{|\boldsymbol{h}_1^T \boldsymbol{m}_1|^2 + |\boldsymbol{h}_2^T \boldsymbol{m}_2|^2}, P^{max})$ and P^{max} is the maximum available power. Schemes (1)-(4) and (6) use the optimal Rx beamforming and relay gain (Section 4.3). The average achievable SINR over 10^3 channel realizations is chosen as the performance metric.

All the plots are generated with $N_0 = 0\,\text{dBm}$ and $P_p = 3\,\text{dBm}$. And each channel coefficient is $\mathcal{CN}(0, 1)$ distributed. To observe the impact of the maximum transmit power, we assume $P_1^{max} = P_2^{max} = P^{max}$ and choose $3\,\text{dBm}$ and $10\,\text{dBm}$, respectively.

Achievable SINR v.s. Interference Temperature Limit I_{th}

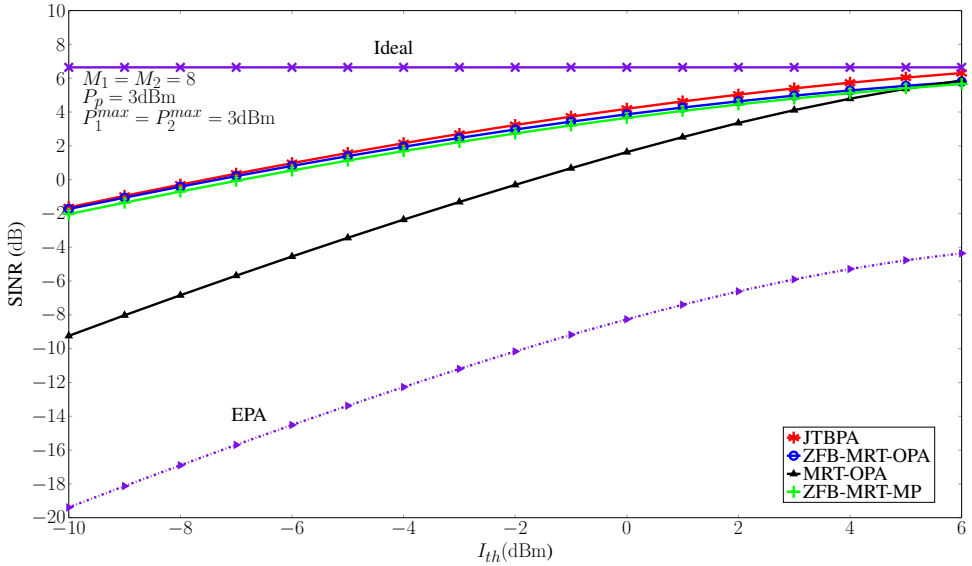

Figure 4.3: SINR v.s. I_{th} with $M_1 = M_2 = 8$ and $P_1^{max} = P_2^{max} = 3\,\text{dBm}$

Figs. 4.3 to 4.5 plot the average SINR as functions of I_{th}. Note that the proposed JTBPA provides over $10\,\text{dB}$ SINR improvement over EPA. As well, the gap between JTBPA and the Ideal case decreases with the increase in I_{th}, e.g., a less than $4\,\text{dB}$ gap exists when $I_{th} = 6\,\text{dBm}$ in Fig. 4.4. The reason for this SINR gap improvement is that at low interference temperature limit, while beamforming at SU$_j$ $(j = 1, 2)$ partially eliminates SU$_j$ $\rightarrow$B interferences, the R$\rightarrow$B interference dominates and hence relay transmit power must be low. But when B has higher interference tolerance, $I_{th} = 6\,\text{dBm}$, the relay can transmit with higher power. Therefore, beamforming and power allocation exploit not only the spatial diversity, but

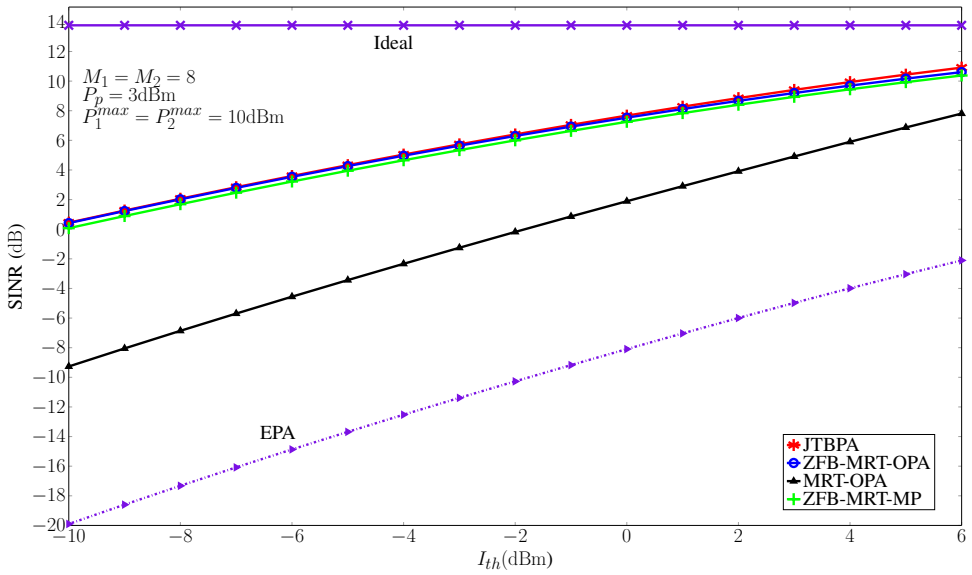

Figure 4.4: SINR v.s. I_{th} with $M_1 = M_2 = 8$ and $P_1^{max} = P_2^{max} = 10\,\text{dBm}$

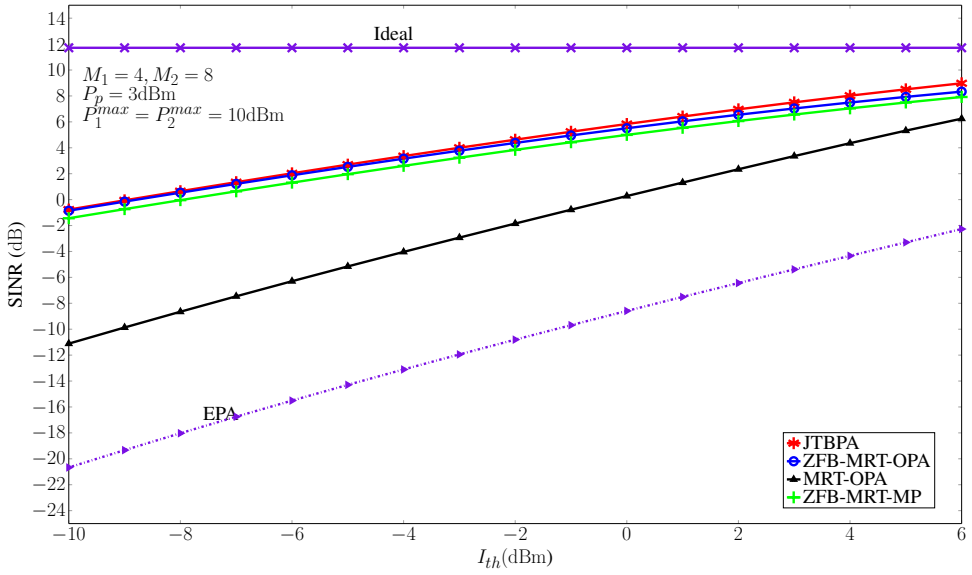

Figure 4.5: SINR v.s. I_{th} with $M_1 = 4,\ M_2 = 8$ and $P_1^{max} = P_2^{max} = 10\,\text{dBm}$

also the interference temperature limit to improve the achievable SINR.

From Figs. 4.3 to 4.5, it is clear that ZFB-MRT-OPA can achieve almost the same performance as JTBPA in low interference temperature limit region (e.g., $I_{th} \leq 2\,\text{dBm}$ with the maximum transmit power of $10\,\text{dBm}$ and $I_{th} \leq -2\,\text{dBm}$ with maximum transmit power of $3\,\text{dBm}$). Fig. 4.3 also shows that with the increase in the interference temperature limit (I_{th}), the gap between ZFB-MRT-OPA and JTBPA increases. This is because using ZFB-MRT, SU_j ($j = 1, 2$) causes no interference at B, therefore, the interference constraint is not exploited. The SINR loss due to not exploiting the interference constraint can be small when I_{th} is low, e.g., less than $0.5\,\text{dB}$ when $I_{th} = -10\,\text{dBm}$ (Fig. 4.3). But when the primary receiver (B) has higher interference tolerance, e.g., $I_{th} = 6\,\text{dBm}$, this SINR loss increases, e.g., $1\,\text{dB}$. However, this problem can be mitigated by either increasing the maximum transmit powers (Fig. 4.4) or equipping more antennas (Fig. 4.6).

With ZFB-MRT, optimal power allocation or maximum power transmission, a less than $1\,\text{dB}$ SINR gap exists throughout the entire interference temperature limit region ($[-10\,\text{dBm},\ 6\,\text{dBm}]$). This $1\,\text{dB}$ gap is because optimal power allocation provides a balance between terminals' and relay's transmissions. In other words, the relay node can transmit with a higher power than that when ZFB-MRT-MP is applied at the two terminals.

When comparing the performance of MRT-OPA in Figs. 4.3 and 4.4, increasing the maximum transmit power dose not benefit the achievable SINR, which is lower than the SINR obtained by JTBPA by over $5\,\text{dB}$ when $I_{th} \leq -4\,\text{dBm}$. But, as the interference temperature limit (I_{th}) increases, MRT-OPA converges to JTBPA. This is reasonable because MRT aims at maximizing the desired signal power. Therefore, the interference factor is not taken into consideration. Consequently, to satisfy the interference constraint in low I_{th} region, the transmit power can not be high, regardless of the maximum available transmit power.

Achievable SINR v.s. Number of Antennas M

Fig. 4.6 shows the average SINR as functions of the number of antennas, where $M_1 = M_2$. Obviously increasing the number of antennas results in higher SINR

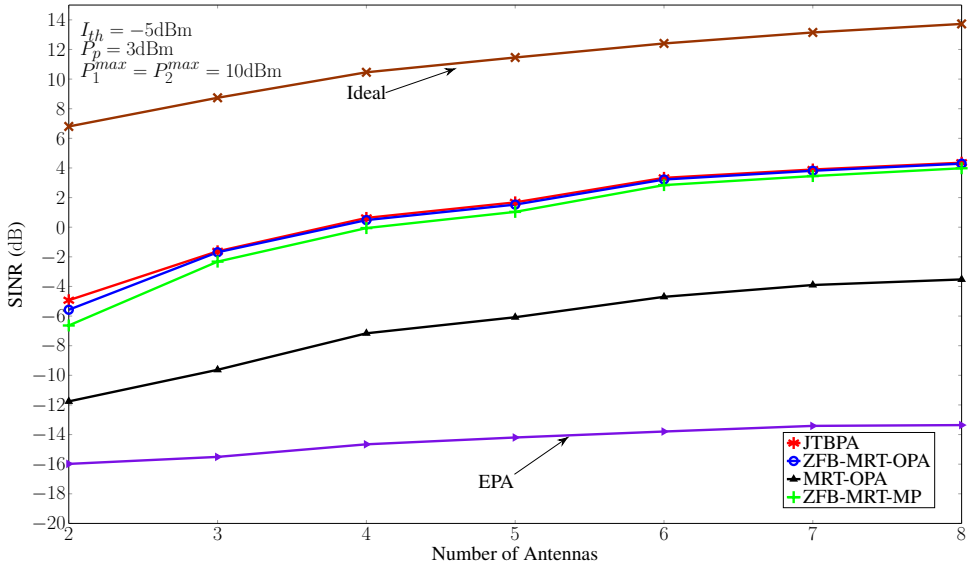

Figure 4.6: SINR v.s. Number of Antennas with $I_{th} = -5\,\text{dBm}$ and $P_1^{max} = P_2^{max} = 10\,\text{dBm}$

as more antennas yield increasing spatial degrees of freedom. Thus the SINR gap between JTBPA and the ideal case is reduced from around $12\,\text{dB}$ to $10\,\text{dB}$. Therefore, the capability of cognitive beamforming in suppressing interferences from/to the primary network is evident. As well, with the increase in the number of antennas, the SINR gap between ZFB-MRT-OPA/ZFB-MRT-MP and JTBPA has been reduced from over $2\,\text{dB}$ with 2 antennas to less than $1\,\text{dB}$ with 8 antennas. This is because, although ZFB-MRT does not exploit the interference temperature limit, the SINR loss due to not having Tx optimal beamforming coefficients can be partially overcome by exploiting more path diversities with more antennas. On the other hand, a large SINR gap, e.g.over $6\,\text{dB}$, exists between MRT-OPA and JTBPA even when more antennas are equipped and more spatial diversities are exploited in MRT. This is because with $I_{th} = -5\,\text{dBm}$, the transmit power determined by MRT-OPA is still relatively low since MRT has no control on the SU_j-to-B ($j = 1, , 2$) interference. Finally, it is obvious that since in EPA, no beamforming is performed, the achievable SINR remains relatively low, e.g., less than $-14\,\text{dB}$, regardless of the increase in the number of antennas. Consequently, the gap between EPA and the ideal case is more than $22\,\text{dB}$.

Running Times Comparison

Table 4.2 shows the comparison of the total running time of 100 channel realizations in a computer equipped with Intel(R)i7-3770CPU at 3.4GHz using JTBPA, ZFB-MRT-OPA and MRT-OPA. In this comparison, I_{th}, P_j^{max} ($j = 1,\ 2$) are set to 0 dBm and 10 dBm, respectively. Clearly, over 99% running time is saved by using sub-optimal beamforming vectors. Besides, the time complexity of JTBPA increases with the increasing number of antennas, while these of the other two are more or less invariant.

Table 4.2: Running Times

	JTBPA	ZFB-MRT-OPA	MRT-OPA
$M_1 = M_2 = 4$	73.463s	0.014s	0.018s
$M_1 = 4,\ M_2 = 8$	90.774s	0.010s	0.010s
$M_1 = M_2 = 8$	110.707s	0.010s	0.009s

4.6 Conclusion

This chapter focused on the transmitter/receiver design for underlay two-way relay networks with multi-antenna terminals. Particularly, considering both S2P and P2S interferences, optimal transmit power, Tx and Rx beamforming have been developed to maximize the worse received SINR. The main contributions of this work are as follows:

1. The optimal Rx beamforming vectors were derived in closed-form and were proven independent of the transmit powers and the Tx beamforming vectors.

2. A bi-section search based algorithm (JTBPA) was proposed to jointly find the optimal Tx beamforming vectors and power allocation. To reduce the high computational complexity of JTBPA, the use of low-complexity sub-optimal Tx beamforming schemes, MRT and ZFB-MRT, was proposed and the corresponding optimal power allocation was derived.

3. Simulation results showed that JTBPA can provide over 20 dB SINR improvement from the EPA approach, where no beamforming is performed and

the transmit power is equally allocated. Besides, ZFB-MRT only has a small SINR loss from JTBPA, e.g., only a less than 1 dB and 2 dB SINR gaps exists when the optimal and the maximum transmit powers are used, respectively, while significantly saves the computational time, e.g., over 99%.

$\sim$

Chapter 5

Distributed Beamforming in Underlay Two-Way Relay Networks with Single-Antenna Nodes

While Chapter 4 investigated beamforming for multi-antenna terminals in an underlay network, this chapter considers multiple single-antenna relay nodes using partial CSI. In this configuration, the spatially separated relays form a distributed beamformer. Then, considering both P2S and S2P interferences, optimal algorithms (Single-Relay Optimal Algorithm (SRO) and Multi-Relay Optimal Algorithm (MRO)) are proposed first to find the optimal power allocation and relay gains for single-relay and multi-relay systems, respectively. Besides, two low-complexity sub-optimal algorithms (Simple Power Allocation (SPA) and Two-Phase Search (TPS)) are also proposed to reduce the high computational complexity of MRO[1]. Moreover, the MRO and TPS algorithms are further adapted for non-cognitive two-way relay networks.

5.1 Introduction

Although Chapter 4 developed the optimal power allocation and Tx and Rx beamforming algorithms for multi-antenna underlay networks, sometimes multiple antennas in wireless devices may be difficult due to the size and the cost constraints [28,29]. Therefore, this chapter investigates the transmit and relay design for single-

[1] *A version of this chapter has been published in IEEE Trans. Signal Process., 62, 5950-5961 (2014).*

antenna networks, where multiple spatially separated relays are available. In this context, multiple spatially-separated relays allow their antenna gain adjustments (i.e., distributed beamforming) to exploit multi-user cooperative diversity [23–25], and thus to provide more robust communications in presence of fading and interference [74].

5.1.1 Prior Related Research

In conventional non-cognitive two-way AF relay networks, where no interference issues exists, the joint distributed beamforming and power allocation problem has been extensively investigated for single-antenna systems [138, 140–142, 144, 145]. Optimal distributed beamforming algorithms have been proposed to minimize the transmit power [140, 141] and to maximize the worse available SNR [141, 142, 144] under total and individual power constraints. And all these studies assumed the availability of perfect instantaneous CSI.

For cognitive systems, this problem has been investigated for overlay [113, 130–133] and underlay [44, 46, 49, 50], respectively. While [44] investigated one-way relays, [46, 49, 50] considered two-way relays. However, the P2S interference was neglected in those works, and the availability of perfect CSI was assumed.

5.1.2 Motivation and Contribution

Since distributed beamforming for underlay two-way relay networks has only been investigated in [46, 49, 50] and only the S2P interference and perfect CSI were considered there, this chapter investigates distributed beamforming for such networks taking into consideration both P2S and S2P interferences and assuming the availability of only partial CSI. Specifically, there are multiple cooperative AF relay nodes (R_i, $i = 1, 2, ..., K$) assisting communications between the two secondary terminals (SU_1 and SU_2). In this configuration, the beamforming vector is formed by the relay gains. We aim at jointly designing the transmit power and relay gains to maximize the worse average SINR between SU_1 and SU_2. Moreover, only partial CSIs, which include the perfect CSI of $\mathrm{SU}_j \leftrightarrow \mathrm{R}_i$ ($j = 1, 2$, $i = 1, 2, ..., K$) channels and the second-order statistics of all the other channels, are assumed at SU_j.

Such a partial CSI assumption can reduce the heavy channel estimation and CSI communication overhead required by full CSI. The contributions of this chapter are given as follows.

1. An optimal algorithm (SRO) [73] is proposed to compute the optimal relay gain and transmit powers for single relay systems. Although it is optimal, its capability of improving the achievable SINR is very limited, e.g., less than 0 dB, since beamforming is impossible when there is only one single-antenna relay.

2. An exhaustive-search based optimal algorithm (MRO) [73] is proposed to find the optimal relay gains (distributed beamforming vectors) and power allocations for multi-relay systems. To reduce the computational complexity, two sub-optimal algorithms (SPA and TPS) [73] are also proposed, both of which first find a sub-optimal power allocation and then derive the optimal relay gains given that sub-optimal power allocation.

3. Simulation results show that since distributed beamforming is performed, MRO can increase the achievable SINR by over 10 dB compared to no beamforming and equal power allocation (EPA). Moreover, the two sub-optimal algorithms (SPA and TPS) achieve near optimal SINRs, e.g., the SINR gaps from MRO are as low as 1 dB, while save 90% running time.

4. The MRO and TPS algorithms are adapted to solve the joint distributed beamforming and power allocation problems for non-cognitive two-way relay networks, where only partial CSI is available [151].

This chapter is organized as follows. Section 5.2 introduces the details of the system configuration and signal flow, then formulates the optimization problem. Section 5.3 develops the necessary conditions for the joint distributed beamforming and power allocation problem. Section 5.4 derives the SRO algorithm to compute the optimal relay gain and transmit powers for single-relay systems. Section 5.5 develops the optimal (MRO) and sub-optimal (SPA and TPS) algorithms to find the relay gains and power allocations for multi-relay systems. Section 5.6 extends

the MRO and TPS algorithms into non-cognitive two-way relay networks. And Section 5.7 concludes this chapter.

5.2 System Configuration, Signal Flow and Problem Formulation

System Configuration

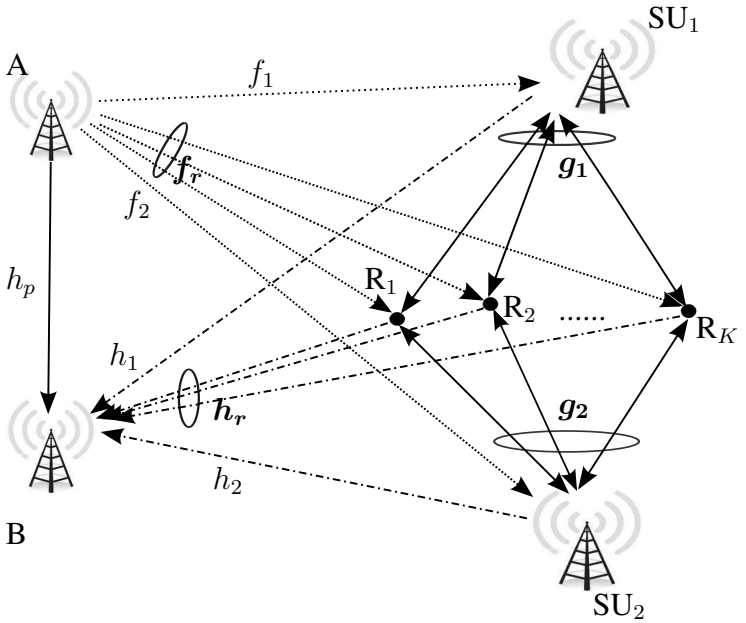

Figure 5.1: Single-Antenna Underlay Two-Way Relay Network

The underlay two-way relay network considered in this chapter is shown in Fig. 5.1, where there are two secondary terminals (SU_1 and SU_2) and K AF relay nodes R_i ($i = 1, 2, ..., K$) coexisting with one primary transmitter(A)-receiver(B) pair. All nodes work in the half-duplex mode. In real applications, this secondary network can be one Peer-to-Peer (P2P) network, which includes a group of devices, such as laptops, smartphones, or tablets. These devices are connected with each other directly without any base station. And the two secondary terminals are any two devices in that group wishing to exchange information, while the remaining devices act as the relays. SU_1 and SU_2 require bidirectional data exchange. Because no direct link exists between them, they can exchange information with each other only by using the K relays R_i ($i = 1, 2, ..., K$).

A stationary flat fading scenario with AWGN is assumed for every channel in

the system, and all channels are independent of each other. The following notations are used throughout this chapter to represent wireless channels in the system. $g_{j_i} \in \mathbb{C}$ ($j = 1, 2$; $i = 1, 2, \ldots, K$) are the reciprocal channels between SU_j and R_i. $f_{r_i} \in \mathbb{C}$ ($i = 1, 2, ..., K$) and $f_j \in \mathbb{C}$ ($j = 1, 2$) are the interference channels from A to the relay R_i and SU_j, respectively. $h_{r_i} \in \mathbb{C}$ ($i = 1, 2, ..., K$) and $h_j \in \mathbb{C}$ ($j = 1, 2$) are the interference channels from R_i and SU_j to B, respectively.

We assume that rather than perfect CSI, only partial CSI is available at the secondary terminals SU_j ($j = 1, 2$), which involves: (1) the second-order statistics (SOS) of all the channels, such as $\mathbb{E}\{\boldsymbol{g}_j \boldsymbol{g}_j^H\}$; and (2) perfect instantaneous CSI of the channels $\boldsymbol{g}_j$ from SU_j ($j = 1\,2$) itself to the relays obtained via an appropriate channel estimation scheme [118, 119]. The assumption of the availability of partial CSI is because the provision of full instantaneous CSI at all nodes can sometimes be difficult in practical systems due to the time-variant nature of wireless channels [152] and the heavy overheads necessary for channel estimation and feedback. Therefore, the provision of partial CSI is less burdensome than providing full CSI. Similar to Chapter 4, we may use a central control device to collect the SOS values of all the channels and broadcast them to the two secondary terminals. Since the SOS values are more static than instant CSIs, they can be updated less frequently, e.g., every 4 ms, which is 1000 symbol durations ($4\,\mu$s) in WLAN networks [158]. Therefore, the associated overhead only depends on the number of relays and how the channel SOSs are communicated, estimated SOSs or reference numbers in a codebook (see Section 4.2).

Moreover, to reduce the cooperation overhead, the transmit powers at SU_j ($j = 1, 2$) and all the relay gains are calculated at the secondary terminals SU_1 and SU_2, and a feedback channel may be employed to deliver the beamforming coefficients to the relays. These ideal assumptions allow us to establish the achievable performance levels of beamforming and two-way relays.

Moreover, AWGN is assumed at every receiving node and unit symbol power are assumed. We also assume perfect time synchronization between the primary and secondary networks.

Signal Flow

With AF two-way relay nodes, one round information exchange between SU_1 and SU_2 requires two consecutive time slots. In the first time slot, A transmits symbol $x^{(1)}$ to B with power P_p. In the meantime, SU_j broadcasts its symbol s_j to the relays by using power P_j ($j = 1, 2$) through the reciprocal channels $\boldsymbol{g}_j$. Consequently, the ith ($i = 1, 2, ..., K$) relay receives signal r_i and the primary receiver B receives interference signal $x_{int}^{(1)}$ as,

$$r_i = \sqrt{P_1} g_{1i} s_1 + \sqrt{P_2} g_{2i} s_2 + \sqrt{P_p} f_{r_i} x^{(1)} + n_{r_i}, \tag{5.1}$$

$$x_{int}^{(1)} = \sqrt{P_1} h_1 s_1 + \sqrt{P_2} h_2 s_2, \tag{5.2}$$

where $n_{r_i} \in \mathbb{C}$ is the zero-mean AWGN of variance σ_r^2.

In the second time slot, A transmits symbol $x^{(2)}$ still with power P_p, while each relay multiplies its received signal r_i ($i = 1, 2, ..., K$) with a complex coefficient ω_i, and broadcasts the resulting signal to SU_j ($j = 1, 2$). Therefore, the interference signal $x_{int}^{(2)}$ at B and the signal y_j ($j = 1, 2$) received at SU_j are given as,

$$x_{int}^{(2)} = \sqrt{P_1} \boldsymbol{\omega} \boldsymbol{H}_r \boldsymbol{g}_1 s_1 + \sqrt{P_2} \boldsymbol{\omega} \boldsymbol{H}_r \boldsymbol{g}_2 s_2 + \sqrt{P_p} \boldsymbol{\omega} \boldsymbol{H}_r \boldsymbol{f}_r x^{(1)} + \boldsymbol{\omega} \boldsymbol{H}_r \boldsymbol{n}_r, \tag{5.3}$$

$$\begin{aligned} y_j = & \underbrace{\sqrt{P_j} \boldsymbol{\omega} \boldsymbol{G}_j \boldsymbol{g}_j s_j}_{\text{Self-Interference}} + \underbrace{\sqrt{P_{\bar{j}}} \boldsymbol{\omega} \boldsymbol{G}_j \boldsymbol{g}_{\bar{j}} s_{\bar{j}}}_{\text{Signal}} + \underbrace{\sqrt{P_p} \boldsymbol{\omega} \boldsymbol{G}_j \boldsymbol{f}_r x^{(1)} + \sqrt{P_p} f_j x^{(2)}}_{\text{P2S Interference}} \\ & + \underbrace{\boldsymbol{\omega} \boldsymbol{G}_j \boldsymbol{n}_r + n_j}_{\text{Noise}}, \end{aligned} \tag{5.4}$$

where $\boldsymbol{g}_j = [g_{j_1}, g_{j_2}, \ldots, g_{j_K}]^T$, $\boldsymbol{f}_r = [f_{r_1}, f_{r_2}, \ldots, f_{r_K}]^T$, $\boldsymbol{\omega} = [\omega_1, \omega_2, \ldots, \omega_K]$, $\boldsymbol{n}_r = [n_{r_1}, n_{r_2}, \ldots, n_{r_K}]^T$, $\boldsymbol{G}_j = diag\{\boldsymbol{g}_j\}$, $\boldsymbol{h}_r = [h_{r_1}, h_{r_2}, \ldots, h_{r_K}]^T$, $\boldsymbol{H}_r = diag\{\boldsymbol{h}_r\}$, $n_j \in \mathbb{C}$ ($j = 1, 2$) is the AWGN at SU_j of zero mean and variance σ_j^2, and $\bar{j} = 1$ if $j = 2$, and vise versa. Note that, $\boldsymbol{\omega}$ is also referred to as the beamforming vector throughout this chapter.

By knowing $\boldsymbol{g}_j$ and s_j, SU_j ($j = 1, 2$) can eliminate its self-interference perfectly, resulting in the self-interference-free signal,

$$\tilde{y_j} = \underbrace{\sqrt{P_{\bar{j}}}\boldsymbol{\omega}\boldsymbol{G}_j\boldsymbol{g}_{\bar{j}}s_{\bar{j}}}_{\text{Signal}} + \underbrace{\sqrt{P_p}\boldsymbol{\omega}\boldsymbol{G}_j\boldsymbol{f}_r x^{(1)} + \sqrt{P_p}f_j x^{(2)}}_{\text{P2S Interference}} + \underbrace{\boldsymbol{\omega}\boldsymbol{G}_j\boldsymbol{n}_r + n_j}_{\text{Noise}}. \tag{5.5}$$

Because only partial CSI is available at the terminals, the SINR at SU$_j$ ($j = 1, 2$) is considered, which is given as,

$$\overline{\text{SINR}}_j = \frac{P_{\bar{j}}\boldsymbol{\omega}\boldsymbol{A}\boldsymbol{\omega}^H}{\boldsymbol{\omega}(\boldsymbol{B}_j + \boldsymbol{B}_{N_j})\boldsymbol{\omega}^H + \hat{\sigma_j^2}}, \tag{5.6}$$

where

$$\begin{aligned}
\boldsymbol{A} \triangleq& \mathbb{E}\{\boldsymbol{G}_1\boldsymbol{g}_2\boldsymbol{g}_2^H\boldsymbol{G}_1^H\} = \mathbb{E}\{\boldsymbol{g}_1\boldsymbol{g}_1^H\} \circ \mathbb{E}\{\boldsymbol{g}_2\boldsymbol{g}_2^H\},\\
\boldsymbol{B}_j \triangleq& P_p\mathbb{E}\{\boldsymbol{G}_j\boldsymbol{f}_r\boldsymbol{f}_r^H\boldsymbol{G}_j^H\} = P_p\mathbb{E}\{\boldsymbol{g}_j\boldsymbol{g}_j^H\} \circ \mathbb{E}\{\boldsymbol{f}_r\boldsymbol{f}_r^H\},\\
\sigma_{f_j}^2 =& P_p\mathbb{E}\{f_j f_j^*\},\\
\boldsymbol{B}_{N_j} \triangleq& \sigma_r^2\mathbb{E}\{\boldsymbol{G}_j\boldsymbol{G}_j^H\} \triangleq \sigma_r^2 diag\{\mathbb{E}\{g_{ji}g_{ji}^*\}\},\\
\hat{\sigma_j^2} \triangleq& \sigma_{f_j}^2 + \sigma_1^2.
\end{aligned}$$

Accordingly, the average interference powers at B in time slot one ($P_I^{(1)}$) and two ($P_I^{(2)}$) are given as,

$$P_I^{(1)} = a_1P_1 + a_2P_2, \tag{5.7a}$$

$$P_I^{(2)} = \boldsymbol{\omega}(P_1\boldsymbol{C}_1 + P_2\boldsymbol{C}_2 + \boldsymbol{C}_3)\boldsymbol{\omega}^H, \tag{5.7b}$$

where

$$\begin{aligned}
a_1 \triangleq& \mathbb{E}\{h_1h_1^*\},\ a_2 \triangleq \mathbb{E}\{h_2h_2^*\},\\
\boldsymbol{C}_1 \triangleq& \mathbb{E}\{\boldsymbol{H}_r\boldsymbol{g}_1\boldsymbol{g}_1^H\boldsymbol{H}_r^H\} = \mathbb{E}\{\boldsymbol{g}_1\boldsymbol{g}_1^H\} \circ \mathbb{E}\{\boldsymbol{h}_r\boldsymbol{h}_r^H\},\\
\boldsymbol{C}_2 \triangleq& \mathbb{E}\{\boldsymbol{H}_r\boldsymbol{g}_2\boldsymbol{g}_2^H\boldsymbol{H}_r^H\} = \mathbb{E}\{\boldsymbol{g}_2\boldsymbol{g}_2^H\} \circ \mathbb{E}\{\boldsymbol{h}_r\boldsymbol{h}_r^H\},\\
\boldsymbol{C}_3 \triangleq& P_p\mathbb{E}\{\boldsymbol{H}_r\boldsymbol{f}_r\boldsymbol{f}_r^H\boldsymbol{H}_r^H\} + \sigma_r^2\mathbb{E}\{\boldsymbol{H}_r\boldsymbol{H}_r^H\}.
\end{aligned}$$

Problem Formulation

Our goal is to design the transmit powers P_j ($j = 1, 2$) and the distributed beamforming coefficients ω_i ($i = 1, 2, ..., K$) such that the two-way outage probability is minimized, or equivalently, the worse average SINR ($\min(\overline{\text{SINR}}_1, \overline{\text{SINR}}_2)$) is

maximized. Meanwhile, both $P_I^{(1)}$ and $P_I^{(2)}$ must be kept under the interference temperature limit I_{th}, and P_1 and P_2 should not exceed their maximum available levels, namely P_1^{max} and P_2^{max}, respectively. Therefore, the optimization problem is formulated as,

$$
\begin{aligned}
\text{(P-5.1)} \quad \max_{P_1,\,P_2,\,\boldsymbol{\omega}} \quad & \min\{\overline{\text{SINR}}_1, \overline{\text{SINR}}_2\} \\
\text{s.t.} \quad & \boldsymbol{\omega}(P_1\boldsymbol{C}_1 + P_2\boldsymbol{C}_2 + \boldsymbol{C}_3)\boldsymbol{\omega}^H \le I_{th}, && \text{(5.8a)} \\
& a_1P_1 + a_2P_2 \le I_{th}, && \text{(5.8b)} \\
& P_1 \le P_1^{max},\, P_2 \le P_2^{max}, && \text{(5.8c)} \\
\text{where} \quad & \overline{\text{SINR}}_1 = \frac{P_2\boldsymbol{\omega}\boldsymbol{A}\boldsymbol{\omega}^H}{\boldsymbol{\omega}(\boldsymbol{B}_1 + \boldsymbol{B}_{N_1})\boldsymbol{\omega}^H + \hat{\sigma_1^2}}, \\
& \overline{\text{SINR}}_2 = \frac{P_1\boldsymbol{\omega}\boldsymbol{A}\boldsymbol{\omega}^H}{\boldsymbol{\omega}(\boldsymbol{B}_2 + \boldsymbol{B}_{N_2})\boldsymbol{\omega}^H + \hat{\sigma_2^2}}.
\end{aligned}
$$

Since we consider only average SINRs, the update of the transmit powers and relay gains is less frequent, e.g., 1000 rounds information exchange between SU_1 and SU_2. Therefore, we assume that either SU_1 and SU_2 solve this optimization problem by our proposed algorithms in the next sections and then broadcasts the results to the relays and the other terminal.

5.3 Necessary Conditions

The optimization problem (P-5.1) is not trivial. However, three necessary conditions for the optimal solution can be found as follows.

Lemma 5. 1. *(P-5.1) is an SINR balancing problem because there is one optimal solution* $(P_1,\ P_2,\ \boldsymbol{\omega})$ *such that (P-5.1) achieves its optimal value with* $\overline{SINR}_1$=$\overline{SINR}_2$.

Proof. See Appendix C.1 for details. □

Lemma 5. 2. *Let* $(P_1^{opt},\ P_2^{opt},\ \boldsymbol{\omega}^{opt})$ *be one optimal solution to (P-5.1). Then at least one of the three inequality constraints in* (5.8b) *and* (5.8c) *are satisfied with equality.*

Proof. See Appendix C.2 for details. □

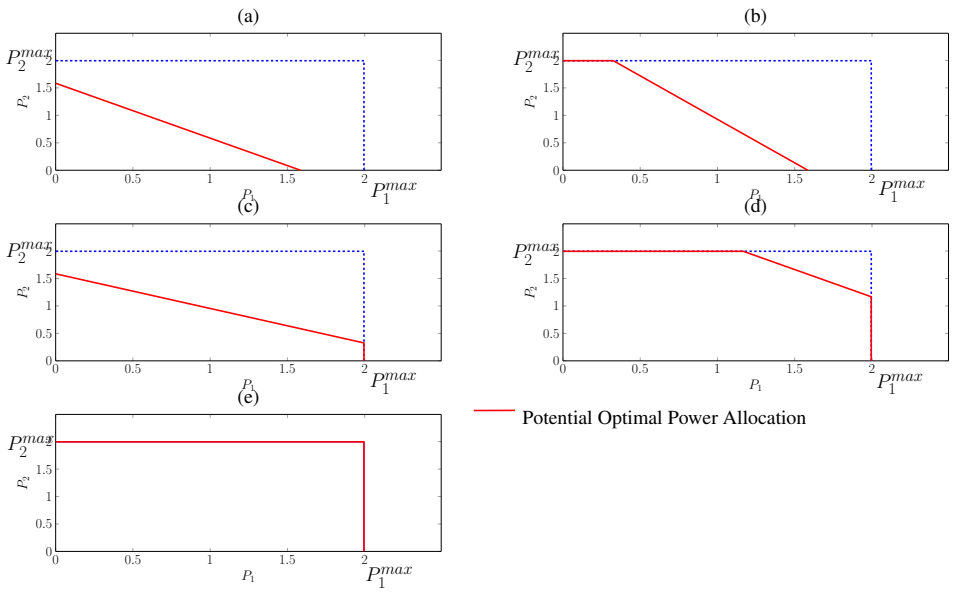

Figure 5.2: Five Cases of Potential Optimal $(P_1,\ P_2)$ Pairs. (a) Case I: $a_1P_1 + a_2P_2 = I_{th}$ is inside the rectangular from $(0, 0)$ to (P_1^{max}, P_2^{max}). (b) Case II: $a_1P_1 + a_2P_2 = I_{th}$ is outside the rectangular when $P_2 > P_2^{max}$. (c) Case III:$a_1P_1 + a_2P_2 = I_{th}$ is outside the rectangular when $P_1 > P_1^{max}$. (d) Case IV: $a_1P_1 + a_2P_2 = I_{th}$ is outside the rectangular when $P_j > P_j^{max}$, $j = 1,\ 2$. (e) Case V: $a_1P_1 + a_2P_2 = I_{th}$ is outside the rectangular.

According to Lemma 3.2, there are five possible cases, as shown in Fig. 5.2, where the optimal power allocation $(P_1,\ P_2)$ must lie on a line, which is referred to as the potential optimal power allocation (POPA) line throughout this chapter.

Lemma 5. 3. *Let* $(P_1^{opt},\ P_2^{opt},\ \boldsymbol{\omega}^{opt})$ *be one optimal solution to (P-5.1). Then the inequality constraint* (5.8a) *is satisfied with equality.*

Proof. See Appendix C.2 for details. □

5.4 Optimal Relaying and Power Allocation for Single Relay Systems

Since generally the optimization problem (P-5.1) is non-convex and difficult to solve, we start with the case where there is only one relay ($K = 1$) assisting the communication between SU_1 and SU_2, and the multi-relay case ($K > 1$) will be treated in the next section.

5.4.1 Optimal Relay Gain and Power Allocation

In a single-relay system, all vectors and matrices become scales and are thus presented in lower-case letters throughout this section. Then the optimization problem (P-5.1) becomes,

$$\text{(P-5.2)} \quad \max_{P_1,\,P_2,\,\omega} \quad \min\{\frac{P_2|g_1|^2|g_2|^2|\omega|^2}{\Delta|g_1|^2|\omega|^2+\hat{\sigma_1^2}}, \frac{P_1|g_1|^2|g_2|^2|\omega|^2}{\Delta|g_2|^2|\omega|^2+\hat{\sigma_2^2}}\}$$

$$\text{s.t.} \quad |h_r|^2(P_1|g_1|^2+P_2|g_2|^2+\Delta)|\omega|^2 \leq I_{th}, \tag{5.9a}$$

$$a_1P_1+a_2P_2 \leq I_{th}, \tag{5.9b}$$

$$P_1 \leq P_1^{max},\ P_2 \leq P_2^{max}, \tag{5.9c}$$

$$|g_j|^2 \triangleq \mathbb{E}\{|g_j|^2\}, \qquad |f_j|^2 \triangleq \mathbb{E}\{|f_j|^2\}, \qquad j=1,\,2,$$
$$|h_r|^2 \triangleq \mathbb{E}\{|h_r|^2\}, \qquad |f_r|^2 \triangleq \mathbb{E}\{|f_r|^2\}, \qquad \Delta \triangleq P_p|f_r|^2+\sigma_r^2.$$

From (P-5.2), it is clear that the phase of ω has no impact on the solution. Therefore, we assume that ω takes only a positive real value. Furthermore, applying Lemma 5.1 and Lemma 5.3, the original three dimensional optimization problem (P-5.2) turns into a two dimensional optimization problem as,

$$\text{(P-5.3)} \quad \max_{P_1,\,P_2} \quad \frac{|g_1|^2|g_2|^2(P_2\hat{\sigma_2^2}-P_1\hat{\sigma_1^2})}{\Delta(|g_1|^2\hat{\sigma_2^2}-|g_2|^2\hat{\sigma_1^2})}$$

$$\text{s.t.} \quad \Phi(P_1,\,P_2)=0, \tag{5.10a}$$

$$a_1P_1+a_2P_2 \leq I_{th}, \tag{5.10b}$$

$$P_1 \leq P_1^{max}, P_2 \leq P_2^{max}, \tag{5.10c}$$

$$|\omega|^2 = \frac{P_2\hat{\sigma_2^2}-P_1\hat{\sigma_1^2}}{(P_1|g_1|^2-P_2|g_2|^2)\Delta} > 0. \tag{5.10d}$$

where

$$\Phi(P_1,\,P_2) \triangleq |h_r|^2|g_2|^2\hat{\sigma_2^2}P_2^2-|h_r|^2|g_1|^2\hat{\sigma_1^2}P_1^2+(|h_r|^2|g_1|^2\hat{\sigma_2^2}-|h_r|^2|g_2|^2\hat{\sigma_1^2})P_1P_2$$
$$+(\Delta|h_r|^2\hat{\sigma_2^2}+\Delta I_{th}|g_2|^2)P_2-(\Delta|h_r|^2\hat{\sigma_1^2}+\Delta I_{th}|g_1|^2)P_1, \tag{5.11}$$

To solve (P-5.3), there are three possible cases to consider:

1) CASE 1: $|g_1|^2\hat{\sigma_2^2} > |g_2|^2\hat{\sigma_1^2}$

In this case, in order to keep both SINRs and $|\omega|^2$ positive, $(P_1,\,P_2)$ must satisfy

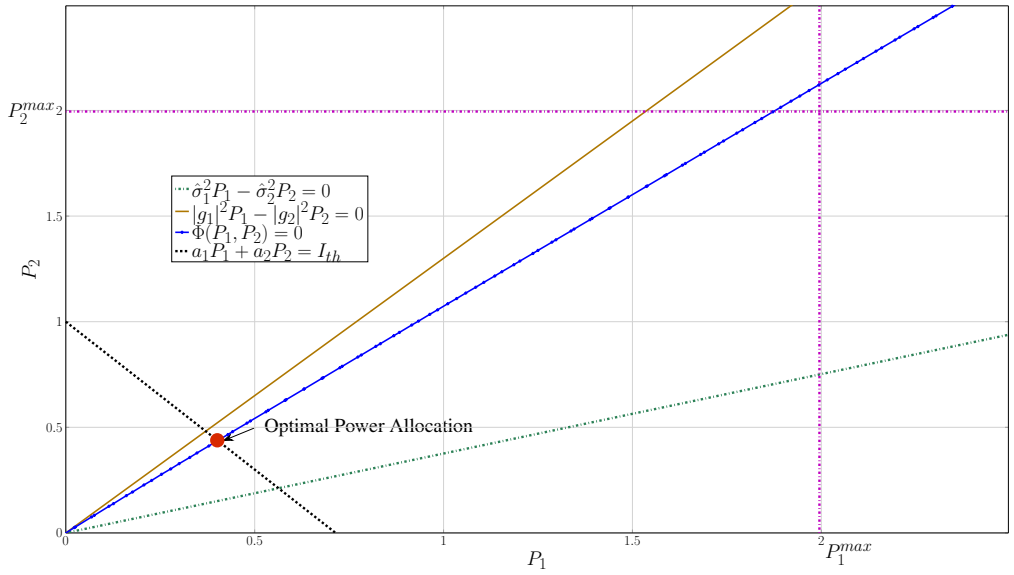

Figure 5.3: Single-Relay System, Case 1: $|g_1|^2\hat{\sigma_2^2} > |g_2|^2\hat{\sigma_1^2}$

$$\frac{\hat{\sigma_1^2}}{\hat{\sigma_2^2}} < \frac{P_2}{P_1} < \frac{|g_1|^2}{|g_2|^2} \tag{5.12}$$

Moreover, we find that the constraint $\Phi(P_1,\, P_2) = 0$ is a hyperbolic curve, which always lies between the lines $P_2 = \frac{\hat{\sigma_1^2}}{\hat{\sigma_2^2}} P_1$ and $P_2 = \frac{|g_1|^2}{|g_2|^2} P_1$ in the first phase, as shown in Fig. 5.3. Therefore, once the constraint (5.10a) is satisfied, (5.10d) must be satisfied. Thus, (P-5.3) is equivalent to,

$$\begin{aligned} \text{(P-5.4)} \quad \max_{P_1,\, P_2} \quad & \frac{|g_1|^2|g_2|^2(P_2\hat{\sigma_2^2} - P_1\hat{\sigma_1^2})}{\Delta(|g_1|^2\hat{\sigma_2^2} - |g_2|^2\hat{\sigma_1^2})} \\ \text{s.t.} \quad & \Phi(P_1,\, P_2) = 0, \\ & a_1 P_1 + a_2 P_2 \le I_{th}, \\ & P_1 \le P_1^{max},\, P_2 \le P_2^{max}. \end{aligned}$$

Since Lemma 5.2 implies that the optimal power allocation should lie on the POPA line, in this case, the optimal power allocation (P_1, P_2) should be the cross point of $\Phi(P_1, P_2) = 0$ and the POPA line, which must be one of (5.13a)–(5.13c). An example of this case is shown in Fig. 5.3.

$$P_1^{(1)} = \frac{-\xi_1 - \sqrt{\xi_1^2 - 4\zeta_1\varrho_1}}{2\zeta_1},\ P_2^{(1)} = P_2^{max}, \tag{5.13a}$$

$$P_1^{(2)} = P_1^{max},\ P_2^{(2)} = \frac{-\xi_2 + \sqrt{\xi_2^2 - 4\zeta_2\varrho_2}}{2\zeta_2}, \tag{5.13b}$$

$$P_1^{(3)} = \frac{-\xi_3 - \sqrt{\xi_3^2 - 4\zeta_3\varrho_3}}{2\zeta_3},\ P_2^{(3)} = \frac{I_{th}}{a_1} - \frac{a_1}{a_2}P_1^{(3)}, \tag{5.13c}$$

where

$$\begin{aligned}
\xi_1 =& |h_r|^2(|g_1|^2\hat{\sigma_2^2} - |g_2|^2\hat{\sigma_1^2})P_2^{max} - \Delta(|h_r|^2\hat{\sigma_1^2} + I_{th}|g_1|^2),\\
\zeta_1 =& -|h_r|^2|g_1|^2\hat{\sigma_1^2},\\
\varrho_1 =& |h_r|^2|g_2|^2\hat{\sigma_2^2}P_2^{max2} + (|h_r|^2\hat{\sigma_2^2} + I_{th}|g_2|^2)\Delta P_2^{max};\\
\xi_2 =& |h_r|^2(|g_1|^2\hat{\sigma_2^2} - |g_2|^2\hat{\sigma_1^2})P_1^{max} + \Delta(|h_r|^2\hat{\sigma_2^2} + I_{th}|g_2|^2),\\
\zeta_2 =& |h_r|^2|g_2|^2\hat{\sigma_2^2},\\
\varrho_2 =& -|h_r|^2|g_1|^2\hat{\sigma_1^2}P_1^{max2} - (|h_r|^2\hat{\sigma_1^2} + I_{th}|g_1|^2)\Delta P_1^{max};\\
\xi_3 =& -\frac{2I_{th}a_1|h_r|^2|g_2|^2\hat{\sigma_2^2}}{a_2^2} - \frac{|h_r|^2\hat{\sigma_2^2} + I_{th}|g_2|^2}{a_2}\Delta a_1 - (|h_r|^2\hat{\sigma_1^2} + I_{th}|g_1|^2)\Delta\\
&+ \frac{(|g_1|^2\hat{\sigma_2^2} - |g_2|^2\hat{\sigma_1^2})I_{th}|h_r|^2}{a_2},\\
\zeta_3 =& \frac{|h_r|^2|g_2|^2\hat{\sigma_2^2}a_1^2}{a_2^2} - \frac{(|g_1|^2\hat{\sigma_2^2} - |g_2|^2\hat{\sigma_1^2})|h_r|^2a_1}{a_2} - |h_r|^2|g_1|^2\hat{\sigma_1^2},\\
\varrho_3 =& \frac{|h_r|^2|g_2|^2\hat{\sigma_2^2}I_{th}^2}{a_2^2} + \frac{(|h_r|^2\hat{\sigma_2^2} + I_{th}|g_2|^2)I_{th}\Delta}{a_2};
\end{aligned}$$

Once the optimal transmit powers (P_1, P_2) are found for this case, the corresponding optimal relaying coefficient ω can be found via,

$$\omega = \sqrt{\frac{P_2\hat{\sigma_2^2} - P_1\hat{\sigma_1^2}}{(P_1|g_1|^2 - P_2|g_2|^2)\Delta}} \tag{5.14}$$

2) CASE 2: $|g_1|^2\hat{\sigma_2^2} < |g_2|^2\hat{\sigma_1^2}$

The analysis of this case is similar to that of CASE 1, and the same solution is obtained.

3) CASE 3: $|g_1|^2\hat{\sigma_2^2} = |g_2|^2\hat{\sigma_1^2}$

Although the probability that this case occurs is nearly zero, when it does happen we have the following approach to find out the optimal solution.

According to the SINR balancing property, we know that $(P_1,\ P_2,\ \omega)$ must fulfil both $P_1\hat{\sigma_1^2} = P_2\hat{\sigma_2^2}$ and $|\omega|^2 = \frac{I_{th}}{|h_r|^2(P_1|g_1|^2+P_2|g_2|^2+\Delta)}$. Therefore, in this case, (P-5.4) is equivalent to,

$$\text{(P-5.5)} \quad \max_{P_2} \quad \frac{P_2|g_1|^2|g_2|^2 I_{th}}{2|h_r|^2|g_1|^2\hat{\sigma_2^2}\hat{\sigma_1^2}P_2 + \hat{\sigma_1^2}|g_1|^2\Delta I_{th} + |h_r|^2\hat{\sigma_1^2}\Delta}$$
$$\text{s.t.} \quad P_2 \le \frac{I_{th}\hat{\sigma_1^2}}{a_1\hat{\sigma_2^2} + a_2\hat{\sigma_1^2}},\ P_2 \le \frac{\hat{\sigma_1^2}}{\hat{\sigma_2^2}}P_1^{max},\ P_2 \le P_2^{max},$$

which obviously achieves its optimal value only when

$$P_2 = \min\left(\frac{\hat{\sigma_1^2}}{\hat{\sigma_2^2}}P_1^{max}, P_2^{max}, \frac{\hat{\sigma_1^2}I_{th}}{a_1\hat{\sigma_2^2} + a_2\hat{\sigma_1^2}}\right). \tag{5.15}$$

Once P_2 is determined, P_1 and ω can be found via,

$$P_1 = \frac{\hat{\sigma_2^2}}{\hat{\sigma_1^2}}P_2, \tag{5.16}$$

$$\omega = \sqrt{\frac{I_{th}}{|h_r|^2(P_1|g_1|^2 + P_2|g_2|^2 + \Delta)}}. \tag{5.17}$$

Algorithm SRO: Closed-Form Solution for Single-Relay System

Input : Δ, $|h_r|^2$, $|g_1|^2$, $|g_2|^2$, $\hat{\sigma_1^2}$, $\hat{\sigma_2^2}$, a_1, a_2, P_1^{max}, P_2^{max}, I_{th}
Output: P_1, P_2, ω

if $|g_1|^2\hat{\sigma_2^2} = |g_2|^2\hat{\sigma_1^2}$ **then**
  $P_1 = \frac{\hat{\sigma_2^2}}{\hat{\sigma_1^2}}P_2,\ P_2 = \min(\frac{\hat{\sigma_1^2}}{\hat{\sigma_2^2}}P_1^{max}, P_2^{max}, \frac{\hat{\sigma_1^2}I_{th}}{a_1\hat{\sigma_2^2}+a_2\hat{\sigma_1^2}})$, $\omega = \sqrt{\frac{I_{th}}{|h_r|^2(P_1|g_1|^2+P_2|g_2|^2+\Delta)}}$;
else
  Compute the following three cross points $(P_1^{(1)},\ P_2^{(1)})$, $(P_1^{(2)},\ P_2^{(2)})$, and $(P_1^{(3)},\ P_2^{(3)})$ according equations (5.13a)–(5.13c)
  Choose the point on the POPA line.
  $\omega = \sqrt{\frac{P_2\hat{\sigma_2^2} - P_1\hat{\sigma_1^2}}{(P_1|g_1|^2 - P_2|g_2|^2)\Delta}}$;
end
return P_1, P_2, ω.

To conclude the analysis above, we generate the SRO Algorithm to compute the optimal power allocation and relay gain in a single-relay system.

5.4.2 Results and Discussions

In this section, we assess the SRO algorithm in single-relay systems through simulations. Since it is critically important to show the performance gain achieved by SRO, we compare it to a system with equal power allocation and simple AF relaying. We label this benchmark system as EPA. It allocates equal powers to the two secondary terminals, $P_1 = P_2 = \min(\frac{I_{th}}{a_1+a_2}, P_T^{max})$ where P_T^{max} is the maximum available power, and computes the relaying coefficient as $\omega = \frac{I_{th}}{\mathbb{E}\{|h_r|^2\}}$.

In the simulations, we assume that wireless channels are flat fading and their complex channel gains are generated via the method used in [44] as,

$$f = \sqrt{\frac{1}{1+\alpha}}\bar{f} + \sqrt{\frac{\alpha}{1+\alpha}}\tilde{f}, \tag{5.18}$$

where $\bar{f} \sim \mathcal{CN}(0,1)$ and $\tilde{f} \sim \mathcal{CN}(0,1)$ are the mean and variable components of the complex channel gain, respectively. Accordingly, α is the uncertainty describing how much the complex channel gain varies from its mean value. Obviously, with a larger α, the channel fluctuates more severely between samples. Same α value is assumed for all channels in each simulation run. We further assume that $P_p = P_1^{max} = P_2^{max} = 3$ dBm. All AWGNs are of 0 dBm power.

The average SINR v.s. I_{th} curves with two different α values, -5 dB and -20 dB, are shown in Fig. 5.4, where a higher SINR can be achieved with a more stable channel, say $\alpha = -20$ dB, compared with $\alpha = -5$ dB. This result is reasonable because besides $\boldsymbol{g}_j$, SU_j $(j = 1, 2)$ knows only the SOS of other channels.

Besides, a constant SINR gap between $\alpha = -20$ dB and $\alpha = -5$ dB exists when I_{th} is lower than 2 dBm. Since I_{th} has increased to 2 dBm, the $\alpha = -5$ dB curve converges to the $\alpha = -20$ dB curve. This result occurs because the increase of I_{th} moves the limitation of the power allocation from the constraint on $P_I^{(1)}$ to its maximum value P^{max}, as shown in Fig. 5.5 and Fig. 5.6.

Moreover, in Fig. 5.4, the relatively low achievable optimal SINR in single-relay systems is not surprising, because in SRO, the relay gain takes only a real value, so that the phase distortions of the signals introduced by the wireless channels have not been taken into account. As a result, the relays' capability to improve the system performance is limited, e.g., only less than 1 dB improvement form EPA.

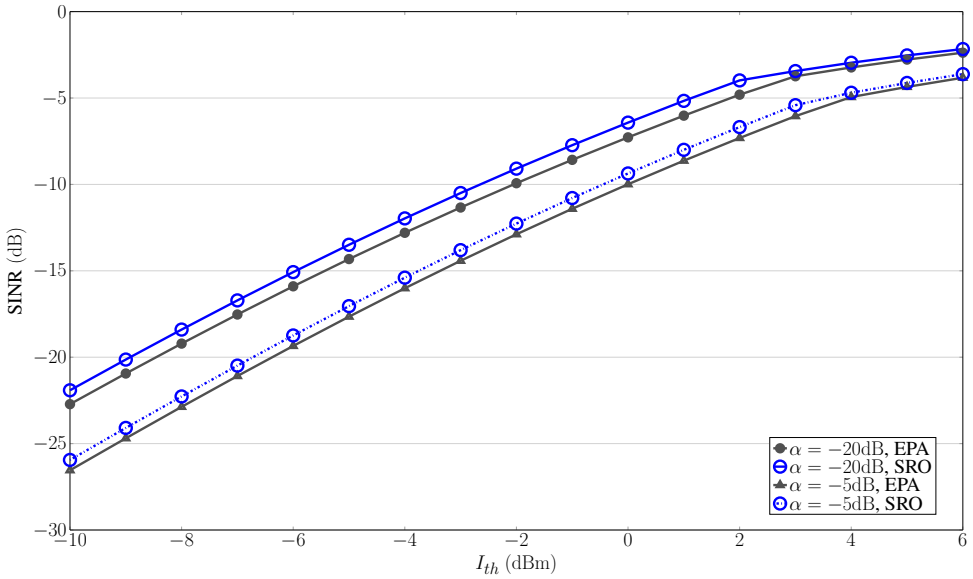

Figure 5.4: SINR v.s. I_{th} in a Single-Relay System

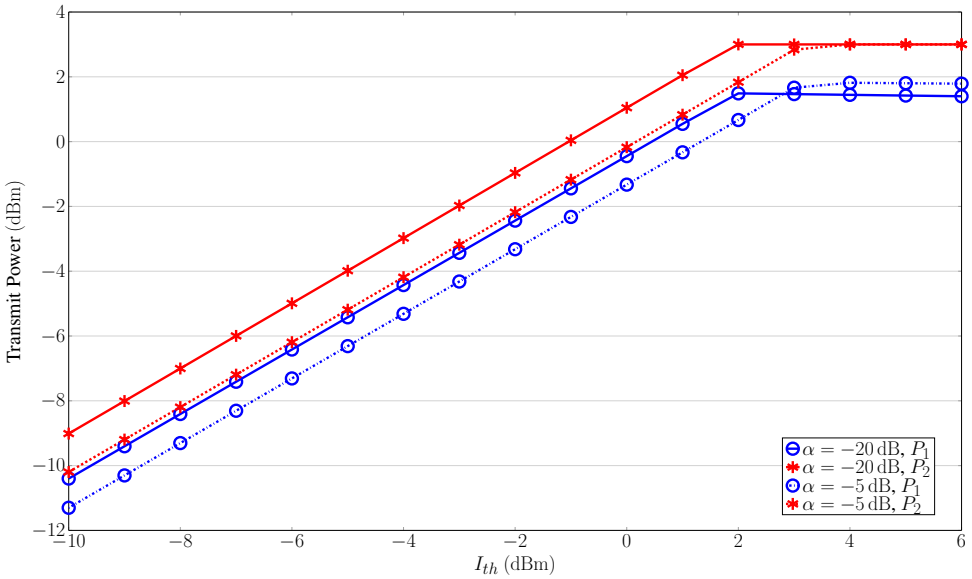

Figure 5.5: Transmit Power v.s. I_{th} in a Single-Relay System

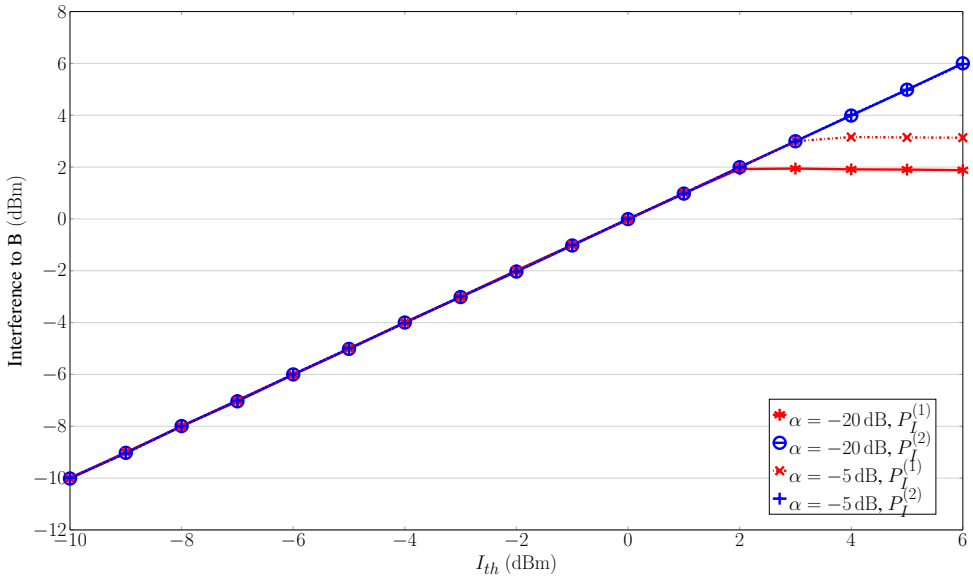

Figure 5.6: Interference v.s. I_{th} in a Single-Relay System

5.5 Joint Distributed Beamforming and Power Allocation for Multiple Relay Systems

While the previous section derived the optimal relay gain and power allocation for single-relay systems, this section develops joint distributed beamforming and power allocation algorithms for multi-relay systems.

5.5.1 Optimal Joint Distributed Beamforming and Power Allocation

When multiple relays are present in the secondary network, we need to solve (P-5.1) to find an optimal distributed beamforming vector $\boldsymbol{\omega}$ and power allocation (P_1, P_2). However, since (P-5.1) is a non-convex optimization problem, it is difficult to solve. Therefore, we start with introducing a slack variable t to (P-5.1), and convert it to,

$$
\begin{aligned}
\text{(P-5.6)} \quad \max_{P_1,\, P_2,\, \boldsymbol{\omega},\, t} \quad & t \\
\text{s.t.} \quad & \frac{P_2 \boldsymbol{\omega} \boldsymbol{A} \boldsymbol{\omega}^H}{\boldsymbol{\omega}(\boldsymbol{B}_1 + \boldsymbol{B}_{N_1})\boldsymbol{\omega}^H + \hat{\sigma_1^2}} \geq t, \\
& \frac{P_1 \boldsymbol{\omega} \boldsymbol{A} \boldsymbol{\omega}^H}{\boldsymbol{\omega}(\boldsymbol{B}_2 + \boldsymbol{B}_{N_2})\boldsymbol{\omega}^H + \hat{\sigma_2^2}} \geq t, \\
& \boldsymbol{\omega}(P_1\boldsymbol{C}_1 + P_2\boldsymbol{C}_2 + \boldsymbol{C}_3)\boldsymbol{\omega}^H = I_{th}, \\
& a_1 P_1 + a_2 P_2 \leq I_{th}, \\
& P_1 \leq P_1^{max},\, P_2 \leq P_2^{max}.
\end{aligned}
$$

This problem is still a non-convex optimization problem. But, if we fix the transmit powers $(P_1,\, P_2)$, which satisfies $a_1 P_1 + a_2 P_2 \leq I_{th}$, $P_1 \leq P_1^{max}$, $P_2 \leq P_2^{max}$, and define the Hermitian and positive definite matrix $\boldsymbol{C} \triangleq P_1\boldsymbol{C}_1 + P_2\boldsymbol{C}_2 + \boldsymbol{C}_3$, the corresponding optimal beamforming vector $\boldsymbol{\omega}$ can be found by our proposed MBSS algorithm. In MBSS, we first decompose $\boldsymbol{\omega}$ as $\boldsymbol{\omega} \triangleq \sqrt{p}\tilde{\boldsymbol{\omega}}\boldsymbol{C}^{-1/2}$, where $\|\tilde{\boldsymbol{\omega}}\|^2 = 1$, $p \geq 0$, and $\boldsymbol{C}^{-1/2}$ is the inverse of $\boldsymbol{C}^{1/2}$. According to Lemma 5.3, it is clear that p should take value of I_{th} to satisfy $\boldsymbol{\omega}(P_1\boldsymbol{C}_1 + P_2\boldsymbol{C}_2 + \boldsymbol{C}_3)\boldsymbol{\omega}^H = I_{th}$. Substituting p and $\boldsymbol{\omega} = \sqrt{p}\tilde{\boldsymbol{\omega}}\boldsymbol{C}^{-1/2}$ into (P-5.6), we obtain the equivalent problem as,

$$
\begin{aligned}
\text{(P-5.7)} \quad \max_{\tilde{\boldsymbol{\omega}},\, t} \quad & t \\
\text{s.t.} \quad & \frac{\tilde{\boldsymbol{\omega}} \hat{\boldsymbol{A}}_1 \tilde{\boldsymbol{\omega}}^H}{\tilde{\boldsymbol{\omega}} \hat{\boldsymbol{B}}_1 \tilde{\boldsymbol{\omega}}^H} \geq t,\, \frac{\tilde{\boldsymbol{\omega}} \hat{\boldsymbol{A}}_2 \tilde{\boldsymbol{\omega}}^H}{\tilde{\boldsymbol{\omega}} \hat{\boldsymbol{B}}_2 \tilde{\boldsymbol{\omega}}^H} \geq t, \\
& \|\tilde{\boldsymbol{\omega}}\|^2 = 1,\, t > 0.
\end{aligned}
\tag{5.19}
$$

where

$$
\begin{cases}
\hat{\boldsymbol{A}}_1 = P_2 I_{th} \boldsymbol{C}^{-1/2} \boldsymbol{A} \boldsymbol{C}^{-1/2}, \\
\hat{\boldsymbol{A}}_2 = P_1 I_{th} \boldsymbol{C}^{-1/2} \boldsymbol{A} \boldsymbol{C}^{-1/2}, \\
\hat{\boldsymbol{B}}_1 = I_{th} \boldsymbol{C}^{-1/2} (\boldsymbol{B}_1 + \boldsymbol{B}_{N_1}) \boldsymbol{C}^{-1/2} + \hat{\sigma_1^2} I, \\
\hat{\boldsymbol{B}}_2 = I_{th} \boldsymbol{C}^{-1/2} (\boldsymbol{B}_2 + \boldsymbol{B}_{N_2}) \boldsymbol{C}^{-1/2} + \hat{\sigma_2^2} I.
\end{cases}
\tag{5.20}
$$

Obviously, (P-5.7) simultaneously maximizes two generalized Rayleigh-Ritz ratios, which can be done by using a bi-section search [125] along the variable t in the range $[t_{low}, t_{up}]$, where t_{low} and t_{up} are the upper and lower bounds to the

Algorithm MBSS: Modified Bi-Section Search

Input : P_1, P_2, $\boldsymbol{A}$, $\boldsymbol{B}_1$, $\boldsymbol{B}_{N_1}$, $\boldsymbol{B}_2$, $\boldsymbol{B}_{N_2}$, $\hat{\sigma_1^2}$, $\hat{\sigma_2^2}$, $\boldsymbol{C}_1$, $\boldsymbol{C}_2$, $\boldsymbol{C}_3$, I_{th}
Output: t, $\boldsymbol{\omega}$
Internal Variables: t_u, t_l, t_m, $\tilde{\boldsymbol{\omega}}_m$

Compute $\boldsymbol{C} = P_1\boldsymbol{C}_1 + P_2\boldsymbol{C}_2 + \boldsymbol{C}_3$;
Compute $\boldsymbol{C}^{1/2}$ and $\boldsymbol{C}^{-1/2}$ such that $\boldsymbol{C}^{1/2}\boldsymbol{C}^{1/2} = \boldsymbol{C}$;
Compute $\hat{\boldsymbol{A}}_1$, $\hat{\boldsymbol{A}}_2$, $\hat{\boldsymbol{B}}_1$, $\hat{\boldsymbol{B}}_2$ by using (5.20);
Compute $(t_i, \tilde{\boldsymbol{\omega}}_i)$, $i = 1, 2$ such that $t_i = \lambda_{max}(\hat{\boldsymbol{A}}_i, \hat{\boldsymbol{B}}_i)$, where $\tilde{\boldsymbol{\omega}}_i$ is the corresponding normalized eigenvector to $\lambda_{max}(\hat{\boldsymbol{A}}_i, \hat{\boldsymbol{B}}_i)$;
if $t_1 < t_2$ **then**
    $t_{up} = t_1$, $\tilde{\boldsymbol{\omega}}_{mid} = \tilde{\boldsymbol{\omega}}_1$, $t_{low} = \frac{\tilde{\boldsymbol{\omega}}_{mid}\hat{\boldsymbol{A}}_2\tilde{\boldsymbol{\omega}}_{mid}^H}{\tilde{\boldsymbol{\omega}}_{mid}\hat{\boldsymbol{B}}_2\tilde{\boldsymbol{\omega}}_{mid}^H}$;
else if $t_1 > t_2$ **then**
    $t_{up} = t_2$, $\tilde{\boldsymbol{\omega}}_{mid} = \tilde{\boldsymbol{\omega}}_2$, $t_{low} = \frac{\tilde{\boldsymbol{\omega}}_{mid}\hat{\boldsymbol{A}}_1\tilde{\boldsymbol{\omega}}_{mid}^H}{\tilde{\boldsymbol{\omega}}_{mid}\hat{\boldsymbol{B}}_1\tilde{\boldsymbol{\omega}}_{mid}^H}$;
else
    $t_{up} = t_1$, $t_1' = \frac{\tilde{\boldsymbol{\omega}}_2\hat{\boldsymbol{A}}_1\tilde{\boldsymbol{\omega}}_2^H}{\tilde{\boldsymbol{\omega}}_2\hat{\boldsymbol{B}}_1\tilde{\boldsymbol{\omega}}_2^H}$, $t_2' = \frac{\tilde{\boldsymbol{\omega}}_1\hat{\boldsymbol{A}}_2\tilde{\boldsymbol{\omega}}_1^H}{\tilde{\boldsymbol{\omega}}_1\hat{\boldsymbol{B}}_2\tilde{\boldsymbol{\omega}}_1^H}$;
    if $t_1' \geq t_2'$ **then** $t_{low} = t_1'$, $\tilde{\boldsymbol{\omega}}_{mid} = \tilde{\boldsymbol{\omega}}_2$;
    else $t_{low} = t_2'$, $\tilde{\boldsymbol{\omega}}_{mid} = \tilde{\boldsymbol{\omega}}_1$
    end
end
if $t_{up} \leq t_{low}$ **then** $t_{mid} = t_{up}$;
else
    while $|t_{up} - t_{low}| > \eta$ **do**
        $t_{mid} = \frac{t_{up}+t_{low}}{2}$, $\tilde{\boldsymbol{\omega}}_{mid} = \boldsymbol{0}$
        if (P-5.8) with $t = t_{mid}$ is feasible **then** $t_{low} = t_{mid}$, $\tilde{\boldsymbol{\omega}}_{mid} =$ any solution of (P-5.8)
        else $t_{up} = t_{mid}$
        end
    end
end
if $t_{mid} \leq 0$ **then** $t = 0$, $\boldsymbol{\omega} = \boldsymbol{0}$;
else $t = t_{mid}$, $\boldsymbol{\omega} = \sqrt{I_{th}}\tilde{\boldsymbol{\omega}}_{mid}\boldsymbol{C}^{-1/2}$
end
return t, $\boldsymbol{\omega}$.

optimal value of (P-5.7). In this bi-section search, given a $t = t_{mid} = \frac{t_{low}+t_{up}}{2}$, it is required to check if there exists an $\tilde{\boldsymbol{\omega}}$ such that t_{mid} is achievable. If an $\tilde{\boldsymbol{\omega}}$ can be found, then we update t_{low} as $t_{low} = t_{mid}$, otherwise we update t_{up} as $t_{up} = t_{mid}$. This is equivalent to solve a feasibility problem [125] as (P-5.8), which can be done by using an interior-point algorithm [125].

$$\text{(P-5.8)} \quad \text{Find} \quad \tilde{\boldsymbol{\omega}}$$
$$\text{s.t.} \quad \frac{\tilde{\boldsymbol{\omega}}\hat{\boldsymbol{A}}_1\tilde{\boldsymbol{\omega}}^H}{\tilde{\boldsymbol{\omega}}\hat{\boldsymbol{B}}_1\tilde{\boldsymbol{\omega}}^H} \geq t_{mid}, \frac{\tilde{\boldsymbol{\omega}}\hat{\boldsymbol{A}}_2\tilde{\boldsymbol{\omega}}^H}{\tilde{\boldsymbol{\omega}}\hat{\boldsymbol{B}}_2\tilde{\boldsymbol{\omega}}^H} \geq t_{mid}, \|\tilde{\boldsymbol{\omega}}\|^2 = 1.$$

Since it has been shown that, at each iteration, the feasibility problem can be solved by an interior-point algorithm, what left is to determine the initial range of the bi-section search. This can be done as follows. Because both $\frac{\tilde{\boldsymbol{\omega}}\hat{\boldsymbol{A}}_1\tilde{\boldsymbol{\omega}}^H}{\tilde{\boldsymbol{\omega}}\hat{\boldsymbol{B}}_1\tilde{\boldsymbol{\omega}}^H}$ and $\frac{\tilde{\boldsymbol{\omega}}\hat{\boldsymbol{A}}_2\tilde{\boldsymbol{\omega}}^H}{\tilde{\boldsymbol{\omega}}\hat{\boldsymbol{B}}_2\tilde{\boldsymbol{\omega}}^H}$ are generalized Rayleigh-Ritz ratios, whose maximum values are their principle generalized eigenvalues, $\lambda_{max}(\hat{\boldsymbol{A}}_1, \hat{\boldsymbol{B}}_1)$ and $\lambda_{max}(\hat{\boldsymbol{A}}_2, \hat{\boldsymbol{B}}_2)$, respectively. Thus, the smaller of $\lambda_{max}(\hat{\boldsymbol{A}}_1, \hat{\boldsymbol{B}}_1)$ and $\lambda_{max}(\hat{\boldsymbol{A}}_2, \hat{\boldsymbol{B}}_2)$ gives an initial upper bound t_{up} to the bi-section search. When computing the initial lower bound t_{low}, since $\hat{\boldsymbol{A}}_j$ and $\hat{\boldsymbol{B}}_j$ $(j = 1, 2)$ are positive definite matrices, $\frac{\tilde{\boldsymbol{\omega}}\hat{\boldsymbol{A}}_1\tilde{\boldsymbol{\omega}}^H}{\tilde{\boldsymbol{\omega}}\hat{\boldsymbol{B}}_1\tilde{\boldsymbol{\omega}}^H}$ and $\frac{\tilde{\boldsymbol{\omega}}\hat{\boldsymbol{A}}_2\tilde{\boldsymbol{\omega}}^H}{\tilde{\boldsymbol{\omega}}\hat{\boldsymbol{B}}_2\tilde{\boldsymbol{\omega}}^H}$ should always be positive and thus t_{low} could be chosen as 0. However, our proposed MBSS algorithm starts with a tighter lower bound, which is calculated as follows. Let $\tilde{\boldsymbol{\omega}}\prime$ be the principle eigenvector corresponding to $\min(\lambda_{max}(\hat{\boldsymbol{A}}_1, \hat{\boldsymbol{B}}_1), \lambda_{max}(\hat{\boldsymbol{A}}_2, \hat{\boldsymbol{B}}_2))$. Then substitute $\tilde{\boldsymbol{\omega}}\prime$ into the other Rayleigh-Ritz ratio, e.g., if $\lambda_{max}(\hat{\boldsymbol{A}}_1, \hat{\boldsymbol{B}}_1) < \lambda_{max}(\hat{\boldsymbol{A}}_2, \hat{\boldsymbol{B}}_2)$, substitute $\tilde{\boldsymbol{\omega}}\prime$ into $\frac{\tilde{\boldsymbol{\omega}}\hat{\boldsymbol{A}}_2\tilde{\boldsymbol{\omega}}^H}{\tilde{\boldsymbol{\omega}}\hat{\boldsymbol{B}}_2\tilde{\boldsymbol{\omega}}^H}$. If $\frac{\tilde{\boldsymbol{\omega}}\prime\hat{\boldsymbol{A}}_2\tilde{\boldsymbol{\omega}}\prime^H}{\tilde{\boldsymbol{\omega}}\prime\hat{\boldsymbol{B}}_2\tilde{\boldsymbol{\omega}}\prime^H} < t_{up}$, we set $t_{low} = \frac{\tilde{\boldsymbol{\omega}}\prime\hat{\boldsymbol{A}}_2\tilde{\boldsymbol{\omega}}\prime^H}{\tilde{\boldsymbol{\omega}}\prime\hat{\boldsymbol{B}}_2\tilde{\boldsymbol{\omega}}\prime^H}$. Otherwise, t_{up} must be the optimal value of (P-5.7).

The above procedure of solving (P-5.7) is concluded in the modified bi-section search (MBSS) algorithm, where η is the predefined stopping threshold of the bi-section search. As mentioned before, our MBSS algorithm starts with a good initial value computed from the upper and lower bounds given by steps 4-11, which might give the optimal solution directly.

Since the optimal beamforming vector $\boldsymbol{\omega}$ can be found via MBSS, given a power allocation (P_1, P_2), an exhaustive search along the POPA line can be performed to find the optimal beamformer and power allocation for the multi-relay system. This process is concluded in the MRO Algorithm.

Algorithm MRO: Optimal Power Allocation and Beamforming for Multi-Relay systems

1 Quantify $(P_1,\ P_2)$ along the POPA line;
2 For each point $(P_1,\ P_2)$, solve (P-5.7) by using MBSS, and store the optimal value $t, \boldsymbol{\omega}$;
3 Compare all t's, choose the largest one, and output the corresponding $P_1,\ P_2,\ \boldsymbol{\omega}$ as optimal power allocation and beamforming vector.

5.5.2 Low-Complexity Sub-Optimal Algorithm I: Simple Power Allocation (SPA) Algorithm

Although MRO can jointly find the optimal distributed beamforming vector $\boldsymbol{\omega}$ and power allocation (P_1, P_2), it has high computational complexity in terms of running time (see Section 5.5.4). Therefore, we propose a low-complexity sub-optimal algorithm (SPA) in this section to reduce the running time required by MRO.

Algorithm SPA: Simple-Power-Allocation Approach

1 Quantify $(P_1,\ P_2)$ along the POPA line;
2 **for** each pair of $(P_1,\ P_2)$ **do**
  | Steps 1-11 in MBSS algorithm
  end
3 Choose $(P_1^{SubOpt}, P_2^{SubOpt})$ with the largest $\min\{t_{low}, t_{up}\}$;
4 Solve (P-5.7) with $(P_1,\ P_2) = (P_1^{SubOpt}, P_2^{SubOpt})$ using MBSS, which returns $\boldsymbol{\omega}^{SubOpt}$;
5 Return $(P_1^{SubOpt}, P_2^{SubOpt})$ and $\boldsymbol{\omega}^{SubOpt}$ as the sub-optimal power allocation and beamformer.

SPA first finds a sub-optimal power allocation $(P_1^{SubOpt}, P_2^{SubOpt})$ as follows. Since steps 4-11 in MBSS give a lower bound or even the optimal value to (P-5.7), we can quantify the POPA line, and apply steps 4-11 in MBSS at each power allocation, then choose the power allocation with the highest lower bound as the sub-optimal power allocation. Once $(P_1^{SubOpt}, P_2^{SubOpt})$ is determined, MBSS is applied to find the sub-optimal $\boldsymbol{\omega}$ corresponding to this sub-optimal power allocation.

Note that, although SPA also does an exhaustive search, no complex algorithm, such as interior-point algorithms, is applied at each iteration. Therefore, SPA's running time reduces significantly compared to that of MRO (see Section 5.5.4).

5.5.3 Low-Complexity Sub-Optimal Algorithm II: Two-Phase Search (TPS) Algorithm

To further eliminate the exhaustive search in SPA, we propose a two-phase search (TPS) algorithm in this section. It first finds a sub-optimal power allocation (Phase I) and then finds the corresponding sub-optimal beamforming vector $\boldsymbol{\omega}$ (Phase II).

Algorithm TPS: Two-Phase Search

1 Compute $(P_1^0,\ P_2^{max})$ and $(P_1^{max},\ P_2^0)$, the cross points of $a_1P_1 + a_2P_2 = I_{th}$ with $P_2 = P_2^{max}$ and $P_1 = P_1^{max}$, respectively;
2 *Phase I:* Solve (P-5.10), (P-5.11) and (P-5.12) by using combined bi-section search and interior-point algorithm, and choose the one with the largest optimal value, compute the corresponding $(P_1^{SubOpt}, P_2^{SubOpt})$;
3 *Phase II:* Let $(P_1,\ P_2) = (P_1^{SubOpt}, P_2^{SubOpt})$. Solve (P-5.7) by using MBSS which will return $\boldsymbol{\omega}^{SubOpt}$;
4 Return $(P_1^{SubOpt},\ P_2^{SubOpt})$ and $\boldsymbol{\omega}^{SubOpt}$ as the sub-optimal power allocation and beamformer.

Phase I: Sub-Optimal Power Allocation Search

To find the sub-optimal power allocation, we first decompose the beamforming vector as $\boldsymbol{\omega} \triangleq \sqrt{p}\tilde{\boldsymbol{\omega}}$, where $\|\tilde{\boldsymbol{\omega}}\|^2 = 1$. According to the SINR balancing property, p should take the value of $\frac{P_2\hat{\sigma_2^2} - P_1\hat{\sigma_1^2}}{\tilde{\boldsymbol{\omega}}[P_1(\boldsymbol{B}_1+\boldsymbol{B}_{N_1}) - P_2(\boldsymbol{B}_2+\boldsymbol{B}_{N_2})]\tilde{\boldsymbol{\omega}}^H}$. Then substituting $\boldsymbol{\omega} \triangleq \sqrt{p}\tilde{\boldsymbol{\omega}}$ and p into (P-5.1) and applying the SINR balancing property, the original problem is converted to,

$$\text{(P-5.9)} \quad \max_{P_1,P_2,\tilde{\boldsymbol{\omega}}} \ \frac{\tilde{\boldsymbol{\omega}}\boldsymbol{A}\tilde{\boldsymbol{\omega}}^H(P_2\hat{\sigma_2^2} - P_1\hat{\sigma_1^2})}{\tilde{\boldsymbol{\omega}}[\hat{\sigma_2^2}(\boldsymbol{B}_1+\boldsymbol{B}_{N_1}) - \hat{\sigma_1^2}(\boldsymbol{B}_2+\boldsymbol{B}_{N_2})]\tilde{\boldsymbol{\omega}}^H}$$

$$\text{s. t.} \quad \|\tilde{\boldsymbol{\omega}}\|^2 = 1, p > 0, \tag{5.21a}$$

$$\Phi(P_1,\ P_2, \tilde{\boldsymbol{\omega}}) = 0, \tag{5.21b}$$

$$a_1P_1 + a_2P_2 \le I_{th}, \tag{5.21c}$$

$$P_1 \le P_1^{max},\ P_2 \le P_2^{max}. \tag{5.21d}$$

$$\Phi(P_1,\ P_2,\ \tilde{\boldsymbol{\omega}}) = k_1P_2^2 + k_2P_1P_2 + k_3P_1^2 + k_4P_2 + k_5P_1, \tag{5.22}$$

where

$$
\begin{aligned}
k_1 =&\hat{\sigma_2^2}\tilde{\boldsymbol{\omega}}\boldsymbol{C}_2\tilde{\boldsymbol{\omega}}^H,\\
k_2 =&\hat{\sigma_2^2}\tilde{\boldsymbol{\omega}}\boldsymbol{C}_1\tilde{\boldsymbol{\omega}}^H - \hat{\sigma_1^2}\tilde{\boldsymbol{\omega}}\boldsymbol{C}_2\tilde{\boldsymbol{\omega}}^H,\\
k_3 =&-\hat{\sigma_1^2}\tilde{\boldsymbol{\omega}}\boldsymbol{C}_1\tilde{\boldsymbol{\omega}}^H,\\
k_4 =&\hat{\sigma_2^2}\tilde{\boldsymbol{\omega}}\boldsymbol{C}_3\tilde{\boldsymbol{\omega}}^H + I_{th}\tilde{\boldsymbol{\omega}}(\boldsymbol{B}_2+\boldsymbol{B}_{N2})\tilde{\boldsymbol{\omega}}^H,\\
k_5 =&-\hat{\sigma_1^2}\tilde{\boldsymbol{\omega}}\boldsymbol{C}_3\tilde{\boldsymbol{\omega}}^H - I_{th}\tilde{\boldsymbol{\omega}}(\boldsymbol{B}_1+\boldsymbol{B}_{N1})\tilde{\boldsymbol{\omega}}^H.
\end{aligned}
$$

Given an $\tilde{\boldsymbol{\omega}}$, the equality constraint (5.21b) $\Phi(P_1,\, P_2) = 0$ becomes a hyperbolic curve, which passes $(0,\, 0)$. Similar to the analysis in the single-relay case, in order to keep both SINRs and p positive, the power allocation $(P_1,\, P_2)$ must be chosen such that $\frac{P_2}{P_1}$ is in the range between $\frac{\hat{\sigma_1^2}}{\hat{\sigma_2^2}}$ and $\frac{\tilde{\boldsymbol{\omega}}(\boldsymbol{B}_1+\boldsymbol{B}_{N_1})\tilde{\boldsymbol{\omega}}^H}{\tilde{\boldsymbol{\omega}}(\boldsymbol{B}_2+\boldsymbol{B}_{N_2})\tilde{\boldsymbol{\omega}}^H}$. Indeed, $\Phi(P_1,\, P_2) = 0$ is always inside this range. Therefore, given an $\tilde{\boldsymbol{\omega}}$, the optimal value of (P-5.9) is achieved at the cross point of $\Phi(P_1,\, P_2) = 0$ and the POPA line. However, this cross point is a complicated function of $\tilde{\boldsymbol{\omega}}$. Thus, we use the first-order Taylor series around point $(0, 0)$ to approximate the original hyperbolic curve $\Phi(P_1,\, P_2) = 0$ in the first phase, which gives,

$$
P_2 = \left.\frac{\partial\Phi(P_1,\, P_2)}{\partial P_1}\right|_{(P_1=0,P_2=0)} P_1 = \frac{-k_5}{k_4}P_1. \tag{5.23}
$$

Accordingly, the sub-optimal power allocation is chosen as the cross point of (5.23) and the POPA line, which is represented as a function of $\tilde{\boldsymbol{\omega}}$. Consequently, (P-5.9) can be approximated by an optimization problem regarding to $\tilde{\boldsymbol{\omega}}$, which will be formulated as follows. As the POPA line must be one of the five cases shown in Fig. 5.2, we use the most complicated case (case (d)), shown in Fig. 5.7, as an example, where the POPA line has three segments. Since the cross point of (5.23) and the POPA line could happen in either segment, we approximate (P-5.9) by a new optimization problem for each segment.

Segment 1: from $(0, P_2^{max})$ **to** (P_1^0, P_2^{max})

In this segment, the cross point of (5.23) and the POPA line is given as,

$$
P_1 = -\frac{k_4}{k_5}P_2^{max},\ P_2 = P_2^{max}. \tag{5.24}
$$

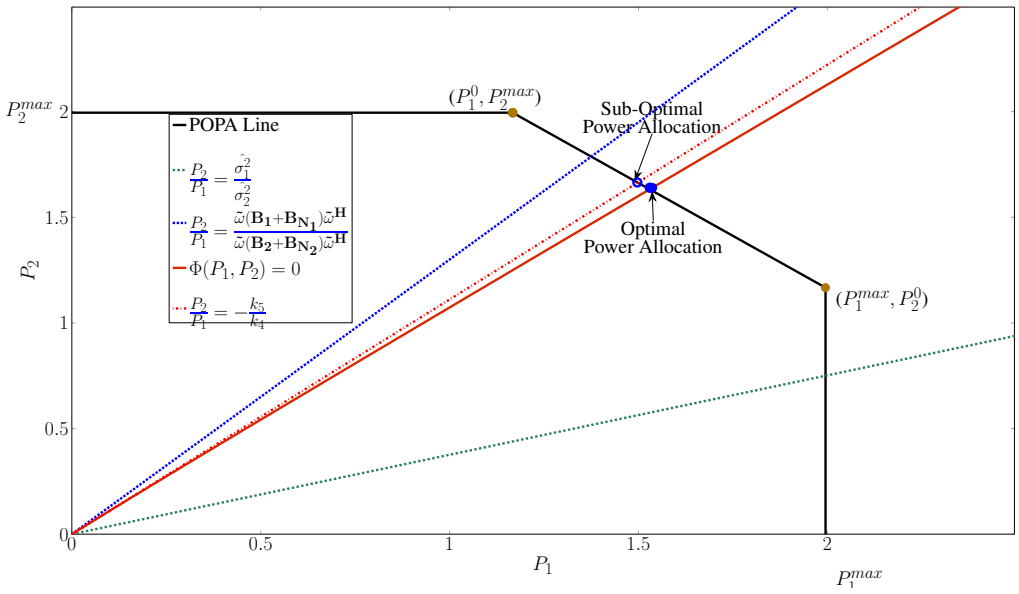

Figure 5.7: An Example of TPS Phase I for Multi-Relay System with $\tilde{\boldsymbol{\omega}}[\hat{\sigma_2^2}(\boldsymbol{B}_1 + \boldsymbol{B}_{N_1}) - \hat{\sigma_1^2}(\boldsymbol{B}_2 + \boldsymbol{B}_{N2})]\tilde{\boldsymbol{\omega}}^H > 0$

Substituting (5.24) into (P-5.9), an approximate problem is obtained as,

$$\text{(P-5.10)} \quad \max_{\tilde{\boldsymbol{\omega}}} \quad I_{th}P_2^{max}\frac{\tilde{\boldsymbol{\omega}}\boldsymbol{A}\tilde{\boldsymbol{\omega}}^H}{\tilde{\boldsymbol{\omega}}[\hat{\sigma_1^2}\boldsymbol{C}_3 + I_{th}(\boldsymbol{B}_1 + \boldsymbol{B}_{N_1})]\tilde{\boldsymbol{\omega}}^H}$$
$$\text{s.t.} \quad P_2^{max}\frac{\tilde{\boldsymbol{\omega}}[\hat{\sigma_2^2}\boldsymbol{C}_3 + I_{th}(\boldsymbol{B}_2 + \boldsymbol{B}_{N_2})]\tilde{\boldsymbol{\omega}}^H}{\tilde{\boldsymbol{\omega}}[\hat{\sigma_1^2}\boldsymbol{C}_3 + I_{th}(\boldsymbol{B}_1 + \boldsymbol{B}_{N_1})]\tilde{\boldsymbol{\omega}}^H} < P_1^0 \ .$$

Segment 2: line $a_1P_1 + a_2P_2 = I_{th}$ with P_1 from P_1^0 to P_1^{max}

In this segment, the cross point of (5.23) and the POPA line is given as,

$$P_1 = -\frac{k_4}{k_5}P_2, \ P_2 = \frac{I_{th}}{a_1} \cdot \frac{a_1k_5}{a_2k_5 + a_1k_4}. \tag{5.25}$$

Then, (P-5.9) is approximated by,

$$\text{(P-5.11)} \quad \max_{\tilde{\boldsymbol{\omega}}} \quad f(\tilde{\boldsymbol{\omega}})$$
$$\text{s.t.} \quad P_1^0 < f_1(\tilde{\boldsymbol{\omega}}) < P_1^{max} \ ,$$

where $f(\tilde{\boldsymbol{\omega}})$ and $f_1(\tilde{\boldsymbol{\omega}})$ are given in (5.26a) and (5.26b).

$$f(\tilde{\boldsymbol{\omega}}) = \frac{I_{th}^2\tilde{\boldsymbol{\omega}}\boldsymbol{A}\tilde{\boldsymbol{\omega}}^H}{\tilde{\boldsymbol{\omega}}[a_1(\hat{\sigma_2^2}\boldsymbol{C}_3 + I_{th}(\boldsymbol{B}_2 + \boldsymbol{B}_{N_2})) + a_2(\hat{\sigma_1^2}\boldsymbol{C}_3 + I_{th}(\boldsymbol{B}_1 + \boldsymbol{B}_{N_1})]\tilde{\boldsymbol{\omega}}^H} \tag{5.26a}$$

$$f_1(\tilde{\boldsymbol{\omega}}) = \frac{\tilde{\boldsymbol{\omega}}[\hat{\sigma_2^2}\boldsymbol{C}_3 + I_{th}(\boldsymbol{B}_2 + \boldsymbol{B}_{N_2})]\tilde{\boldsymbol{\omega}}^H}{\tilde{\boldsymbol{\omega}}[a_1(\hat{\sigma_2^2}\boldsymbol{C}_3 + I_{th}(\boldsymbol{B}_2 + \boldsymbol{B}_{N_2})) + a_2(\hat{\sigma_1^2}\boldsymbol{C}_3 + I_{th}(\boldsymbol{B}_1 + \boldsymbol{B}_{N_1})]\tilde{\boldsymbol{\omega}}^H}I_{th} \tag{5.26b}$$

Segment 3: from (P_1^{max}, P_2^0) **to** $(P_1^{max}, 0)$

In this segment, the cross point of (5.23) and the POPA line is given as,

$$P_1 = P_1^{max},\ P_2 = -\frac{k_5}{k_4} P_1^{max}. \tag{5.27}$$

Then, (P-5.9) is approximated by,

$$\text{(P-5.12)} \quad \max_{\tilde{\boldsymbol{\omega}}} \quad I_{th} P_1^{max} \frac{\tilde{\boldsymbol{\omega}} \boldsymbol{A} \tilde{\boldsymbol{\omega}}^H}{\tilde{\boldsymbol{\omega}} [\hat{\sigma_2^2} \boldsymbol{C}_3 + I_{th}(\boldsymbol{B}_2 + \boldsymbol{B}_{N_2})] \tilde{\boldsymbol{\omega}}^H}$$
$$\text{s.t.} \quad \frac{\tilde{\boldsymbol{\omega}} [\hat{\sigma_2^2} \boldsymbol{C}_3 + I_{th}(\boldsymbol{B}_2 + \boldsymbol{B}_{N_2})] \tilde{\boldsymbol{\omega}}^H}{\tilde{\boldsymbol{\omega}} [\hat{\sigma_1^2} \boldsymbol{C}_3 + I_{th}(\boldsymbol{B}_1 + \boldsymbol{B}_{N_1})] \tilde{\boldsymbol{\omega}}^H} P_1^{max} < P_2^0 \ .$$

It is obvious that the fractions in (P-5.10), (P-5.11) and (P-5.12) are Rayleigh-Ritz ratios. Therefore, the nested bi-section search and interior-point algorithm can be employed to solve these problems. Once (P-5.10), (P-5.11) and (P-5.12) are solved, we choose the one with the largest optimal value and use the corresponding beamforming vector $\tilde{\boldsymbol{\omega}}$ to compute the sub-optimal power allocation $(P_1^{SubOpt}, P_2^{SubOpt})$ via the corresponding equation from (5.24), (5.25), and (5.27).

Phase II: Sub-Optimal Beamforming Vector Search

Once $(P_1,\ P_2) = (P_1^{SubOpt}, P_2^{SubOpt})$ is determined,the sub-optimal beamforming vector $\boldsymbol{\omega}^{SubOpt}$ can be derived by solving (P-5.7) with the MBSS algorithm.

5.5.4 Complexity Analysis

The complexity of the proposed three algorithms (MRO, SPA and TPS) are analysed and compared in terms of running time in this section.

Since all these algorithms employ our proposed MBSS algorithm, we start with the analysis of the running time required by it. In MBSS, a bi-section search is executed, whose worst-case total number of search points is given as $\log_2(\frac{t_{up}-t_{low}}{\eta})$ [124], where η is the stopping threshold, and $[t_{low},\ t_{up}]$ is the initial searching interval. In each iteration, an interior-point algorithm is used to find the optimal solution, which requires running time of $\mathcal{O}(K^{4.5}\log(1/\epsilon))$, given the approximation accuracy $\epsilon > 0$ [126]. Therefore, MBSS requires $\mathcal{O}(\log_2(\frac{t_{up}-t_{low}}{\eta})K^{4.5}\log(1/\epsilon))$ running time. Besides, MRO, SPA and TPS all need to compute the generalized eigenvalues of two $K \times K$ matrices, which requires the running time of $\mathcal{O}(K^3)$.

Accordingly, MRO requires running time of $\mathcal{O}(N\log_2(\frac{t_{up}-t_{low}}{\eta})K^{4.5}\log(1/\epsilon))$, where N is the total number of quantization power allocations $(P_1,\ P_2)$. Although SPA also performs an exhaustive search along the POPA line, in each iteration, only the generalized eigenvalues of two Rayleigh-Ritz ratios are computed. In addition, MBSS is executed only once in the entire process. Therefore, the SPA running time is $\mathcal{O}(NK^3 + \log_2(\frac{t_{up}-t_{low}}{\eta})K^{4.5}\log(1/\epsilon))$. Unlike MRO and SPA, TPS allocates sub-optimal power directly by using an approximation process, and requires at most four executions of the nested bi-section search and interior-point algorithm. Accordingly, the TPS running time is $\mathcal{O}(\log_2(\frac{t_{up}-t_{low}}{\eta})K^{4.5}\log(1/\epsilon))$.

A clear comparison of the running time required by these three algorithms is shown in Table 5.1 Obviously, both of TPS and SPA reduce the impact of N on the total running time, and thus the computational complexity is reduced dramatically by using either of the two sub-optimal algorithms. For example, if N takes value of 100, both TPS and SPA can reduce over 90% running time, compared with the optimal method.

Table 5.1: Comparison of Running Times

Algorithms	Running Times
MRO	$\mathcal{O}(N\log_2(\frac{t_{up}-t_{low}}{\eta})K^{4.5}\log(1/\epsilon))$
SPA	$\mathcal{O}(NK^3 + \log_2(\frac{t_{up}-t_{low}}{\eta})K^{4.5}\log(1/\epsilon))$
TPS	$\mathcal{O}(\log_2(\frac{t_{up}-t_{low}}{\eta})K^{4.5}\log(1/\epsilon))$

5.5.5 Results and Discussions

This section assesses our proposed three algorithms (MRO, SPA and TPS) through simulations. We also compare our algorithms to a system with the EPA approach. For multi-relay systems, EPA allocates equal powers to the two secondary terminals, $P_1 = P_2 = \min(\frac{I_{th}}{a_1+a_2}, P_T^{max})$ where P_T^{max} is the maximum available power, and restricts each $\mathrm{R}_i \rightarrow$B $(i = 1, 2, ..., K)$ interference under I_{th}/K. Therefore, the ith $(i = 1, 2, ..., K)$ relay computes its relaying coefficient as $\omega_i = \frac{I_{th}}{K\mathbb{E}\{|h_{r_i}|^2\}}$.

In the simulations, we generate the channel coefficients using the same method

as those in single-relay systems,

$$f = \sqrt{\frac{1}{1+\alpha}}\bar{f} + \sqrt{\frac{\alpha}{1+\alpha}}\tilde{f}. \tag{5.28}$$

Therefore, their second-order statistics are computed as,

$$\mathbb{E}\{|f|^2\} = \frac{1}{1+\alpha}(|\bar{f}|^2 + \alpha), \tag{5.29}$$

$$\mathbb{E}\{\boldsymbol{f}\boldsymbol{f}^H\} = \frac{1}{1+\alpha}(\bar{\boldsymbol{f}}\bar{\boldsymbol{f}}^H + \alpha I). \tag{5.30}$$

We further assume that all AWGN components follow $\mathcal{CN}(0,1)$ distribution, and $P_p = P_1^{max} = P_2^{max}$ =3 dBm. The $(P_1,\ P_2)$ trajectory in MRO is quantified with a step size of 0.001.

Figs. 5.8 to 5.13 compare MRO, SPA, TPS, and EPA with different α values in 10-relay and 20-relay systems from the SINR and power allocation perspectives, respectively.

Achievable Average SINR v.s. Interference Temperature Limit I_{th}

As shown in Figs. 5.8 and 5.9, just like the single-relay case, a higher SINR is synonymous with more stable channels, such as α =-20 dB. Unlike the single-relay systems, the phase distortions are compensated for by the MRO beamforming vector. Consequently, joint distributed beamforming and power allocation dramatically improves the SINR, e.g., over 10 dB more than EPA. Additionally, Figs. 5.8 and 5.9 indicate that more relays facilitating the communication achieves higher SINRs. However, the number of relays only mildly affects the optimal power allocation (see Figs. 5.10 to 5.13). The reason is that the interference limit $P_I^{(1)}$, which is unrelated to the number of relays, significantly impacts power allocation.

When comparing SPA with MRO, Figs. 5.8 and 5.9 show that their SINR gap is less than 0.8 dB and 1.5 dB with α =-20 dB and α =-5 dB, respectively. Moreover, the SPA power allocations have larger differences when α =-5 dB, as shown in Figs. 5.10 to 5.13. These differences are due to the sub-optimal SPA power allocations. Indeed, the true optimal solution might have a slightly lower lower bound.

Unlike SPA, TPS achieves SINRs closer to the optimal values, with SINR gap less than 0.12 dB. Moreover, TPS even provides almost the same power allocation as MRO, as shown in Figs. 5.10 to 5.13.

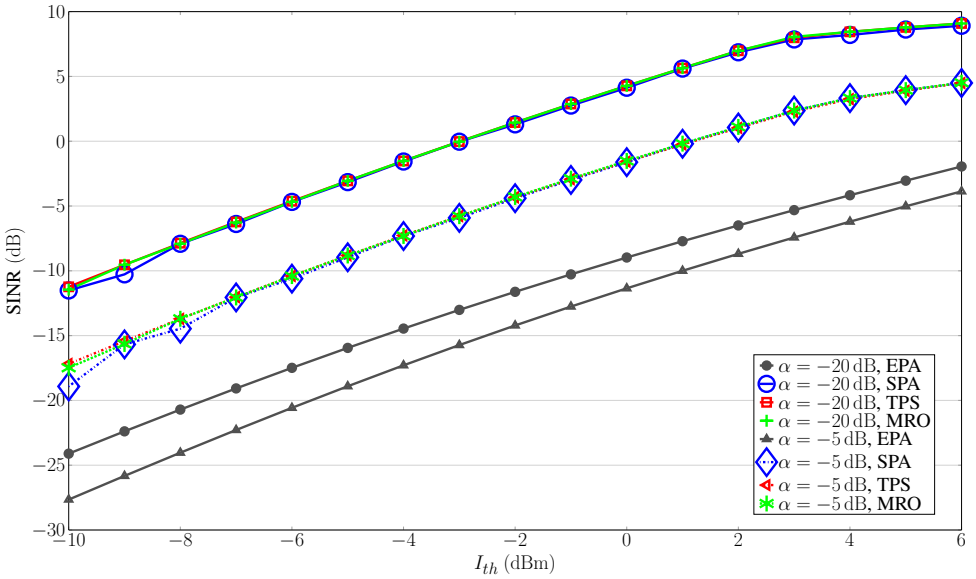

Figure 5.8: SINR v.s. I_{th} in a 10-relay system

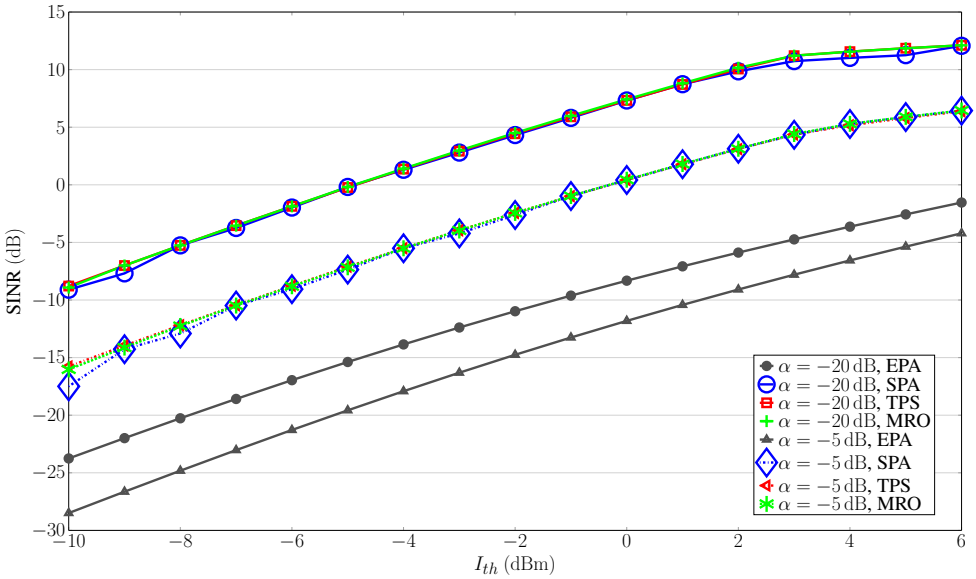

Figure 5.9: SINR v.s. I_{th} in a 20-relay system

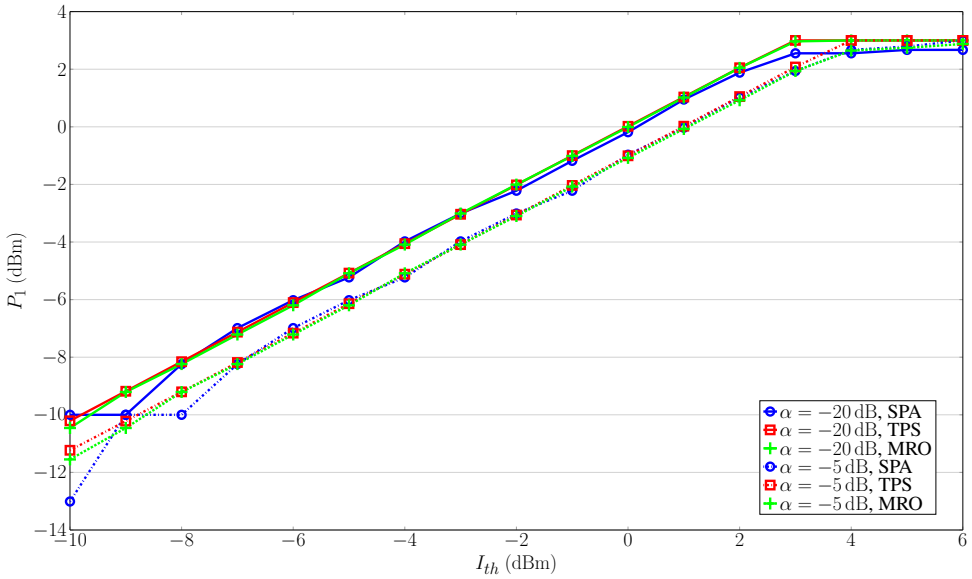

Figure 5.10: P_1 v.s. I_{th} in a 10-relay System

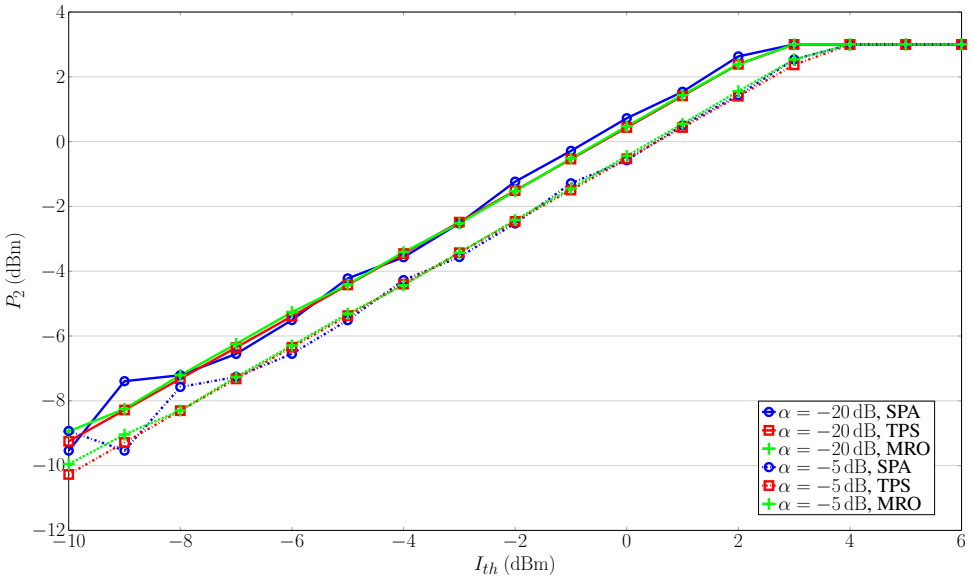

Figure 5.11: P_2 v.s. I_{th} in a 10-relay System

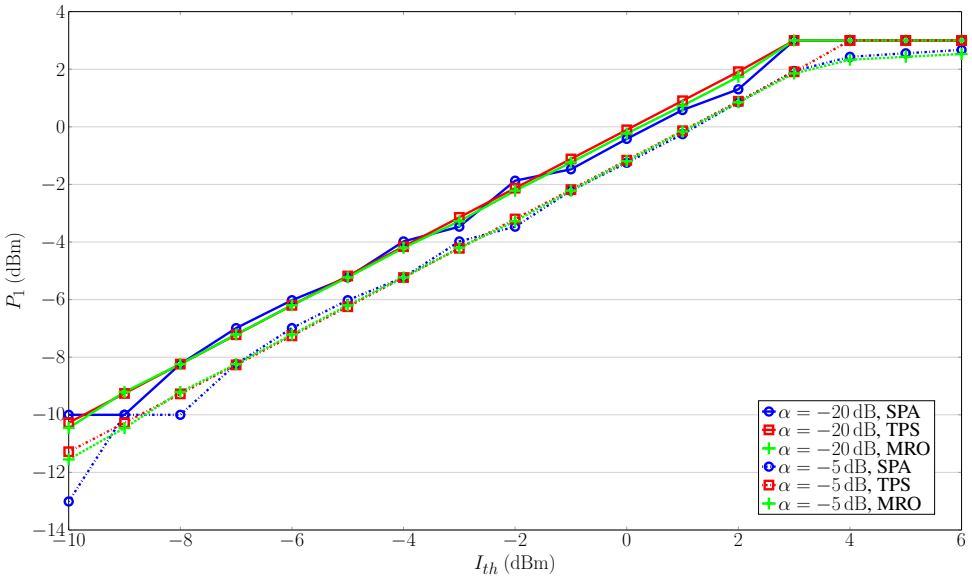

Figure 5.12: P_1 v.s. I_{th} in a 20-relay System

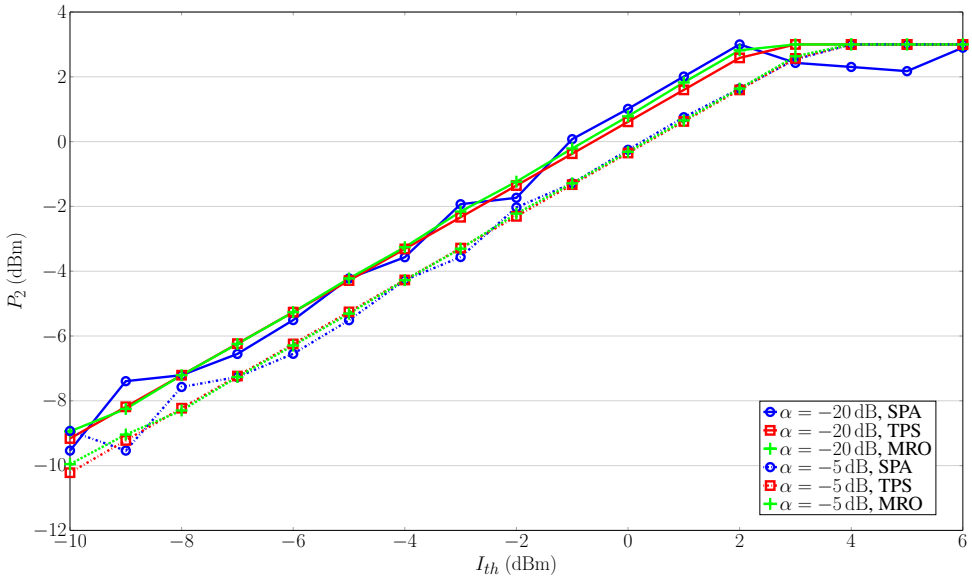

Figure 5.13: P_2 v.s. I_{th} in a 20-relay System

Running Times Comparison

Table 5.2 shows the comparison of the total running time of 100 channel realizations in a computer equipped with Intel(R)i7-3770CPU at 3.4GHz using MRO, SPA and TPS. In this comparison, I_{th}, P_j^{max} ($j = 1,\ 2$) are set to 0 dBm and 3 dBm, respectively. And the channel uncertainty α is set to -20 dB. The quantization step is set to 0.001. Clearly, over 97% running time is saved by using sub-optimal algorithms.

Table 5.2: Running Times

	MRO	SPA	TPS
$K = 10$	446.338s	0.021s	2.520s
$K = 20$	601.744s	1.716s	1.503s

5.6 Extension to Non-Cognitive Two-Way Relay Networks

In this section, the MRO and TPS algorithms are extended into non-cognitive two-way relay networks with the knowledge of partial CSI.

5.6.1 System Configuration, Signal Flow and Problem Formulation

System Configuration

The non-cognitive two-way relay network is shown as the secondary network in Fig. 5.1 which consists of only terminals SU_j ($j = 1,\ 2$) and AF two-way relay nodes R_i ($i = 1,\ 2,\ ...,\ K$). The channel assumptions and notations in the cognitive case (Section 5.2) are adopted here.

Signal Flow

The mutual information exchange between SU_1 and SU_2 also requires two time slots. In the first time slot, SU_1 and SU_2 broadcast their symbols s_j ($j = 1, 2$) with power P_j simultaneously. Then, the ith ($i = 1, 2, ..., K$) relay receives signal r_i as,

$$r_i = \sqrt{P_1} g_{1i} s_1 + \sqrt{P_2} g_{2i} s_2 + n_{r_i}, \tag{5.31}$$

where $n_{r_i} \in \mathbb{C}$ is the AWGN at R_i with zero mean and $\sigma_{r_i}^2$ variance.

In the second time slot, the ith relay multiplies r_i with a complex coefficient ω_i, then broadcasts the result to SU_j ($j = 1, 2$). Then the two signals y_1 and y_2 received at SU_1 and SU_2 respectively are given as,

$$y_1 = \underbrace{\sqrt{P_1}\boldsymbol{\omega}\boldsymbol{G}_1\boldsymbol{g}_1 s_1}_{\text{self-interference}} + \underbrace{\sqrt{P_2}\boldsymbol{\omega}\boldsymbol{G}_1\boldsymbol{g}_2 s_2}_{\text{signal}} + \underbrace{\boldsymbol{\omega}\boldsymbol{G}_1\boldsymbol{n}_r + n_1}_{\text{noise}}, \tag{5.32}$$

$$y_2 = \underbrace{\sqrt{P_1}\boldsymbol{\omega}\boldsymbol{G_2}\boldsymbol{g_1} s_1}_{\text{signal}} + \underbrace{\sqrt{P_2}\boldsymbol{\omega}\boldsymbol{G}_2\boldsymbol{g}_2 s_2}_{\text{self-interference}} + \underbrace{\boldsymbol{\omega}\boldsymbol{G}_2\boldsymbol{n}_r + n_2}_{\text{noise}}, \tag{5.33}$$

where $n_j \in \mathbb{C}$ is the zero mean AWGN at SU_j of σ_j^2 variance, $\boldsymbol{\omega} = [\omega_1, \omega_2, , ..., \omega_K]$, $\boldsymbol{n}_r = [n_{r_1}, n_{r_2}, \ldots, n_{r_K}]^T$, and $\boldsymbol{G}_j = diag\{\boldsymbol{g}_j\}$.

Partial CSI is also assumed here. Thus, SU_j $(j = 1, 2)$ only knows (1) the instantaneous CSI, $\boldsymbol{g}_j$, between the relays and itself, and (2) the SOS of all the other channels, $\mathbb{E}\{\boldsymbol{g}_j\boldsymbol{g}_j^H\}$. Therefore, the self-interference part in (5.31) and (5.32) can be eliminated perfectly. After this self-interference cancellation, the received signals become,

$$\tilde{y_1} = \sqrt{P_2}\boldsymbol{\omega}\boldsymbol{G}_1\boldsymbol{g}_2 s_2 + \boldsymbol{\omega}\boldsymbol{G}_1\boldsymbol{n}_r + n_1, \tag{5.34}$$

$$\tilde{y_2} = \sqrt{P_1}\boldsymbol{\omega}\boldsymbol{G}_2\boldsymbol{g}_1 s_1 + \boldsymbol{\omega}\boldsymbol{G}_2\boldsymbol{n}_r + n_2, \tag{5.35}$$

We further assume identical noise powers, $\sigma_{r_i}^2 = \sigma_1^2 = \sigma_2^2 = \sigma^2$, and unit symbol powers, $\mathbb{E}\{|s_1|^2\} = \mathbb{E}\{|s_2|^2\} = 1$. The transmit powers P_j $(j = 1, 2)$ and the relay coefficients ω_i $(i = 1, 2, ..., K)$ are calculated at the two terminals, then SU_j $(j = 1, 2)$ transmits the relay coefficients to the relays via an error-free feedback channel.

Problem Formulation

Our aim is to design the transmit powers P_j $(j = 1, 2)$ and the relay coefficients ω_i $(i = 1, 2, ..., K)$ to maximize the worse of the average SNRs at both terminals $(\min(\overline{\mathrm{SNR}}_1, \overline{\mathrm{SNR}}_2))$. Meanwhile the total transmit power in each time slot $P_T^{(i)}$

($i = 1, 2$) should be kept below the maximum value P_T^{max}. With these concerns, an optimization problem is formulated as,

$$\text{(P-5.13)} \max_{P_1,\, P_2,\, \boldsymbol{\omega}} \min\{\overline{\text{SNR}}_1,\, \overline{\text{SNR}}_2\} \text{ s.t. } P_T^{(i)} \leq P_T^{max},$$

where $\overline{\text{SNR}}_1$ and $\overline{\text{SNR}}_2$ are given as,

$$\overline{\text{SNR}}_1 = \frac{P_2 \boldsymbol{\omega} \boldsymbol{A} \boldsymbol{\omega}^H}{\sigma^2(\boldsymbol{\omega} \boldsymbol{D}_1 \boldsymbol{\omega}^H + 1)}, \tag{5.36}$$

$$\overline{\text{SNR}}_2 = \frac{P_1 \boldsymbol{\omega} \boldsymbol{A} \boldsymbol{\omega}^H}{\sigma^2(\boldsymbol{\omega} \boldsymbol{D}_2 \boldsymbol{\omega}^H + 1)}, \tag{5.37}$$

where $\boldsymbol{A} = \mathbb{E}\{\boldsymbol{G}_1 \boldsymbol{g}_2 \boldsymbol{g}_2^H \boldsymbol{G}_1^H\} = \mathbb{E}\{\boldsymbol{g}_1 \boldsymbol{g}_1^H\} \circ \mathbb{E}\{\boldsymbol{g}_2 \boldsymbol{g}_2^H\}$, $\boldsymbol{D}_j = \mathbb{E}\{\boldsymbol{G}_j \boldsymbol{G}_j^H\}$, $j = 1, 2$. And $P_T^{(i)}$ ($i = 1, 2$) are given as,

$$P_T^{(1)} = P_1 + P_2, \tag{5.38}$$

$$P_T^{(2)} = \boldsymbol{\omega}(P_1 \boldsymbol{D}_1 + P_2 \boldsymbol{D}_2 + \sigma^2 \boldsymbol{I}_K)\boldsymbol{\omega}^H. \tag{5.39}$$

Similar to the cognitive case, it can be proven that there is an optimal solution $(P_1,\, P_2,\, \boldsymbol{\omega})$ to (P-5.13) such that $\overline{\text{SNR}}_1 = \overline{\text{SNR}}_2$. Besides, at the optimal solution, both $P_1 + P_2 \leq P_T^{max}$ and $\boldsymbol{\omega}(P_1 \boldsymbol{D}_1 + P_2 \boldsymbol{D}_2 + \sigma^2 \boldsymbol{I}_K)\boldsymbol{\omega}^H \leq P_T^{max}$ should be satisfied with equality. The proofs are similar to those for Lemma 5.1, Lemma 5.2, and Lemma 5.3, respectively.

5.6.2 Optimal and Sub-Optimal Distributed Beamforming

As shown in (P-5.13), this optimization problem is non-convex [125] with $2(K + 1)$ variables. To find the optimal solution, we first propose an exhaustive search algorithm [151], which is an extension of the MRO algorithm. Secondly, to reduce the computational complexity, we propose a sub-optimal algorithm [151], which is an extension of the TPS algorithm.

Optimal Distributed Beamforming

By applying $\overline{\text{SNR}}_1 = \overline{\text{SNR}}_2$ and $P_1 + P_2 = P_T^{max}$, we first rewrite the optimization problem (P-5.13) as,

$$\text{(P-5.14)} \quad \max_{P_1, P_2, \boldsymbol{\omega}} \quad \frac{P_1 \boldsymbol{\omega} \boldsymbol{A} \boldsymbol{\omega}^H}{\sigma^2(\boldsymbol{\omega} \boldsymbol{D}_2 \boldsymbol{\omega}^H + 1)}$$

$$\text{s.t.} \quad P_1(\boldsymbol{\omega} \boldsymbol{D}_1 \boldsymbol{\omega}^H + 1) = P_2(\boldsymbol{\omega} \boldsymbol{D}_2 \boldsymbol{\omega}^H + 1), \tag{5.40a}$$

$$P_1 + P_2 = P_T^{max}, \tag{5.40b}$$

$$\boldsymbol{\omega}(P_1 \boldsymbol{D}_1 + P_2 \boldsymbol{D}_2 + \sigma^2 \boldsymbol{I}_K)\boldsymbol{\omega}^H = P_T^{max}. \tag{5.40c}$$

Substituting (5.40a) and (5.40b) into (5.40c), the variable P_2 can be eliminated and we have $\boldsymbol{\omega} \boldsymbol{D} \boldsymbol{\omega}^H = 2(P_T^{max} - P_1)$, where $\boldsymbol{D} = (2P_1 \boldsymbol{D}_1 + \sigma^2 \boldsymbol{I}_K)$ is a positive-definite real-valued diagonal matrix. If P_1 is given, then (P-5.14) is reduced to an optimization problem regarding to the variable $\boldsymbol{\omega}$ only. Following the analysis in the cognitive case, we define $\boldsymbol{\omega} = \sqrt{p} \tilde{\boldsymbol{\omega}} \boldsymbol{D}^{-1/2}$, where $\|\tilde{\boldsymbol{\omega}}\|^2 = 1$ and p should take value of $2(P_T^{max} - P_1)$ to satisfy (5.40c). Then, we can reformulate (P-5.14) as,

$$\max_{\tilde{\boldsymbol{\omega}}} \ \frac{P_1 p \tilde{\boldsymbol{\omega}} \hat{\boldsymbol{A}} \tilde{\boldsymbol{\omega}}^H}{\sigma^2 \tilde{\boldsymbol{\omega}}(p \hat{\boldsymbol{D}}_{\boldsymbol{2}} + \boldsymbol{I}_K)\tilde{\boldsymbol{\omega}}^H} \ \text{ s.t. } \|\tilde{\boldsymbol{\omega}}\|^2 = 1, \tag{5.41}$$

where, $\hat{\boldsymbol{A}} = \boldsymbol{D}^{-1/2} \boldsymbol{A} \boldsymbol{D}^{-1/2}$ and $\hat{\boldsymbol{D}}_{\boldsymbol{2}} = \boldsymbol{D}^{-1/2} \boldsymbol{A} \boldsymbol{D}^{-1/2}$. Since $\frac{\tilde{\boldsymbol{\omega}} \hat{\boldsymbol{A}} \tilde{\boldsymbol{\omega}}^H}{\tilde{\boldsymbol{\omega}}(p \hat{\boldsymbol{D}}_{\boldsymbol{2}} + \boldsymbol{I}_K)\tilde{\boldsymbol{\omega}}^H}$ is a generalized Rayleigh-Ritz Ratio maximization problem, its maximum value is the principal generalized eigenvalue of the two matrices, $\lambda_{max}\{\hat{\boldsymbol{A}}, p \hat{\boldsymbol{D}}_{\boldsymbol{2}} + \boldsymbol{I}_K\}$, and $\tilde{\boldsymbol{\omega}}$ should be chosen as the corresponding normalized principle eigenvector. Accordingly, given P_1, the achievable average SNR is given by,

$$\overline{\text{SNR}}^{opt}(P_1) = \frac{P_1 p}{\sigma^2} \lambda_{max}\{\hat{\boldsymbol{A}}, p \hat{\boldsymbol{D}}_{\boldsymbol{2}} + \boldsymbol{I}_K\}. \tag{5.42}$$

Therefore, to find the optimal solution to (P-5.13), we can first quantify P_1 in the range $[0,\ P_T^{max}]$. At each P_1, we solve the corresponding optimization problem (5.41), and choose P_1 with the largest $\overline{\text{SNR}}^{opt}(P_1)$ as the optimal power allocation for SU_1. Then, the optimal P_2 and $\boldsymbol{\omega}$ could be calculated according to (5.40b) and $\boldsymbol{\omega} = \sqrt{p} \tilde{\boldsymbol{\omega}} \boldsymbol{D}^{-1/2}$, respectively.

Sub-Optimal Distributed Beamforming

In this section, we propose a sub-optimal distributed beamforming method. It is an extension as of TPS, and also uses an approximation process to find a sub-optimal P_1 directly, then compute $\lambda_{max}\{\hat{\boldsymbol{A}}, p\hat{\boldsymbol{D}}_{\boldsymbol{2}} + \boldsymbol{I}_K\}$ and its corresponding eigenvector, which leads to the sub-optimal achievable average SNR and the sub-optimal beamforming vector.

To find the sub-optimal P_1, we start with rewriting the beamforming vector $\boldsymbol{\omega}$ as $\boldsymbol{\omega} = \sqrt{p}\hat{\boldsymbol{\omega}}$, where $\|\hat{\boldsymbol{\omega}}\|^2 = 1$. Substituting it to (5.40a), p is represented as,

$$p = \frac{P_2 - P_1}{\hat{\boldsymbol{\omega}}(P_1\boldsymbol{D}_1 - P_2\boldsymbol{D}_2)\hat{\boldsymbol{\omega}}^H}. \tag{5.43}$$

Then substituting (5.43) into (P-5.14), the original optimization problem is equivalent to,

$$\begin{aligned}
\text{(P-5.15)} \quad \max_{P_1, P_2, \hat{\boldsymbol{\omega}}} \quad & \frac{\hat{\boldsymbol{\omega}}\boldsymbol{A}\hat{\boldsymbol{\omega}}^H}{\sigma^2\hat{\boldsymbol{\omega}}(\boldsymbol{D}_1 - \boldsymbol{D}_2)\hat{\boldsymbol{\omega}}^H}(P_2 - P_1) \\
\text{s.t.} \quad & \|\hat{\boldsymbol{\omega}}\|^2 = 1, && \text{(5.44a)} \\
& \frac{P_2 - P_1}{\hat{\boldsymbol{\omega}}(P_1\boldsymbol{D}_1 - P_2\boldsymbol{D}_2)\hat{\boldsymbol{\omega}}^H} > 0, && \text{(5.44b)} \\
& P_1 + P_2 = P_T^{max}, && \text{(5.44c)} \\
& \Phi(P_1, P_2, \hat{\boldsymbol{\omega}}) = 0, && \text{(5.44d)}
\end{aligned}$$

where $\Phi(P_1, P_2, \hat{\boldsymbol{\omega}}) = k_1P_2^2 + k_2P_1P_2 + k_3P_1^2 + k_4P_2 + k_5P_1,$

$$\begin{aligned}
k_1 &= \hat{\boldsymbol{\omega}}\boldsymbol{D}_2\hat{\boldsymbol{\omega}}^H, && \text{(5.45a)} \\
k_2 &= \hat{\boldsymbol{\omega}}(\boldsymbol{D}_1 - \boldsymbol{D}_2)\hat{\boldsymbol{\omega}}^H, && \text{(5.45b)} \\
k_3 &= -\hat{\boldsymbol{\omega}}\boldsymbol{D}_1\hat{\boldsymbol{\omega}}^H, && \text{(5.45c)} \\
k_4 &= \hat{\boldsymbol{\omega}}(P_T^{max}\boldsymbol{D}_2 + \sigma^2\boldsymbol{I}_K)\hat{\boldsymbol{\omega}}^H, && \text{(5.45d)} \\
k_5 &= -\hat{\boldsymbol{\omega}}(P_T^{max}\boldsymbol{D}_1 + \sigma^2\boldsymbol{I}_K)\hat{\boldsymbol{\omega}}^H. && \text{(5.45e)}
\end{aligned}$$

Similar to the analysis in Phase I of TPS, given an $\hat{\boldsymbol{\omega}}$, (P-5.15) can achieve its optimal value at the cross point (P_1, P_2) of (5.44c) and $\Phi(P_1, P_2) = 0$. To simplify the representation of (P_1, P_2), we use the first order Taylor series around point $(0, 0)$

to approximate the original hyperbolic curve $\Phi(P_1, P_2) = 0$ in the first phase. The approximation function is given as,

$$P_2 = \left.\frac{\partial \Phi(P_1, P_2)}{\partial P_1}\right|_{(P_1=0, P_2=0)} P_1 = \frac{-k_5}{k_4} P_1 = \frac{\hat{\boldsymbol{\omega}}(P_T^{max}\boldsymbol{D}_1 + \sigma^2 \boldsymbol{I}_K)\hat{\boldsymbol{\omega}}^H}{\hat{\boldsymbol{\omega}}(P_T^{max}\boldsymbol{D}_2 + \sigma^2 \boldsymbol{I}_K)\hat{\boldsymbol{\omega}}^H} P_1. \tag{5.46}$$

Then the cross point of (5.44c) and (5.46), is represented as,

$$P_1 = \frac{\hat{\boldsymbol{\omega}}(\boldsymbol{D}_2 P_T^{max} + \sigma^2 \boldsymbol{I}_K)\hat{\boldsymbol{\omega}}^H}{\hat{\boldsymbol{\omega}}[P_T^{max}(\boldsymbol{D}_1 + \boldsymbol{D}_2) + 2\sigma^2 \boldsymbol{I}_K]\hat{\boldsymbol{\omega}}^H} P_T^{max},\ P_2 = P_T^{max} - P_1. \tag{5.47}$$

Substituting (5.47) into (P-5.15), the optimization problem is reformulated as,

$$\max_{\hat{\boldsymbol{\omega}}} \frac{P_T^{max2}\hat{\boldsymbol{\omega}}\boldsymbol{A}\hat{\boldsymbol{\omega}}^H}{\sigma^2\hat{\boldsymbol{\omega}}[P_T^{max}(\boldsymbol{D}_1 + \boldsymbol{D}_2) + 2\sigma^2 \boldsymbol{I}_K]\hat{\boldsymbol{\omega}}^H},\ \text{s.t. } \|\hat{\boldsymbol{\omega}}\|^2 = 1. \tag{5.48}$$

Obviously, the optimal value of (5.48) is $\frac{P_T^{max2}}{\sigma^2}\lambda_{max}\{\boldsymbol{A}, P_T^{max}(\boldsymbol{D}_1 + \boldsymbol{D}_2) + 2\sigma^2 \boldsymbol{I}_K\}$. And it is achieved when $\hat{\boldsymbol{\omega}}$ is taken as the corresponding normalized eigenvector. Once $\hat{\boldsymbol{\omega}}$ is obtained, the sub-optimal power allocation $(P_1, P_2)^{SubOpt}$ us determined via (5.47), and the corresponding sub-optimal beamformer $\boldsymbol{\omega}^{SubOpt}$ should be re-calculated using the method as solving (5.41).

To sum up, in this sub-optimal method, only two steps are required: 1) to search for sub-optimal power allocation $(P_1, P_2)^{SubOpt}$ approximately, and 2) to search for the sub-optimal beamformer $\boldsymbol{\omega}^{SubOpt}$, given this sub-optimal power allocation.

5.6.3 Results and Discussions

This section shows the simulation results and compares the optimal and sub-optimal methods for non-cognitive two-way relay networks. The channel and noise are generated using the same method as those in Section 5.5.5. In the optimal method, P_1 is quantified with a step size of 0.001. To observe the impact of the number of relays, we generate 10-relay and 20-relay systems.

Fig. 5.14 and Fig. 5.15 show the power allocation versus P_T^{max} curves for 10 relays and 20 relays, respectively. It is shown that the uncertainty α of the channel and the number of relays have only a slight impact on the power allocation. This is because power allocation is mainly decided by the constraint $P_1 + P_2 = P_T^{max}$.

Fig. 5.16 and Fig. 5.17 plot the achievable average SNR versus P_T^{max} curves for 10 relays and 20 relays, respectively. Clearly, under the assistance from more

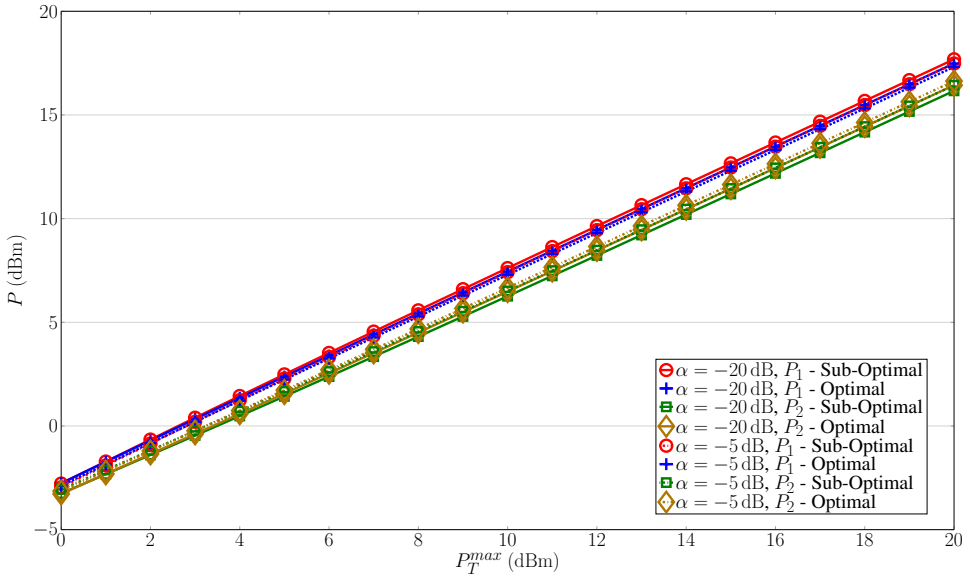

Figure 5.14: Transmit Power v.s. P_T^{max} in a 10-Relay System

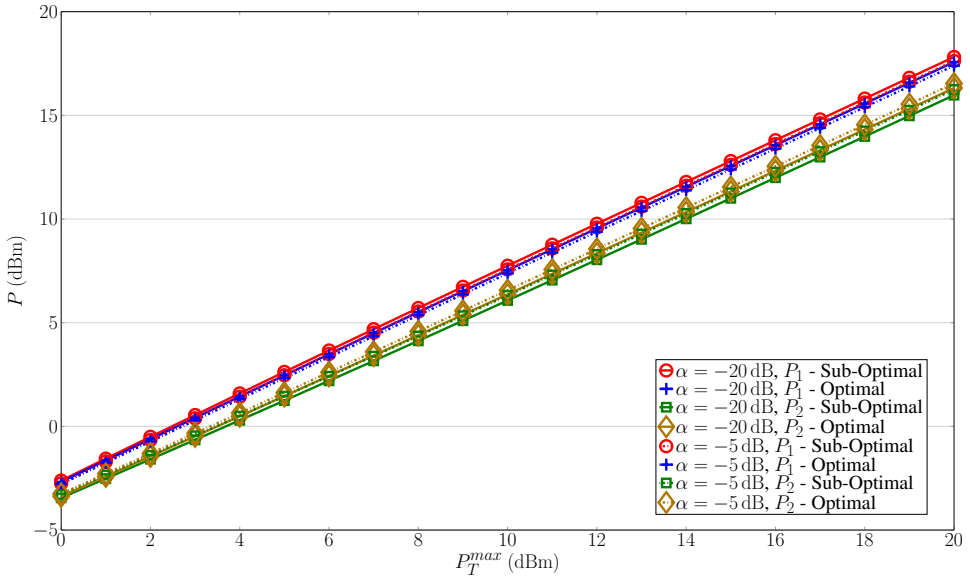

Figure 5.15: Transmit Power v.s. P_T^{max} in a 20-Relay System

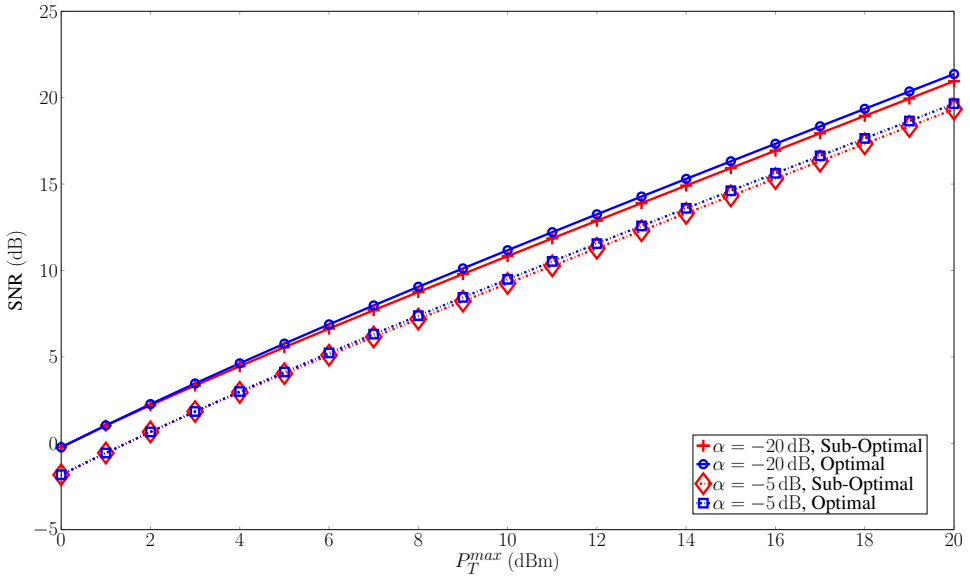

Figure 5.16: SNR v.s. P_T^{max} in a 10-Relay System

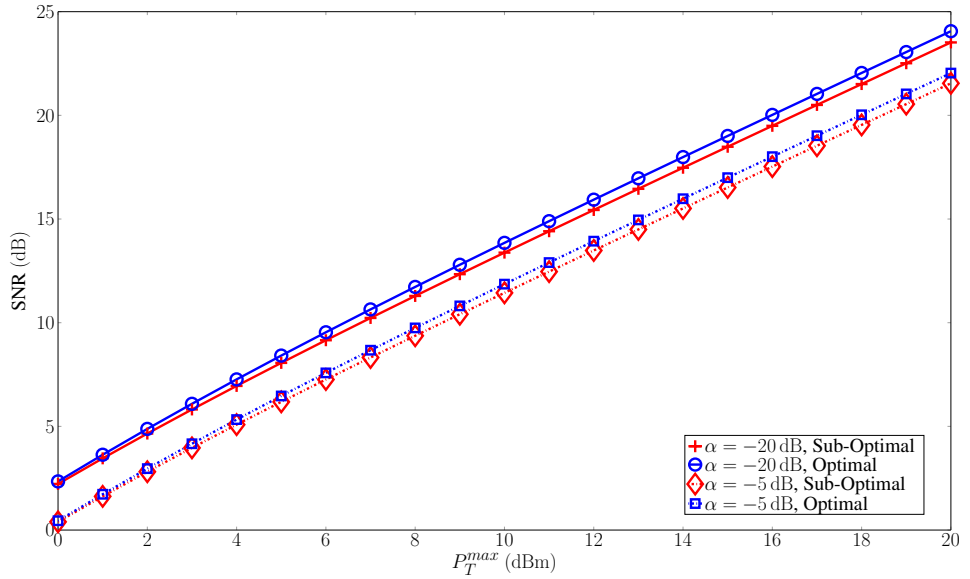

Figure 5.17: SNR v.s. P_T^{max} in a 20-Relay System

relays, higher SNR can be achieved because more spatial diversities are exploited. It is also shown that there is nearly a 2 dB gap between $\alpha = -20$ dB and $\alpha = -5$ dB cases in both 10-relay and 20-relay systems. Therefore, in a comparatively stabler channel scenario where α is small, higher SNR can be achieved.

When comparing the performances of the sub-optimal method and the optimal method, it is shown in Fig. 5.14 and Fig. 5.15 that both methods give almost the same power allocation. And the sub-optimal method can also give a near optimal SNR as shown in Fig. 5.16 and Fig. 5.17. However, the sub-optimal method can reduce the computational time dramatically. For instance, running in a computer equipped with Intel(R) i7-3770 CPU at 3.40 GHz, the suboptimal method only spends 10^{-3} of the time required by the optimal method where the quantifying step is set to 0.001 and the power constraint P_T^{max} is set to 6 dBm. So we get complexity saving of 3-orders of magnitude.

5.7 Conclusion

This chapter investigated joint distributed beamforming and power allocation in underlay two-way relay networks with only single-antenna nodes. Considering both S2P and P2S interferences and assuming the availability of partial CSI, optimal (SRO and MRO) and sub-optimal (SPA and TPS) algorithms were developed to generate the distributed beamforming vectors and to compute the transmit powers. The main contributions include:

- For a single relay, the optimal relay gain and power allocation were developed through numerical computations. However, since no beamforming is performed in this case, the achievable SINR is relatively low, e.g., lower than 0 dB.

- For $K > 1$ relays, an exhaustive-search algorithm (MRO) was proposed for the optimal distributed beamforming vector and power allocation. To reduce the computational complexity, two sub-optimal algorithms (SPA and TPS) were also proposed, which can reduce over 90% running time compared to MRO.

- Simulation results showed that MRO can improve the achievable SINR by over $10\,$dB, and only a small SINR gap exists between SPA, TPS and MRO. For instance, TPS differs only $0.15\,$dB from MRO, while SPA differs from MRO less than $0.8\,$dB and $1.5\,$dB in stabler channels and more fluctuating channels, respectively.

- The MRO and TPS algorithms were further extended into non-cognitive two-way relay networks with the knowledge of partial CSI.

$\sim$

Chapter 6

Conclusions and Future Work

6.1 Conclusion

Next-generation wireless systems must not only address the problem of spectrum congestion but also increase the utilization of spectrum. To achieve these goals, spectrum must be more efficiently and more frequently used. An obvious way to do so is to allow the licensed spectrum bands to be accessed by unlicensed (secondary) nodes. Such access policies are covered under the umbrella of underlay cognitive radio. In such underlay secondary networks, interference issues are critical and must be mitigated. This thesis thus investigated (1) beamforming (exploiting space diversity via multiple antennas); and (2) two-way AF relaying (exploiting space diversity and improving spectral efficiency while enlarging the geographical coverage via intermediate nodes).

In the resulting underlay two-way AF relay networks, taking both P2S and S2P interferences into consideration, this thesis: (1) showed the effectiveness of beamforming in addressing the bi-directional interference issues and thus in improving the reliability, and (2) developed new beamforming algorithms for underlay networks. Specific contributions are as follows.

- Chapter 3 characterized the performance of sub-optimal beamforming algorithms, ZFB-MRT/MRC, in underlay two-way relay networks consisting of multi-antenna terminals considering both path loss and small-scale fading effects. Specifically, the closed-form exact and asymptotic E2E outage probabilities were derived, which showed that (1) only the location of the relay

significantly impacts the outage, and (2) as the secondary transmit power $P_s \to \infty$ or the interference temperature limit $I_{th} \to \infty$, the diversity order is zero, but if $\frac{I_{th}}{P_s}$ is a constant, a diversity of order $(\min(M_1, M_2) - 1)$ is achieved as $P_s \to \infty$. Moreover, simulation results also showed that beamforming can provide a preferable outage, e.g., as low as 10^{-4}. Therefore, beamforming is effective in addressing the bi-directional interference issues in underlay two-way relay networks.

- Chapter 4 investigated the transmitter/receiver designs for the underlay two-way relay network with multi-antenna terminals to improve the reliability. Specifically, assuming perfect knowledge of CSI, the optimal Rx beamforming vectors were derived in closed-form first. Then the optimal Tx beamforming vectors and transmitter powers were generated jointly via our proposed optimal algorithm (JTBPA), which exploits both the spatial diversity and the interference temperature limit and improves the achievable SINR by as much as 20 dB. Next, to reduce the computational complexity, the two beamforming strategies (MRT and ZFB-MRT) were employed and the corresponding optimal power allocation was derived. Simulation results showed that ZFB-MRT has only less than 2 dB SINR loss compared to that of JTBPA. On the other hand, the time-complexity savings are significant, e.g., as much as 99%.

- Chapter 5 studied the transmitter and relay design for two single-antenna terminals and $K \geq 1$ single-antenna relays. In this configuration, the set of spatially-separated relays act as a beamformer, where the relay gains form the beamforming vector. And a form of partial CSI, using seconder-order channel statistics, is used to compute the relay gains. When $K = 1$, the optimal relay gain and transmitter powers were derived via numerical computations. But the achievable SINR is very limited in this case, e.g., lower than 0 dB, because no beamforming is performed and thus no spatial diversity is exploited. However, when $K > 1$, the optimal power allocation and relay gains (distributed beamforming vector) were computed via the optimal algorithm MRO, which can improve the achievable SINR by 10 dB or more. Due

to its high computational complexity, two low-complexity sub-optimal algorithms (SPA and TPS) were proposed as well. Both of the two sub-optimal algorithms dramatically reduce the computational complexity, by over 90% running time, and provide near optimal achievable SINR, e.g., the SINR gaps from MRO are less than 1 dB.

The above contributions demonstrate the benefits of beamforming and relay techniques and provide us with following insights.

1. Two-way relays in underlay networks help to address the problem of limited transmit powers due to the S2P interference constraint and to provide higher spectral efficiency compared to that of one-way relays.

2. Beamforming in underlay two-way relay networks can control both S2P and P2S interferences while exploiting the interference temperature limit. Therefore, beamforming can improve the communication reliability, e.g., the outage probability can be as low as 10^{-4} with sub-optimal beamforming algorithms (ZFB-MRT/MRC) in Chapter 3 and the achievable SINR can be improved by over 20 dB and 10 dB via optimal beamforming algorithms in Chapter 4 and Chapter 5, respectively.

Overall, the research findings in this thesis facilitate the use of underlay cognitive radio in real applications.

6.2 Future Research Directions

This thesis has shown the capability of beamforming in addressing the bi-directional interference issues and improving the reliability in underlay two-way relay networks. It also opens up many interesting questions to extend the researches in this thesis.

1. This thesis assumed the availability of true CSI at all nodes. However, in real applications, estimated CSI, which is the sum of true CSI and Gaussian error terms [153–156], must be used. In such a scenario, the impact of the

Gaussian error term must be characterized through performance analysis. To further overcome its impact, effective beamforming algorithms and transmitter/receiver, relay design must be developed.

2. This thesis assumed that the relays are limited to the AF mode and a single-antenna. This assumption enabled the analysis and design of the algorithms. However, it can be relaxed in several ways, e.g., the relays can be AF or DF types and have more than one antenna. With multi-antenna relays, the availability of more spatial degrees of freedom can be exploited to mitigate primary-to/from-relay interferences. Also, DF relaying can avoid the interference propagation from the first time slot to the second time slot. Therefore, more sophisticated beamforming algorithms can be developed to improve the reliability.

3. This thesis focused on half-duplex nodes only. This is because all radio nodes currently operate the half-duplex mode. However, if full-duplex nodes are available, spectral efficiency will be doubled and hence the development of such nodes is being researched recently. In full-duplex nodes, the received signal is subject to self-interference [157]. Therefore, self-interference and P2S and S2P interferences must be mitigated by beamforming. Thus, new beamforming algorithms can be developed.

4. This thesis considered only one secondary link. If multiple secondary links exist, inter-pair interferences must also be considered. In this case, beamforming and transmitter/receiver, relay design must be developed to address both the bi-directional interference issues in underlay networks and the inter-pair interference among secondary users.

$\sim$

Bibliography

[1] B. Butterworth. (2013, Jan.) How do I know if the 4G broadband will overload my freeview? [Online]. Available: http://www.ukfree.tv/article/1107052059/How_do_I_know_if_the_4G_broadband_will_overload_my

[2] I. F. Akyildiz, W.-Y. Lee, M. C. Vuran, and S. Mohanty, "Next generation/dynamic spectrum access/cognitive radio wireless networks: A survey," *Computer Networks*, vol. 50, no. 13, pp. 2127 – 2159, 2006. [Online]. Available: http://www.sciencedirect.com/science/article/pii/S1389128606001009

[3] M. Ghosh. (2014, Jun.) 22 interesting insights on global mobile usage: Ericsson. [Online]. Available: http://trak.in/tags/business/2014/06/04/22-interesting-insights-global-mobile-usage/

[4] (2014, Feb.) Cisco visual networking index: Global mobile data traffic forecast update, 20132018. [Online]. Available: http://www.cisco.com/en/US/solutions/collateral/ns341/ns525/ns537/ns705/ns827/white_paper_c11-520862.html

[5] N. Gompa. (2014, Oct.) FCC begins research into 24GHz for gigabit ultra-dense 5G mobile networks. [Online]. Available: http://www.extremetech.com/electronics

[6] Q. Zhao and B. Sadler, "A survey of dynamic spectrum access," *IEEE Signal Processing Mag.*, vol. 24, no. 3, pp. 79 –89, May. 2007.

[7] Federal Communications Commission, "Spectrum Policy Task Force," Rep. ET Docket, Tech. Rep. 02-135, Nov. 2002.

[8] S. Haykin, "Cognitive radio: brain-empowered wireless communications," *IEEE J. Sel. Areas Commun.*, vol. 23, no. 2, pp. 201 – 220, Feb. 2005.

[9] "IEEE Standard Definitions and Concepts for Dynamic Spectrum Access: Terminology Relating to Emerging Wireless Networks, System Functionality, and Spectrum Management," *IEEE Std 1900.1*, Sep. 2008.

[10] "IEEE Standard for Information technology– Local and metropolitan area networks– Specific requirements– Part 22: Cognitive Wireless RAN Medium Access Control (MAC) and Physical Layer (PHY) specifications: Policies and procedures for operation in the TV Bands," *IEEE Std 802.22*, Jul. 2011.

[11] C. Cordeiro, K. Challapali, D. Birru, and S. S. N., "IEEE 802.22: An introduction to the first wireless standard based on cogntive radios," *J. Commun. (JCM)*, vol. 1, pp. 38–47, Apr. 2006.

[12] C. Stevenson, G. Chouinard, Z. Lei, W. Hu, S. Shellhammer, and W. Caldwell, "IEEE 802.22: the first cognitive radio wireless regional area network standard," *IEEE Commun. Mag.*, vol. 47, no. 1, pp. 130–138, Jan. 2009.

[13] ECMA-International. (2012, Jun.) MAC and PHY for operation in TV white space. [Online]. Available: http://www.ecma-international.org/publications/files/ECMA-ST/ECMA-392.pdf

[14] J. Wang, M. Ghosh, and K. Challapali, "Emerging cognitive radio applications: a survey," *IEEE Commun. Mag.*, vol. 49, no. 3, pp. 74–81, Mar. 2011.

[15] C. S. Sum, H. Harada, F. Kojima, Z. Lan, and R. Funada, "Smart utility netowrks in TV white space," *IEEE Commun. Mag.*, vol. 49, no. 7, pp. 132–139, Jul. 2011.

[16] Connecting-America. (2010) The national broadband plan. [Online]. Available: http://download.broadband.gov/plan/national-broadband-plan.pdf

[17] B. Van Veen and K. Buckley, "Beamforming: a versatile approach to spatial filtering," *IEEE ASSP Magazine*, vol. 5, no. 2, pp. 4–24, Apr. 1988.

[18] "IEEE Standard for Information technology–Telecommunications and information exchange between systems–Local and metropolitan area networks–Specific requirements-Part 11: Wireless LAN Medium Access Control (MAC) and Physical Layer (PHY) Specifications Amendment 3: Enhancements for Very High Throughput in the 60 GHz Band," *IEEE Std 802.11ad-2012*, pp. 1–628, Dec. 2012.

[19] "Technical Specication Group Radio Access Network; Evolved Universal Terrestrial Radio Access (E-UTRA); LTE physical layer; General description (Release 11)," *3GPP 3GPP TS 36.201 V11.0.0 Std.*, Oct. 2012.

[20] W. Ajib and D. Haccoun, "An overview of scheduling algorithms in MIMO-based fourth-generation wireless systems," *IEEE Network*, vol. 19, no. 5, pp. 43–48, Sep. 2005.

[21] G. Boudreau, J. Panicker, N. Guo, R. Chang, N. Wang, and S. Vrzic, "Interference coordination and cancellation for 4G networks," *IEEE Commun. Mag.*, vol. 47, no. 4, pp. 74–81, Apr. 2009.

[22] S. Mohammad Razavizadeh, M. Ahn, and I. Lee, "Three-dimensional beamforming: A new enabling technology for 5G wireless networks," *IEEE Signal Process. Mag.*, vol. 31, no. 6, pp. 94–101, Nov. 2014.

[23] A. Sendonaris, E. Erkip, and B. Aazhang, "User cooperation diversity– Part I. System description," *IEEE Trans. Commun.*, vol. 51, pp. 1927–1938, Nov. 2003.

[24] ——, "User cooperation diversity– Part II. Implementation aspects and performance analysis," *IEEE Trans. Commun.*, vol. 51, pp. 1939–1948, Nov. 2003.

[25] J. Laneman, D. Tse, and G. Wornell, "Cooperative diversity in wireless networks: Efficient protocols and outage behavior," *IEEE Trans. Inf. Theory*, vol. 50, pp. 3062–3080, Dec. 2004.

[26] Q. Li, R. Hu, Y. Qian, and G. Wu, "Cooperative communications for wireless networks: techniques and applications in LTE-advanced systems," *IEEE Wireless Commun.*, vol. 19, no. 2, pp. 22–29, Apr. 2012.

[27] A. Goldsmith, *Wireless Communications*. Cambridge, U.K.: Cambridge Univ. Press, 2005.

[28] H. Katiyar and R. Bhattacharjee, "Performance of regenerative relay network operating in uplink of multi-antenna base station under Rayleigh fading channel," in *Proc. TENCON 2009 - 2009 IEEE Region 10 Conf.*, Jan. 2009, pp. 1–5.

[29] N. Yang, P. Yeoh, M. Elkashlan, I. Collings, and Z. Chen, "Two-way relaying with multi-antenna sources: Beamforming and antenna selection," *IEEE Trans. Veh. Technol.*, vol. 61, no. 9, pp. 3996–4008, Nov. 2012.

[30] "FCC: In the matter of unlicensed operation in the TV broadcast bands docket 04-186 incremental reform toward a broadcast underlay, and the radio traffic signal," FCC2008, Tech. Rep.

[31] B. Lembrikov, Ed., *Novel Applications of the UWB Technologies*. InTech, 2011.

[32] M. Chraiti, H. Hakim, W. Ajib, and H. Boujemaa, "Spectrum sharing techniques for broadcast cognitive radio networks," *IEEE Trans. Wireless Commun.*, vol. 12, no. 11, pp. 5880–5888, Nov. 2013.

[33] K. Cumanan, R. Krishna, L. Musavian, and S. Lambotharan, "Joint beamforming and user maximization techniques for cognitive radio networks based on branch and bound method," *IEEE Trans. Wireless Commun.*, vol. 9, no. 10, pp. 3082–3092, Oct. 2010.

[34] K. Cumanan, L. Musavian, S. Lambotharan, and A. Gershman, "SINR balancing technique for downlink beamforming in cognitive radio networks," *IEEE Signal Process. Lett.*, vol. 17, no. 2, pp. 133–136, Feb. 2010.

[35] N. Jamal and P. Mitran, "Performance tradeoffs offered by beamforming in cognitive radio systems: An analytic approach," *IEEE Trans. Wireless Commun.*, vol. 11, no. 10, pp. 3766–3777, Oct. 2012.

[36] M.-L. Ku, L.-C. Wang, and Y.-T. Su, "Toward optimal multiuser antenna beamforming for hierarchical cognitive radio systems," *IEEE Trans. Commun.*, vol. 60, no. 10, pp. 2872–2885, Oct. 2012.

[37] K. Phan, S. Vorobyov, N. Sidiropoulos, and C. Tellambura, "Spectrum sharing in wireless networks via QoS-aware secondary multicast beamforming," *IEEE Trans. Signal Process.*, vol. 57, no. 6, pp. 2323–2335, Jun. 2009.

[38] Y. Rahulamathavan, K. Cumanan, and S. Lambotharan, "A mixed SINR-balancing and SINR-target-constraints-based beamformer design technique for spectrum-sharing networks," *IEEE Trans. Veh. Technol.*, vol. 60, no. 9, pp. 4403–4414, Nov. 2011.

[39] R. Ramamonjison, A. Haghnegahdar, and V. Bhargava, "Joint optimization of clustering and cooperative beamforming in green cognitive wireless networks," *IEEE Trans. Wireless Commun.*, vol. 13, no. 2, pp. 982–997, Feb. 2014.

[40] G. Huang and J. Tugnait, "On energy efficient MIMO-assisted spectrum sharing for cognitive radio networks," in *Proc. 2013 IEEE Int. Conf. Commun. (ICC)*, Jun. 2013, pp. 2644–2649.

[41] T. Luan, F. Gao, X.-D. Zhang, J. Li, and M. Lei, "Rate maximization and beamforming design for relay-aided multiuser cognitive networks," *IEEE Trans. Veh. Technol.*, vol. 61, no. 4, pp. 1940–1945, May 2012.

[42] M. Beigi and S. Razavizadeh, "Cooperative beamforming in cognitive radio networks," in *2009 2nd IFIP Wireless Days (WD)*, Dec. 2009, pp. 1–5.

[43] A. Piltan, S. Salari, and R. Sadeghzadeh, "Network beamforming in cognitive relay networks with QoS constraints," in *2011 IFIP Wireless Days (WD)*, Oct. 2011, pp. 1–3.

[44] A. Piltan and S. Salari, "Distributed beamforming in cognitive relay networks with partial channel state information," *IET Commun.*, vol. 6, pp. 1011 –1018, Jan. 2012.

[45] K. Zarifi, S. Affes, and A. Ghrayeb, "Joint power control and relay design in underlay cognitive networks with multiple transmitter-receiver pairs," in *Proc. 2011 Conf. Record Forty Fifth Asilomar Conf. Signals, Systems and Computers (ASILOMAR)*, Nov. 2011, pp. 1216–1221.

[46] S. Safavi, M. Ardebilipour, V. Jamali, and M. Ahmadian, "Distributed beamforming for SINR balancing approach in cognitive two-way relay networks with imperfect channel state information," in *Proc. 20nd Iranian Conf. Elect. Eng.*, May 2012, pp. 1342 –1346.

[47] T. M. Chinh Chu, H. Phan, T. Q. Duong, M. Elkashlan, and H.-J. Zepernick, "Beamforming transmission in cognitive AF relay networks with feedback delay," in *Proc. Int. Conf. in Comput., Manage. and Telecommun. (ComManTel)*, Jan. 2013, pp. 117–122.

[48] Q. Li, Q. Zhang, R. Feng, L. Luo, and J. Qin, "Optimal relay selection and beamforming in mimo cognitive multi-relay networks," *IEEE Commun. Lett.*, vol. 17, no. 6, pp. 1188–1191, Jun. 2013.

[49] S. Safavi, M. Ardebilipour, R. Zadeh, and A. Piltan, "SINR balancing approach for network beamforming in cognitive two-way relay networks," in *Proc. 11th Int. Conf. Hybrid Intelligent Systems*, dec. 2011, pp. 481 –485.

[50] S. Safavi, M. Ardebilipour, and S. Salari, "Relay beamforming in cognitive two-way networks with imperfect channel state information," *IEEE Wireless Commun. Lett.*, vol. 1, no. 4, pp. 344 –347, Aug. 2012.

[51] K. Tourki, K. Qaraqe, and M. Alouini, "Outage analysis for underlay relay-assisted cognitive networks," in *2012 IEEE Global Commun. Conf. (GLOBECOM)*, Dec. 2012, pp. 1248–1253.

[52] K. Tourki, K. Qaraqe, and M.-S. Alouini, "Outage analysis for underlay cognitive networks using incremental regenerative relaying," *IEEE Trans. Veh. Technol.*, vol. 62, no. 2, pp. 721–734, Feb. 2013.

[53] K. J. Kim, T. Duong, and H. Poor, "Outage probability of single-carrier cooperative spectrum sharing systems with decode-and-forward relaying and selection combining," *IEEE Trans. Wireless Commun.*, vol. 12, no. 2, pp. 806–817, Feb. 2013.

[54] X. Zhang, Z. Yan, Y. Gao, and W. Wang, "On the study of outage performance for cognitive relay networks (CRN) with the nth best-relay selection in Rayleigh-fading channels," *IEEE Wireless Commun. Lett.*, vol. 2, no. 1, pp. 110–113, Feb. 2013.

[55] K. J. Kim, T. Duong, and X.-N. Tran, "Performance analysis of cognitive spectrum-sharing single-carrier systems with relay selection," *IEEE Trans. Signal Process.*, vol. 60, no. 12, pp. 6435–6449, Dec. 2012.

[56] L. Luo, P. Zhang, G. Zhang, and J. Qin, "Outage performance for cognitive relay networks with underlay spectrum sharing," *IEEE Commun. Lett*, vol. 15, no. 7, pp. 710–712, Jul. 2011.

[57] V. Asghari and S. Aissa, "End-to-end performance of cooperative relaying in spectrum-sharing systems with quality of service requirements," *IEEE Trans. Veh. Technol.*, vol. 60, no. 6, pp. 2656–2668, Jul. 2011.

[58] Z. Yan, X. Zhang, and W. Wang, "Exact outage performance of cognitive relay networks with maximum transmit power limits," *IEEE Commun. Lett.*, vol. 15, no. 12, pp. 1317–1319, Dec. 2011.

[59] Y. Zou, J. Zhu, B. Zheng, and Y.-D. Yao, "An adaptive cooperation diversity scheme with best-relay selection in cognitive radio networks," *IEEE Trans. Signal Process.*, vol. 58, no. 10, pp. 5438–5445, Oct. 2010.

[60] H. Hakim, H. Boujemaa, and W. Ajib, "Performance comparison between adaptive and fixed transmit power in underlay cognitive radio networks," *IEEE Trans. Commun.*, vol. 61, no. 12, pp. 4836–4846, Dec. 2013.

[61] J. Si, Z. Li, X. Chen, B. Hao, and Z. Liu, "On the performance of cognitive relay networks under primary user's outage constraint," *IEEE Commun. Lett.*, vol. 15, no. 4, pp. 422 –424, Apr. 2011.

[62] V. N. Q. Bao, T. Duong, D. Benevides da Costa, G. Alexandropoulos, and A. Nallanathan, "Cognitive amplify-and-forward relaying with best relay selection in non-identical Rayleigh fading," *IEEE Commun. Lett*, vol. 17, no. 3, pp. 475–478, Mar. 2013.

[63] G. Chen, O. Alnatouh, and J. Chambers, "Outage probability analysis for a cognitive amplify-and-forward relay network with single and multi-relay selection," *IET Commun.*, vol. 7, no. 17, pp. 1974–1981, Nov. 2013.

[64] B. Zhong, Z. Zhang, X. Zhang, J. Wang, and K. Long, "Partial relay selection with fixed-gain relays and outdated CSI in underlay cognitive networks," *IEEE Trans. Veh. Technol.*, vol. 62, no. 9, pp. 4696–4701, Nov. 2013.

[65] M. Xia and S. Aissa, "Cooperative AF relaying in spectrum-sharing systems: Performance analysis under average interference power constraints and Nakagami-m fading," *IEEE Trans. Commun.*, vol. 60, no. 6, pp. 1523–1533, Jun. 2012.

[66] K. Fredj and S. Aissa, "Performance of amplify-and-forward systems with partial relay selection under spectrum-sharing constraints," *IEEE Trans. Wireless Commun.*, vol. 11, no. 2, pp. 500–504, Feb. 2012.

[67] M. Seyfi, S. Muhaidat, and J. Liang, "Relay selection in cognitive radio networks with interference constraints," *IET Commun.*, vol. 7, no. 10, pp. 922–930, Jul. 2013.

[68] M. Xia and S. Aissa, "Cooperative AF relaying in spectrum-sharing systems: Outage probability analysis under co-channel interferences and relay selection," *IEEE Trans. Commun.*, vol. 60, no. 11, pp. 3252–3262, Nov. 2012.

[69] A. Afana, V. Asghari, A. Ghrayeb, and S. Affes, "Enhancing the performance of spectrum-sharing systems via collaborative distributed beamforming and AF relaying," in *Proc. IEEE Global Commun. Conf. (GLOBECOM)*, Dec. 2012, pp. 1314–1319.

[70] ——, "On the performance of cooperative relaying spectrum-sharing systems with collaborative distributed beamforming," *IEEE Trans. Commun.*, vol. 62, no. 3, pp. 857–871, Mar. 2014.

[71] Y. Cao and C. Tellambura, "Outage analysis of ZFB-MRT/MRC underlay two-way relay systems," *IEEE Commun. Lett.*, Accepted for publication.

[72] ——, "Cognitive beamforming in underlay two-way relay networks with multi-antenna terminals," *IEEE Trans. Cognitive Commun. Network.*, submitted.

[73] ——, "Joint distributed beamforming and power allocation in underlay cognitive two-way relay links using second-order channel statistics," *IEEE Trans. Signal Process.*, vol. 62, no. 22, pp. 5950–5961, Nov. 2014.

[74] A. Molisch, *Wireless Communication*, 2nd ed. New York: Wiley-IEEE press, 2011.

[75] J. G. Proakis and M. Salehi, *Digital Communications*, 5th ed. McGraw-Hill Science/Engineering/Math, Nov. 2007.

[76] B. Rankov and A. Wittneben, "Spectral efficient protocols for half-duplex fading relay channels," *IEEE J. Select. Areas Commun.*, vol. 25, no. 2, pp. 379–389, Feb. 2007.

[77] X. Gao, B. Jiang, X. You, Z. Pan, Y. Xue, and E. Schulz, "Efficient channel estimation for MIMO single-carrier block transmission with dual cyclic timeslot structure," *IEEE Trans. Commun.*, vol. 55, no. 11, pp. 2210–2223, Nov 2007.

[78] H.-M. Kim, D. Kim, T.-K. Kim, and G.-H. Im, "Frequency domain channel estimation for MIMO SC-FDMA systems with CDM pilots," *J. Commun. and Networks*, vol. 16, no. 4, pp. 447–457, Aug. 2014.

[79] T.-H. Chang, W.-C. Chiang, Y. Hong, and C.-Y. Chi, "Training sequence design for discriminatory channel estimation in wireless MIMO systems," *IEEE Trans. Signal Process.*, vol. 58, no. 12, pp. 6223–6237, Dec. 2010.

[80] Y. Jing and X. Yu, "ML-based channel estimations for non-regenerative relay networks with multiple transmit and receive antennas," *IEEE J. Sel. Areas Commun.*, vol. 30, no. 8, pp. 1428–1439, Sep. 2012.

[81] S. Sun and Y. Jing, "Channel training design in Amplify-and-Forward MIMO relay networks," *IEEE Trans. Wireless Commun.*, vol. 10, no. 10, pp. 3380–3391, Oct. 2011.

[82] ——, "Training and decodings for cooperative network with multiple relays and receive antennas," *IEEE Trans. Commun.*, vol. 60, no. 6, pp. 1534–1544, Jun. 2012.

[83] C. Wu, D. Wang, and Y. Jing, "MSE and outage probability based training power allocations for relay networks," *IEEE Trans. Commun.*, vol. 62, no. 7, pp. 2260–2270, Jul. 2014.

[84] T. Duong, H. Suraweera, H. Zepernick, and C. Yuen, "Beamforming in two-way fixed gain amplify-and-forward relay systems with CCI," in *2012 IEEE Int. Conf. Commun. (ICC)*, Jun. 2012, pp. 3621–3626.

[85] I. Chatzigeorgiou, W. Guo, I. Wassell, and R. Carrasco, "Exact and asymptotic outage probability analysis for decode-and-forward networks," *IEEE Trans. Commun.*, vol. 59, no. 2, pp. 376–381, Feb. 2011.

[86] S. Jin, M. McKay, X. Gao, and I. Collings, "Asymptotic SER and outage probability of MIMO MRC in correlated fading," *IEEE Signal Process. Lett.*, vol. 14, no. 1, pp. 9–12, Jan. 2007.

[87] B. Lee and C. Lee, "Performance analysis of cooperative multi-hop networks with hop selection in Nakagami-m fading channels," *IEEE Trans. Wireless Commun.*, vol. 12, no. 8, pp. 3851–3859, Aug. 2013.

[88] G. Amarasuriya, C. Tellambura, and M. Ardakani, "Joint relay and antenna selection for dual-hop amplify-and-forward MIMO relay networks," *IEEE Trans. Wireless Commun.*, vol. 11, no. 2, pp. 493–499, Feb. 2012.

[89] ——, "Performance analysis framework for transmit antenna selection strategies of cooperative MIMO AF relay networks," *IEEE Trans. Veh. Technol.*, vol. 60, no. 7, pp. 3030–3044, Sep. 2011.

[90] W. Xu, J. Zhang, P. Zhang, and C. Tellambura, "Outage probability of decode-and-forward cognitive relay in presence of primary user's interference," *IEEE Commun. Lett.*, vol. 16, no. 8, pp. 1252–1255, Aug. 2012.

[91] G. Amarasuriya, C. Tellambura, and M. Ardakani, "Performance analysis of hop-by-hop beamforming for dual-hop MIMO AF relay networks," *IEEE Trans. Commun.*, vol. 60, no. 7, pp. 1823–1837, Jul. 2012.

[92] ——, "Asymptotically-exact performance bounds of AF multi-hop relaying over Nakagami fading," *IEEE Trans. Commun.*, vol. 59, no. 4, pp. 962–967, Apr. 2011.

[93] S. Kusaladharma and C. Tellambura, "Aggregate interference analysis for underlay cognitive radio networks," *IEEE Wireless Commun. Lett.*, vol. 1, no. 6, pp. 641–644, Dec. 2012.

[94] M. Hasna and M.-S. Alouini, "End-to-end performance of transmission systems with relays over Rayleigh-fading channels," *IEEE Trans. Wireless Commun.*, vol. 2, no. 6, pp. 1126–1131, Nov. 2003.

[95] E. Biglieri, R. Calderbank, A. Constrantinides, A. Goldsmith, A. Paulraj, and H. V. Poor, *MIMO Wireless Communications*. New York: USA: Cambridge University Press, 2007.

[96] G. J. Foschini, "Layered space-time architecture for wireless communication in a fading environment when using multi-element antennas," *Bell Labs Technical Journal*, vol. 1, no. 2, pp. 41–59, Aug. 1996.

[97] R. Mailloux and T. K. Sarkar, *History of Wireless*. John Wiley & Sons, 2006.

[98] N. Gross, "Telecom's Contrarian," *BusinessWeek*, Jun. 2000.

[99] C. Peel, B. Hochwald, and A. Swindlehurst, "A vector-perturbation technique for near-capacity multiantenna multiuser communication-part I: channel inversion and regularization," *IEEE Trans. Commun.*, vol. 53, no. 1, pp. 195–202, Jan. 2005.

[100] B. Hochwald, C. Peel, and A. Swindlehurst, "A vector-perturbation technique for near-capacity multiantenna multiuser communication-part II: perturbation," *IEEE Trans. Commun.*, vol. 53, no. 3, pp. 537–544, Mar. 2005.

[101] T. M. C. Chu, T. Duong, and H. Zepernick, "Performance analysis for multiple-input multiple-output-maximum ratio transmission systems with channel estimation error, feedback delay and co-channel interference," *IET Commun.*, vol. 7, no. 4, pp. 279–285, Mar. 2013.

[102] L. Zhao, K. Zheng, H. Long, H. Zhao, and W. Wang, "Performance analysis for downlink massive multiple-input multiple-output system with channel state information delay under maximum ratio transmission precoding," *IET Commun.*, vol. 8, no. 3, pp. 390–398, Feb. 2014.

[103] Y. Chen and C. Tellambura, "Performance analysis of maximum ratio transmission with imperfect channel estimation," *IEEE Commun. Lett.*, vol. 9, no. 4, pp. 322–324, Apr. 2005.

[104] Y. Dhungana, N. Rajatheva, and C. Tellambura, "Performance analysis of antenna correlation on LMS-based dual-hop AF MIMO systems," *IEEE Trans. Veh. Technol.*, vol. 61, no. 8, pp. 3590–3602, Oct. 2012.

[105] L. Najafizadeh and C. Tellambura, "BER analysis of arbitrary QAM for MRC diversity with imperfect channel estimation in generalized ricean fading channels," *IEEE Trans. Veh. Technol.*, vol. 55, no. 4, pp. 1239–1248, Jul. 2006.

[106] P. Kalansuriya, M. Soysa, and C. Tellambura, "Performance of a cooperative network using rate adaptation and cooperative combining," in *Proc. 2010 IEEE Wireless Commun. and Networking Conference (WCNC)*, Apr. 2010, pp. 1–6.

[107] S. Atapattu, C. Tellambura, and H. Jiang, "Performance of an energy detector over channels with both multipath fading and shadowing," *IEEE Trans. Wireless Commun.*, vol. 9, no. 12, pp. 3662–3670, Dec. 2010.

[108] S. Atapattu, N. Rajatheva, and C. Tellambura, "Performance analysis of TDMA relay protocols over Nakagami- m fading," *IEEE Trans. Veh. Technol.*, vol. 59, no. 1, pp. 93–104, Jan. 2010.

[109] S. Atapattu, C. Tellambura, and H. Jiang, "Analysis of area under the ROC curve of energy detection," *IEEE Trans. Wireless Commun.*, vol. 9, no. 3, pp. 1216–1225, Mar. 2010.

[110] C. Tellambura, "Bounds on the distribution of a sum of correlated lognormal random variables and their application," *IEEE Trans. Commun.*, vol. 56, no. 8, pp. 1241–1248, Aug. 2008.

[111] T. K. Y. Lo, "Maximum ratio transmission," *IEEE Trans. Commun.*, vol. 47, no. 10, pp. 1458–1461, Oct. 1999.

[112] A. Afana, A. Ghrayeb, V. Asghari, and S. Affes, "On the performance of spectrum sharing two-way relay networks with distributed beamforming," in *2013 IEEE 14th Workshop Signal Process. Advances in Wireless Commun. (SPAWC)*, Jun. 2013, pp. 365–369.

[113] S. Song, M. Hasna, and K. Letaief, "Prior zero forcing for cognitive relaying," *IEEE Trans. Wireless Commun.*, vol. 12, no. 2, pp. 938–947, Feb. 2013.

[114] M. Di Renzo, F. Graziosi, and F. Santucci, "A unified framework for performance analysis of CSI-assisted cooperative communications over fading channels," *IEEE Trans. Commun.*, vol. 57, no. 9, pp. 2551–2557, Sep. 2009.

[115] M. Hasna and M.-S. Alouini, "A performance study of dual-hop transmissions with fixed gain relays," *IEEE Trans. Wireless Commun.*, vol. 3, no. 6, pp. 1963–1968, Nov. 2004.

[116] Tanendaum and A. S., *Comptuer Networks*. Prentice Hall, 2003.

[117] A. Sabharwal, P. Schniter, D. Guo, D. Bliss, S. Rangarajan, and R. Wichman, "In-band full-duplex wireless: Challenges and opportunities," *IEEE J. Sel. Areas Commun.*, vol. 32, no. 9, pp. 1637–1652, Sep. 2014.

[118] T. Cui, C. Tellambura, and Y. Wu, "Low-complexity pilot-aided channel estimation for OFDM systems over doubly-selective channels," in *Proc. 2005 IEEE Int. Conf. Commun.*, vol. 3. IEEE, May 2005, pp. 1980–1984.

[119] Z. Zhang, W. Zhang, and C. Tellambura, "Cooperative OFDM channel estimation in the presence of frequency offsets," *IEEE Trans. Veh. Technol.*, vol. 58, no. 7, pp. 3447–3459, Sep. 2009.

[120] R. Menon, R. Buehrer, and J. Reed, "Outage probability based comparison of underlay and overlay spectrum sharing techniques," in *2005 First IEEE Int. Symp. New Frontiers in Dynamic Spectrum Access Networks*, Nov. 2005, pp. 101–109.

[121] R. Blasco-Serrano, J. Lv, R. Thobaben, E. Jorswieck, A. Kliks, and M. Skoglund, "Comparison of underlay and overlay spectrum sharing strategies in MISO cognitive channels," in *Proc. 2012 7th Int. ICST Conf. Cognitive Radio Oriented Wireless Networks and Commun. (CROWNCOM)*, Jun. 2012, pp. 224–229.

[122] W. Zhang, *State Space Search: Algorithms, Complexity and Applications*. New York: Springer-Verlag, 1999.

[123] J. M. Rabaey, A. Chandrakasan, and B. Nikolic, *Digital integrated circuits-a design perspective*. Prentice Hall, 2004.

[124] T. H. Cormen, C. E. Leiserson, R. L. Rivest, and C. Stein, *Introduction to algorithms*. The MIT Press, 2009.

[125] S. Boyd and L. Vandenberghe, *Convex Optimization*. Cambridge, U.K.: Cambridge Univ. Press, 2004.

[126] Z.-Q. Luo, W.-K. Ma, A.-C. So, Y. Ye, and S. Zhang, "Semidefinite relaxation of quadratic optimization problems," *IEEE Signal Processing Mag.*, vol. 27, no. 3, pp. 20–34, May 2010.

[127] Y. Huang and S. Zhang, "Complex matrix decomposition and quadratic programming," *Math. Oper. Res.*, vol. 32, pp. 758–768, Aug. 2007.

[128] X. Gong, S. Vorobyov, and C. Tellambura, "Optimal bandwidth and power allocation for sum ergodic capacity under fading channels in cognitive radio networks," *IEEE Trans. Signal Process.*, vol. 59, no. 4, pp. 1814–1826, Apr. 2011.

[129] ——, "Joint bandwidth and power allocation with admission control in wireless multi-user networks with and without relaying," *IEEE Trans. Signal Process.*, vol. 59, no. 4, pp. 1801–1813, Apr. 2011.

[130] K. Hamdi, M. Hasna, A. Ghrayeb, and K. Letaief, "Priority-based zero-forcing in spectrum sharing cognitive systems," *IEEE Commun. Lett.*, vol. 17, no. 2, pp. 313–316, Feb. 2013.

[131] J. Tang and S. Lambotharan, "Beamforming and temporal power optimisation for an overlay cognitive radio relay network," *IET Signal Process.*, vol. 5, no. 6, pp. 582–588, 2011.

[132] Z. Dai, J. Liu, C. Wang, and K. Long, "An adaptive cooperation communication strategy for enhanced opportunistic spectrum access in cognitive radios," *IEEE Commun. Lett.*, vol. 16, no. 1, pp. 40–43, Jul. 2012.

[133] J. Liu, W. Chen, Z. Cao, and Y. Zhang, "Cooperative beamforming for cognitive radio networks: A cross-layer design," *IEEE Trans. Commun.*, vol. 60, no. 5, pp. 1420–1431, May 2012.

[134] G. Amarasuriya, C. Tellambura, and M. Ardakani, "Joint beamforming and antenna selection for two-way amplify-and-forward MIMO relay networks," in *Proc. IEEE Int. Conf. Commun.(ICC)*, Dec. 2012, pp. 4829–4834.

[135] H. Bagheri, M. Ardakani, and C. Tellambura, "Power allocation for two-way amplify-forward relaying with receive channel knowledge," in *Proc. IEEE 22nd Int. Symp. Personal Indoor and Mobile Radio Commun. (PIMRC),*, Toronto, ON, 2011, pp. 1708–1712.

[136] ——, "Resource allocation for two-way af relaying with receive channel knowledge," *IEEE Trans. Wireless Commun.*, vol. 11, no. 6, pp. 2002–2007, Jun. 2012.

[137] G. Amarasuriya, C. Tellambura, and M. Ardakani, "Performance analysis of zero-forcing for two-way MIMO AF relay networks," *IEEE Wireless Commun. Lett.*, vol. 1, no. 2, pp. 53–56, Apr. 2012.

[138] M. Zeng, R. Zhang, and S. Cui, "On design of collaborative beamforming for two-way relay networks," *IEEE Trans. Signal Process.*, vol. 59, pp. 2284–2295, May 2011.

[139] S. ShahbazPanahi and M. Dong, "A semi-closed-form solution to optimal distributed beamforming for two-way relay networks," *IEEE Trans. Signal Process.*, vol. 60, pp. 1511 –1516, Mar. 2012.

[140] S. Shahbazpanahi and M. Dong, "Achievable rate region under joint distributed beamforming and power allocation for two-way relay networks," *IEEE Trans. Wireless Commun.*, vol. 11, pp. 4026–4037, Nov. 2012.

[141] V. Havary-Nassab, S. ShahbazPanahi, and A. Grami, "Optimal distributed beamforming for two-way relay networks," *IEEE Trans. Signal Process.*, vol. 58, pp. 1238 –1250, Mar. 2010.

[142] S. ShahbazPanahi and M. Dong, "A semi-closed form solution to the SNR balancing problem of two-way relay network beamforming," in *Proc. IEEE Int. Conf. Acoustics Speech and Signal Process. (ICASSP),*, Mar. 2010, pp. 2514 –2517.

[143] Y. Jing and H. Jafarkhani, "Network beamforming using relays with perfect channel information," *IEEE Trans. Inf. Theory*, vol. 55, pp. 2499–2517, Jun. 2009.

[144] Y. Jing and S. ShahbazPanahi, "Max-min optimal joint power control and distributed beamforming for two-way relay networks under per-node power constraints," *IEEE Trans. Signal Process.*, vol. 60, pp. 6576 –6589, Dec. 2012.

[145] V. Havary-Nassab, S. Shahbazpanahi, A. Grami, and Z.-Q. Luo, "Distributed beamforming for relay networks based on second-order statistics of the channel state information," *IEEE Trans. Signal Process.*, vol. 56, pp. 4306–4316, Sep. 2008.

[146] D. Tse, P. Viswanath, and L. Zheng, "Diversity-multiplexing tradeoff in multiple-access channels," *IEEE Trans. Inf. Theory*, vol. 50, no. 9, pp. 1859–1874, Sep 2004.

[147] J. Yang, S. Jang, and D. K. Kim, "Sum rate approximation of zero-forcing beamforming with semi-orthogonal user selection," *J. Commun. and Networks*, vol. 12, no. 3, pp. 222–230, Jun. 2010.

[148] I. Gradshteyn and I. Ryzhik, *Table of Integrals, Series, and Products*. Academic Press, 2007.

[149] S. Puntanen, G. P. Styan, and J. Isotalo, *Matrix Tricks for Linear Statistical Models: our personal top twenty*. Springer, 2011.

[150] W. H. Press, S. A. Teukolsky, W. T. Vetterling, and B. P. Flannery, "Numerical recipes in C: The art of scientific computing. second edition," 1992.

[151] Y. Cao and C. Tellambura, "Distributed beamforming and power allocation in two-way multi-relay networks with second-order channel statistics," in *2013 Int. Conf. Wireless Commun. Signal Process. (WCSP)*, Oct 2013, pp. 1–6.

[152] C. Li, L. Yang, and W.-P. Zhu, "Robust distributed beamforming for two-way wireless relay systems," in *Proc. IEEE Int. Symp. Circuits and Systems (ISCAS)*, 2010, pp. 3108–3111.

[153] P. Ubaidulla and A. Chockalingam, "Relay precoder optimization in MIMO-relay networks with imperfect CSI," *IEEE Trans. Signal Process.*, vol. 59, no. 11, pp. 5473–5484, Nov. 2011.

[154] Y. Chen and C. Tellambura, "Performance analysis of maximum ratio transmission with imperfect channel estimation," *IEEE Commun. Lett*, vol. 9, no. 4, pp. 322–324, Apr. 2005.

[155] V. N. Q. Bao, T. Duong, A. Nallanathan, and C. Tellambura, "Effect of imperfect channel state information on the performance of cognitive multihop relay networks," in *2013 IEEE Global Commun. Conf. (GLOBECOM)*, Dec. 2013, pp. 3458–3463.

[156] Z. Peng, W. Xu, L.-C. Wang, and C. Zhao, "Achievable rate analysis and feedback design for multiuser MIMO relay with imperfect CSI," *IEEE Trans. Wireless Commun.*, vol. 13, no. 2, pp. 780–793, Feb. 2014.

[157] D. Senaratne and C. Tellambura, "Beamforming for space division duplexing," in *2011 IEEE Int. Conf. Commun. (ICC)*, Jun. 2011, pp. 1–5.

[158] LANCOM, "IEEE 802.11n Overview," *LANCOM Techpaper*, [Online]. Available: www.lancom-systems.de

[159] K. Kim, T. Kim, D.J. Love and I.H. Kim, "Differential Feedback in Codebook-Based Multiuser MIMO Systems in Slowly Varying Channels," *IEEE Trans. Commun.*, vol. 60, no. 2, pp. 578–588, Feb. 2012.

[160] S. Atapattu, C. Tellambura, and H. Jiang, " Energy Detection for Spectrum Sensing in Cognitive Radio," SpringerBriefs in Computer Science, 2014.

[161] V. N. Q. Bao, T. Duong, and C. Tellambura, "On the performance of cognitive underlay multihop networks with imperfect channel state information," *IEEE Trans. Commun.*, vol. 61, no. 12, pp. 4864–4873, Dec. 2013.

[162] D.T., Ngo, C. Tellambura, and H.H.!Nguyen, "Efficient Resource Allocation for OFDMA Multicast Systems With Spectrum-Sharing Control," *IEEE Trans. Veh. Technol.*, vol. 58, no. 9, pp. 4878–4889, Nov. 2009.

$\sim$

Appendix A

Comparison of Interweave, Overlay, and Underlay Modes

For the system mentioned in Section 2.1.6, the capacities when using the three cognitive modes are computed as follows.

Capacity of the interweave cognitive network

The secondary transmitter is allowed to transmit only when the primary transmitter is idle. Therefore, the secondary transmitter can transmits with its maximum available power P_s^{max} once it gets the spectrum. Thus, the capacity of the interweave cognitive network $C_{interweave}$ is given as,

$$C_{interweave} = \kappa \log_2(1 + \frac{P_s^{max}}{N_0}) \tag{A.1}$$

Capacity of the overlay cognitive network

Two cases need to be considered: (1) when the primary transmitter is active; and (2) when the primary transmitter is idle.

- When the primary transmitter is active

  In the overlay cognitive network, the secondary transmitter needs to assist primary communication. Therefore, AF relaying is assumed at the secondary transmitter and one-round communication thus requires two consecutive time slots:

1. In time slot one, the primary transmitter transmits message x by using power P_p, where $|x|^2 = 1$. Consequently, the secondary transmitter receives signal r, and the primary receiver receives signal $y_p^{(1)}$,

$$r = \sqrt{P_p}x + n_1 \tag{A.2}$$

$$y_p^{(1)} = \sqrt{P_p}x + n_p^{(1)} \tag{A.3}$$

where n_1 and $n_p^{(1)}$ are the AWGN of power N_0.

2. In time slot two, the secondary transmitter amplifies signal r to power $P_{s_1} \geq 0$ then transmits the resultant, and its own message s, $|s|^2 = 1$, with power $P_{s_2} = P_s^{max} - P_{s_1} \leq P_s^{max}$. Consequently, the transmitted signal is $\sqrt{\frac{P_{s_1}}{P_p+N_0}}r + \sqrt{P_{s_2}}s$, where $\sqrt{P_p + N_0}$ is the normalizing factor. Thus the secondary receiver receives signal y_s and the primary receiver receives signal $y_p^{(2)}$,

$$y_s = \sqrt{\frac{P_{s_1}}{P_p + N_0}}r + \sqrt{P_{s_2}}s + n_2 \tag{A.4}$$

$$y_p^{(2)} = \sqrt{\frac{P_{s_1}}{P_p + N_0}}r + \sqrt{P_{s_2}}s + n_p^{(2)} \tag{A.5}$$

where n_2 and $n_p^{(2)}$ are the AWGN of power N_0.

Then the primary receiver decodes the sum y_p of $y_p^{(1)}$ and $y_p^{(2)}$ to obtain the message x.

$$y_p = \sqrt{P_p}x + n_p^{(1)} + \sqrt{\frac{P_{s_1}}{P_p + N_0}}r + \sqrt{P_{s_2}}s + n_p^{(2)} \tag{A.6}$$

Therefore, the data rate of the primary network is given as,

$$\begin{aligned} R_1 &= \frac{1}{2}\log_2(1 + \text{SINR}_p) \\ &= \frac{1}{2}\log_2(1 + \frac{P_p + \alpha P_{s_1}}{(1-\alpha)P_{s_1} + P_{s_2} + N_0}) \end{aligned} \tag{A.7}$$

where $\alpha = \frac{P_p}{P_p+N_0}$, and the factor $\frac{1}{2}$ is due to the use of two time slots. Solving the equation $R_1 = R_1^{min}$ using the fact that $P_{s_1} + P_{s_2} = P_s^{max}$, the power P_{s_1}

used to forward the primary message and the power P_{s_2} used to transmit the secondary message are,

$$P_{s_1} = \min\left(\frac{(2^{2R_1^{min}} - 1)(N_0 + P_s^{max}) - P_p}{2^{2R_1^{min}}\alpha}, 0\right) \tag{A.8}$$

$$P_{s_2} = P_s^{max} - P_{s_1} \tag{A.9}$$

Then according to (A.4), the capacity of the secondary network when the primary transmitter is active is,

$$C_{overlay}^{(1)} = \frac{1}{2}(1-\kappa)\log_2\left(1 + \frac{P_{s_2}}{P_p + P_{s_1} + N_0}\right), \tag{A.10}$$

where the factor $\frac{1}{2}$ is due to the use of two time slots.

- When the primary transmitter is idle

  When the primary transmitter is idle, the secondary transmitter can transmit with its maximum available power P_2^{max}. Therefore, the capacity of the secondary network in this case is,

$$C_{overlay}^{(2)} = \kappa\log_2\left(1 + \frac{P_s^{max}}{N_0}\right). \tag{A.11}$$

Therefore, the overall capacity of the overlay cognitive networks is,

$$C_{overlay} = \frac{1}{2}(1-\kappa)\log_2\left(1 + \frac{P_{s_2}}{P_p + P_{s_1} + N_0}\right) + \kappa\log_2\left(1 + \frac{P_s^{max}}{N_0}\right). \tag{A.12}$$

Capacity of the underlay cognitive network

To compute the capacity of the underlay cognitive network, two cases need to be consider as well: (1) when the primary transmitter is active; and (2) when the primary transmitter is idle.

- When the primary transmitter is active

  Since in the underlay cognitive network, the secondary nodes do not assist the primary nodes transmission, thus the secondary transmitter only needs to adjust its transmit power P_s to comply with the interference constraint such that the data rate of the primary network is R_1^{min}. Using the equation

$R_1^{min} = \log_2(1 + \frac{P_p}{N_0+P_s})$, when the primary transmitter is active, the secondary transmit power is compute as,

$$P_s = \min(\frac{P_p}{2^{R_1^{min}-1}} - N_0, P_2^{max}). \tag{A.13}$$

Thus, the capacity of the underlay cognitive network in this case is given as,

$$C_{underlay}^{(1)} = (1-\kappa)\log_2(1 + \frac{P_s}{P_p + N_0}). \tag{A.14}$$

- When the primary transmitter is idle

  When the primary transmitter is idle, the secondary transmitter can transmit with its maximum available power P_2^{max}. Therefore, the capacity of the secondary network in this case is,

$$C_{underlay}^{(2)} = \kappa\log_2(1 + \frac{P_s^{max}}{N_0}). \tag{A.15}$$

Therefore, the overall capacity of the overlay cognitive networks is,

$$C_{underlay} = (1-\kappa)\log_2(1 + \frac{P_s}{P_p + N_0}) + \kappa\log_2(1 + \frac{P_s^{max}}{N_0}). \tag{A.16}$$

Appendix B

Proof of Lemmas in Multi-Antenna Cognitive Networks

B.1 Proof of Lemma 4.1

Since $\text{SINR}_j > 0$ and $\gamma_{Rj} > 0$, we have,

$$\frac{\partial \text{SINR}_j}{\partial \gamma_{Rj}} = \frac{\gamma_{\bar{j}R}[\gamma_{1R} + \gamma_{2R} + (\gamma_{Rj}+1)\Delta] - \Delta\gamma_{\bar{j}R}\gamma_{Rj}}{[\gamma_{1R} + \gamma_{2R} + (\gamma_{Rj}+1)\Delta]^2} \tag{B.1}$$

$$= \frac{\gamma_{\bar{j}R}[\gamma_{1R} + \gamma_{2R} + \Delta]}{[\gamma_{1R} + \gamma_{2R} + (\gamma_{Rj}+1)\Delta]^2} > 0. \tag{B.2}$$

Thus, SINR_j increases with γ_{Rj}.

B.2 Proof of Lemma 4.2

Let $(P_1^o,\ P_2^o,\ \boldsymbol{m}_1^o,\ \boldsymbol{m}_2^o)$ be an optimal solution to (P-4.2). Without loss of generality, we assume that $\text{SINR}_1^o < \text{SINR}_2^o$. Therefore the corresponding optimal value SINR^o of (P-4.2) satisfies $\text{SINR}^o = \text{SINR}_1^o$.

Define $\kappa = \frac{\text{SINR}_1^o}{\text{SINR}_2^o}$, then $\kappa < 1$ and $\text{SINR}^o = \kappa\text{SINR}_2^o$. Define a new power allocation $\tilde{P}_1 = \kappa P_1^o$, $\tilde{P}_2 = P_2^o$. $(\tilde{P}_1,\ P_2^o,\ \boldsymbol{m}_1^{opt},\ \boldsymbol{m}_2^{opt})$ is also a feasible point of (P-4.2), and the resulting $\widetilde{\text{SINR}_1} > \text{SINR}_1^o$ and $\widetilde{\text{SINR}_2} > \text{SINR}^o$. This contradicts that $(P_1^o,\ P_2^o,\ \boldsymbol{m}_1^o,\ \boldsymbol{m}_2^o)$ is an optimal solution to (P-4.2).

Appendix C

Proof of Lemmas in Single-Antenna Cognitive Networks

C.1 Proof of SINR Balancing Property

Assume $(P_1^{opt},\ P_2^{opt},\ \boldsymbol{\omega}^{opt})$ is one optimal solution to (P-5.1) and the corresponding optimal SINRs are not equal, e.g. $\overline{\text{SINR}}_1^{opt} \neq \overline{\text{SINR}}_2^{opt}$. Without loss of generality, we assume that $\overline{\text{SINR}}_1^{opt} > \overline{\text{SINR}}_2^{opt}$.

Define $\kappa \triangleq \frac{\overline{\text{SINR}}_2^{opt}}{\overline{\text{SINR}}_1^{opt}}$ which satisfies $\kappa < 1$. If we reduce P_2^{opt} to $\tilde{P}_2 \triangleq \kappa P_2^{opt}$, it is obvious that $(P_1^{opt},\ \tilde{P}_2,\ \boldsymbol{\omega}^{opt})$ is also a feasible solution to (P-5.1) and

$$\widetilde{\overline{\text{SINR}}}_1 \;=\; \kappa \frac{P_2^{opt}\boldsymbol{\omega}^{opt}\boldsymbol{A}(\boldsymbol{\omega}^{opt})^H}{\boldsymbol{\omega}^{opt}(\boldsymbol{B}_1+\boldsymbol{B}_{N_1})(\boldsymbol{\omega}^{opt})^H+\hat{\sigma_1^2}} = \overline{\text{SINR}}_2^{opt}.$$

Therefore, $(P_1^{opt},\ \tilde{P}_2,\ \boldsymbol{\omega}^{opt})$ is another optimal solution.

C.2 Proof of POPA Line

Assume $(P_1^{opt},\ P_2^{opt},\ \boldsymbol{\omega}^{opt})$ is an optimal solution to (P-5.1) with the optimal value $\overline{\text{SINR}}^{opt}$. Further assume that (5.8b) and (5.8c) are satisfied with inequality, $a_1P_1^{opt}+a_2P_2^{opt} < I_{th}$, $P_1^{opt} < P_1^{max}$, and $P_2^{opt} < P_2^{max}$.

Define $\kappa \triangleq \min\{\frac{P_1^{max}}{P_1^{opt}},\ \frac{P_2^{max}}{P_2^{opt}},\ \frac{I_{th}}{a_1P_1^{opt}+a_2P_2^{opt}}\}$ which satisfies $\kappa > 1$. Next, we define,

$$\tilde{P}_1 \triangleq \kappa P_1^{opt}\ \ ,\ \ \ \tilde{P}_2 \triangleq \kappa P_2^{opt}\ \ ,\ \ \ \tilde{\boldsymbol{\omega}} \triangleq \frac{1}{\sqrt{\kappa}}\boldsymbol{\omega}^{opt}\ .$$

$(\tilde{P}_1,\ \tilde{P}_2,\ \tilde{\boldsymbol{\omega}})$ is also a feasible point of (P-5.1), and $\min\{\overline{\text{SINR}}_1(\tilde{P}_2,\tilde{\boldsymbol{\omega}}), \overline{\text{SINR}}_2(\tilde{P}_1,\ \tilde{\boldsymbol{\omega}})\} > \overline{\text{SINR}}^{opt}$, which contradicts with that $(P_1^{opt},\ P_2^{opt},\ \boldsymbol{\omega}^{opt})$ is an optimal solu-

tion to (P-5.1). Therefore, at least one of the three inequalities in (5.8b) and (5.8c) should be satisfied with equality at the optimal point.

C.3 Proof of Lemma 5.3

Assume $(P_1^{opt},\ P_2^{opt},\ \boldsymbol{\omega}^{opt})$ is an optimal solution to (P-5.1) with the optimal value $\overline{\text{SINR}}^{opt}$. Further, we assume that (5.8a) is satisfied with inequality.

Define $\kappa \triangleq I_{th}/[\boldsymbol{\omega}^{opt}(P_1^{opt}\boldsymbol{C}_1 + P_2^{opt}\boldsymbol{C}_2 + \boldsymbol{C}_3)(\boldsymbol{\omega}^{opt})^H]$, which is obviously larger than 1. Then define a new beamforming vector $\tilde{\boldsymbol{\omega}} \triangleq \sqrt{\kappa}\boldsymbol{\omega}^{opt}$. $(P_1^{opt},\ P_2^{opt},\ \tilde{\boldsymbol{\omega}})$ also satisfies the constraints (5.8b) and (5.8c). And the constraint (5.8a) is satisfied with equality. We even have,

$$\begin{aligned}
\overline{\text{SINR}}_1(P_2^{opt}, \tilde{\boldsymbol{\omega}}) &> \overline{\text{SINR}}_1(P_2^{opt}, \boldsymbol{\omega}^{opt}), \\
\overline{\text{SINR}}_2(P_1^{opt}, \tilde{\boldsymbol{\omega}}) &> \overline{\text{SINR}}_2(P_1^{opt}, \boldsymbol{\omega}^{opt}),
\end{aligned}$$

which contradicts with that $(P_1^{opt},\ P_2^{opt},\ \boldsymbol{\omega}^{opt})$ is an optimal solution to (P-5.1).